2025-05

Assessing Evapotranspiration Dynamics In Ethiopia: A Case Study Of The Grand Ethiopian Renaissance Dam And Its Vicinity

Enatihun, Yesigat

BAHIRDARUNIVERSITY
FACULTY SOCIAL SCIENCES

DEPARTMENT OF GEOGRAPHY AND ENVIRONMENTAL STUDIES

PROGRAM: MSc IN GEO-INFORMATION SCIENCE

A RESEARCH ON

ASSESSING EVAPOTRANSPIRATION DYNAMICS IN ETHIOPIA: A CASE STUDY OF THE GRAND ETHIOPIAN RENAISSANCE DAM AND ITS VICINITY

BY:

ENATIHUN YESIGAT

MAY, 2025

BAHIR DAR, ETHIOPIA

BAHIR DAR UNIVERSITY

SCHOOL OF GRADUATE STUDIES

FACULTY OF SOCIAL SCIENCE

DEPARTMENT OF GEOGRAPHY AND ENVIRONMENTAL STUDIES

ASSESSING EVAPOTRANSPIRATION DYNAMICS IN ETHIOPIA: A CASE STUDY OF THE GRAND ETHIOPIAN RENAISSANCE DAM AND ITS VICINITY

BY

ENATIHUN YESIGAT

ADVISOR`

ADVISOR: DANIEL A. BEKELE

A THESIS SUBMITTED TO THE FACULTY OF SOCIAL SCIENCE, BA-HIR DAUNIVERSITY, IN PARTIAL FULFILLMENT OF THE RE-QUIREMENTS FOR THEDEGREE OF MASTER OF SCIENCE IN GEO-INFORMATION SCIENCE MAY, 2025

BAHIR DAR, ETHIOPIA

DECLARATION

This is to certify that the thesis entitled "**Assessing evapotranspiration in Ethiopia: a case study of the Grand Ethiopian Renaissance Dam and its vicinity**", submitted in partial fulfilment of the requirements for the degree of Master of science in Geo-Information Science of department of Geography and Environmental Studies, Bahir Dar University, is a record of original work carried out by me and has never been submitted to this or any other institution to get any other degree or certificates. The assistance and help I received during the course of this investigation have been duly acknowledged**.**

_____	_____	_____
Name of the candidate	Signature	Date

BAHIR DAR UNIVERSITY

FACULTY OF SOCIAL SCIENCES

DEPARTMENT OF GEOGRAPHY AND ENVIRONMENTAL STUDIES

APPROVAL OF THESIS FOR DEFENSE RESULT

As members of the board of examiners, we examined this thesis entitled "**Assessing evapotranspiration dynamics in Ethiopia: a case study of the Grand Ethiopian Renaissance Dam and its vicinity**" by Enatihun yesigat. We hereby certify that the thesis is accepted for fulfilling the requirements for the Master of science (MSc) in Geo-information science.

Board of Examiners

_____	_____	_____
Internal Examiner name	Signature	Date
_____	_____	_____
External Examiner name	Signature	Date
_____	_____	_____
Chairperson's name	Signature	Date

ACKNOWLEDGEMENT

First and for most, I would like to thank and praise the Almighty God and his mother, Virgin Mary for providing patience, strength and power to accomplish my study. I am very grateful to advisor: **DANIEL.A. BEKELE** for his professional guidance, constructive comments; close follow up by spending his time and encouragement throughout of this study. I also thank him for his positive response when I called him any time and welcome at his office and his brotherly advice. Generally, without his encouragement, insight and professional expertise, the completion of this work would not have been possible.

LIST OF ABBREVIATION AND ACRONYM

AET	Actual Evapotranspiration
BC	Blaney-Criddle Method
CHIRPS	Climate Hazards Group Infrared Precipitation with Station data
EB	Energy Balance
ERDAS	Earth Resources Data Analysis System
ET	Evapotranspiration
ETM	Enhanced Thematic Mapper
FAO	Food and Agriculture Organization
GERD	Great Ethiopia Renaissance Dam
LST	Land Surface Temperature
LULC	Land Use Land Cover
MK	Mann–Kendall
MODIS	Moderate Resolution Imaging Spectra diameter
MSE	Mean Square
NDVI	Normalized Difference Vegetation Index
OLI	Operational Land Imagery
PET	Potential Evapotranspiration
RMSE	Root Mean Square
RS	Remote Sensing
SEBAL	Surface Energy Balance for Land
SEBS	Surface Energy Balance System
TCF	Thermal Condition Factor
TM	Thematic Mapper

TABLE OF CONTENT

Contents **Page Nº**

LIST OF TABLES

LIST OF FIGURES

ABSTRCT

Actual evapotranspiration (AET) is the process through which water is transported from land surfaces to the atmosphere through evaporation from water bodies and soil, and transpiration from vegetation. This study analyzes the spatial and temporal patterns of AET in the Grand Ethiopian Renaissance Dam (GERD) region from 2001 to 2023, with a focus on climate variability and land use/land cover (LULC) changes. Aquantitative methods explanatory research design was adopted, AET was simulated using the Surface Energy Balance Algorithm for Land (SEBAL), executed on Landsat and MODIS imagery within Google Earth Engine (GEE). To analyze rainfall variability, CHIRPS (Climate Hazards Group InfraRed Precipitation with Station data) was used to provide high-resolution precipitation estimates, offering a more detailed understanding of temporal and spatial rainfall patterns. LULC change was measured through a Random Forest classifier to identify changes in forest cover, agricultural land, water bodies, and built-up land use. Random Forest regression analysis was utilized to explore the relationship between AET and climatic drivers, such as rainfall and land surface temperature (LST). An overall increase in AET post-GERD reservoir impoundment was recorded, from 5.4 mm/day in 2020 to 6 mm/day in 2023, driven by rising rainfall ($R^2 = 0.93$) and falling LST ($R^2 = 0.87$). The Mann-Kendall trend test showed no notable change in annual rainfall (Kendall's tau = 0.047, p = 0.77), but a weak negative trend in LST (Kendall's tau = 0.27, p = 0.073). The LULC analysis revealed deforestation and decline cropland, along with the expansion of water bodies and built-up areas, due to the GERD construction and water filling. The Random Forest model was resulting showed rainfall was highly explained with value ($R^2 = 0.93$, MAE = 0.32), confirming a strong correlation between AET and climatic variables. The findings underscore the vital role of the GERD in managing local hydrological cycles and climate, necessitating adaptive management strategies and continuous monitoring It is recommended to implement interventions such as utilizing innovative technologies to reduce evaporation, promoting sustainable land and water management practices, enhancing climate monitoring, supporting reforestation efforts, and engaging local communities. Effective management of natural resources is crucial for achieving long-term ecological resilience in the region.

. **Keywords**: Grand Ethiopian Renaissance Dam (GERD), Evapotranspiration, Climate variability LULC, Google earth engine.

CHAPTER ONE

1. INTRODUCTION

1.1. Background of the Study

Water is a valuable and finite resource permanently linked with life on Earth, climate balance, and sustenance of both ecosystem and human communities (Mishra, 2023). The hydrologic cycle, being a system of interconnected processes that entails precipitation, infiltration, evaporation, transpiration, and runoff, is accountable for maintaining the balance of our world's systems (Pagano & Sorooshian,2002). Especially, evapotranspiration (ET) the process of water evaporation from water bodies & land and plants' transpiration is an integral part of the hydrological cycle as it defines the supply of water in ecosystems, fields, and cities (Pagano & Sorooshian, 2002).ET is regulated by different climatic factors including temperature, humidity, solar radiation, wind speed, and land use & land cover (LULC) changes also significantly influence its rates (Li et al.,2017).

With rising global populations and climate patterns becoming ever more unstable, the demand for effective water resource management has accelerated (Sivakumar, 2011). In fact, the United Nations reports that by 2025, close to 1.8 billion people will live in regions of absolute water scarcity, and two-thirds of the world's population will be experiencing water stress (Vanham et al., 2018). These projections underscore the need for innovative and effective water management solutions especially in vulnerable regions such as Africa, where the impacts of global warming are experienced most sharply.

The distribution and availability of freshwater resources in Africa are largely dictated by diverse and in some cases extreme climatic conditions that range from arid deserts to tropical areas of high vegetation (Urama & Ozor, 2010). Climate variability like rising temperatures and erratic precipitation patterns therefore has a great impact on water resources, exacerbating both droughts and floods (Niang et al., 2014). Additionally, Sub-Saharan Africa contains some of Africa's most water-stressed countries. It becomes even riskier because the majority of African nations such as Ethiopia rely heavily on rain-fed agriculture, thereby making food security even more vulnerable to climatic variability (Mastrorillo et al., 2016).

These factors are especially relevant to nations like Ethiopia, where climate change as well as land use changes make water management increasingly challenging and heighten water resource tensions (Gelete, 2020). At the center of the Nile Basin lies Ethiopia, with especially urgent issues of shifting rainfall patterns and temperature rises. Both of these endanger agricultural productivity and complicate water resource management (Thornton & Herrero, 2010). In addition, Ethiopia's rapidly growing population has brought about dramatic land use and land cover changes further stressing an already limited water re-source supply (Thornton & Herrero, 2010). Such coupled stresses of climate change and land-use changes contribute to increasingly complex water availability issues. Therefore, innovative solutions and detailed analyses are necessary in order to make development sustainable (Gelete, 2020). Further, mega infrastructure developments like the Grand Ethiopian Renaissance Dam (GERD) usher in drastic alteration of the local hydrology, thereby changing ET patterns and the general availability of water (World Bank, 2020). Creation of large water bodies that are dam reservoirs has the potential to increase evaporation losses, decrease water storage capacity, and damage downstream assets, further worsening water management in the area (Wang et al., 2018).

For a better understanding of these processes, evapotranspiration is expressed in two simple ways: potential evapotranspiration (PET) and actual evapotranspiration (AET). PET is the potential maximum under ideal conditions for evaporation as a function of atmospheric conditions like temperature, humidity, and solar radiation (Juárez et al., 2022). On the other hand, AET represents the actual water loss under current conditions, that affected by soil moisture availability and vegetation cover (Lawrence et al., 2007). Understanding the interplay between these factors is essential for effective water resource management as it directly influences soil moisture levels, crop water demand, and the sustainability of freshwater resources within river basins (Schlosser et al., 2014). Changes in temperature, precipitation patterns, wind speed, and humidity as well as shifts in land cover can significantly impact ET rates and therefore local water availability (Zeppel et al., 2014). In Ethiopia, where land use changes, population increase, and climate change are escalating pressures on already scarce water resources, the significance of these factors is especially clear (Gelete, 2020). Climate change is also expected to strongly influence the water supply by enhancing excessive water loss by evapotranspiration in the Gilgel Gibe basin (Alemayehu et al., 2023), Tekeze basin (Gebremeskel & Kebede, 2018), and upper Blue Nile basin (Haile et al., 2017). Additionally, the GERD which leds to significant land cover changes in the

Benishangul Gumuz region further complicates water management and evapotranspiration dynamics (World Bank, 2020). Therefore, understanding how these factors interact to influence ET rates is crucial for sustainable water resource management. Therefore, this study aims to assessing evapotranspiration in the vicinity of the GERD by integrating the effects of both land cover changes and climatic variability. By utilizing satellite imagery and local meteorological data, this study seeks to explain how these factors influence ET rates and water availability.

1.2 Statement of the Problem

One of the increasingly global issues, water shortage impacts over 2 billion individuals and is a result of the advanced interrelationship between population increase, climatic uncertainty, and ineffective policies for water resource management (UN Water, 2021). One of the greatest issues the world is fighting in the twenty-first century is water scarcity that has impacted millions of people's daily lives (Rosegrant, 1997). It has been estimated that nearly 40% of the global population are facing some form of water scarcity. Population increases, mismanagement of water, and climate change (Lal et al., 2010) are the primary causes of water scarcity in Asia and the Middle East. Numerous studies have documented a sudden fall in the semi-arid regions of Asia and the Middle East groundwater level primarily as a result of over drawal of water for agriculture (Priyan, 2021).

Climate fluctuation highly disturbs the hydrologic cycle, typified by unpredictable patterns of rain and rising temperatures. This deeply affects evapotranspiration (ET) processes, which are responsible for sustaining water systems at local levels (Allan et al., 2020). The impact is rather devastating in the majority of African nations, where approximately 300 million individuals lack guaranteed access to clean drinking water (Okesanya et al., 2024). This crisis is further exacerbated by in-creasing water demand caused by rapid urbanization and agricultural expansion, both of which are also influenced by land cover and land use changes (Mastrorillo et al., 2016). For instance, deforestation and natural landscape conversion to agricultural or urban land reduces the coverage of vegetation capable of transpiring, which is a critical component of ET (Teuling et al., 2019). As vegetation cover diminishes, soil moisture content levels decrease, and the resulting higher evaporation rates subsequently decrease freshwater resource levels (Carpente et al., 1992).

In Ethiopia, where around 65% of its population rely on agriculture for their livelihood, it places them in a vulnerable situation (Moreda, 2023). The country is highly vulnerable to the impacts of climate variability, including persistent droughts and out-of-season rainfall, further affecting farm production and food security (Berhane, 2018). LULC dynamics, driven by population pressures and economic development activities, cause reduced transpiration rates and increased evaporation, which result in negative feedback mechanisms aggravating water scarcity (Hirsch & Johnson, 2020). The impact of altered ET dynamics is tremendous, not only in agricultural production but also in ecosystems and in community resilience that relies on such natural resources.

The assessment of evapotranspiration (ET) dynamics in the Grand Ethiopian Renaissance Dam (GERD) and its surrounding areas is a complex and critical problem that directly affects water resource management in the Blue Nile basin. ET, which combines evaporation from the reservoir surface and transpiration from surrounding vegetation, represents a major pathway of water loss, yet its quantification remains uncertain due to several interrelated factors.

Climate variability plays a significant role in influencing ET rates. The GERD region experiences highly variable rainfall patterns, temperatures, and potential evapotranspiration (PET) rates, which fluctuate seasonally and spatially due to the basin's complex topography and climate systems. Studies show that rainfall in the Upper Blue Nile basin ranges from 1000 mm to 2200 mm annually, with potential evapotranspiration varying between 1000 and 1800 mm per year (HESS, 2023). Climate change projections suggest an increase in ET rates by approximately 8.3%, driven by rising temperatures and altered precipitation regimes, which could intensify water losses through ET (MDPI, 2022). This variability complicates the ability to accurately model and predict ET, especially under changing climatic conditions.

Land use and land cover (LULC) changes in the GERD vicinity further influence ET dynamics. The Ethiopian Highlands surrounding the dam have undergone significant transformations due to agricultural expansion, deforestation, and urbanization. These changes alter vegetation types, density, and health, which in turn affect transpiration rates. Vegetation acts as a natural regulator of water fluxes, and shifts in LULC modify the balance between evaporation and transpiration, impacting the overall ET budget. However, current hydrological models and remote sensing ap-

proaches often lack detailed integration of LULC dynamics, limiting their capacity to capture these effects accurately (HESS, 2023).

Furthermore, the study by Stonestrom et al. (2009) addressed the impacts of land use and land cover changes on water resources, as concurrent trends have been achieved in the context of water reservoirs, particularly delineated by Mostafa et al. (2016) within the Aswan Dam area. Badawy (2009) studied the impacts of climate change on Aswan High Dam Reservoir evaporation losses and concluded that temperature and humidity rise are to be anticipated, while declining wind speed would have negligible effects on evaporation rates. Analysis has further been made of climate variability interactions with land use changes and their subsequent effects on the hydrologic cycle, particularly in semi-arid and arid regions experiencing severe water scarcity conditions, as in the case study by Bao (2019) in the Middle Yellow River Basin in China. Simultaneously, Zhang et al. (2020) noted the significance of land use change effects on hydrological processes as well as the need to formulate integrated water resource. Liu et al. (2015) discussed the consequences of ET for water resource management in different climatic zones, whereas basic research, such that of Allen et al. (1998b), has offered sophisticated methodologies to estimate ET. While Vicente-Serrano et al. (2014) investigated spatiotemporal changes in ET using MODIS data to provide information on water usage efficiency, Dai et al. (2018) highlighted the significance of climate change as a primary cause producing ET variability, particularly across semi-arid regions.

Despite this wealth of information, many studies focus on land use change or climatic impacts alone at the expense of the other factors, and even less often examine the synergistic interactions among all these variables and their combined impact on ET processes. These are especially important given the large-scale land cover changes triggered by the GERD construction. Previous research has highlighted various dimensions of land cover, land use, and evaporation trends, often overlooking an integrated consideration of interlinkages between these changes and their influences on ET This omission limits understanding of complex interlinkages between climate variability, land use change, and ET in the GERD basin. Therefore, there is a strong need for an

integrated approach that combines quantitative and qualitative analysis to enhance comprehension of the linkage among land use patterns, climate variability, and ET processes. To address these gaps, the present study aims to assess the dynamics of evapotranspiration with the aim of enhancing water resource management in the Benishangul Gumuz region that includes the GERD.

1.3. Objectives

1.3.1 General objective

The general objective the study was to assess the evapotranspiration dynamics for improved water resource management in the Benishangul-Gumuz region, Ethiopia focusing on GERD and its vicinity.

1.3.2 Specific objectives

The specific objectives of the study were

- To assess the spatiotemporal variations of evapotranspiration in the GERD and its vicinity for the period of 2001 to 2023
- To assess the climate variability in the GERD and its vicinity from the period of 2001 to 2023
- To investigate land cover change dynamics in the study area from the period of 2001,2012 and 2023
- To analyze the relationship LULC changes, climate variability and with evapotranspiration dynamics from the period of 2001 to 2023

1.4. Research Questions

1. How can the spatial and temporal variations of evapotranspiration be accurately assessed in the GERD and its vicinity?
2. What is the extent and nature of climate change or variability in the GERD and its vicinity?
3. What are dynamics of land cover changes in the GERD and its vicinity?

4. How does land use/land cover changes and climate variability influence on the dynamics of evapotranspiration in around the GERD and its vicinity?

1.5 Scope of the Study

This study investigated into understanding how water loss through evaporation and plant transpiration changes over time in the Benishangul Gumuz region of Ethiopia, specifically around the Grand Ethiopian Renaissance Dam (GERD) and its neighboring areas. The primary aim was to assess that could help improve the management of water resources in this region, with a special focus on providing insights and recommendations tailored to the GERD project.

1.6. Significance of the Study

By exploring evapotranspiration patterns, the study provides essential input for future research and offers a foundation for those interested in understanding land-water vegetation interactions. The results can support better environmental planning, contribute to sustainable land use, and help protect natural resources.

1.7. Organization of the Thesis

This research document is structured into five comprehensive chapters. Chapter one provides a brief introduction to the study, statement of the problem, research objectives, discussing the significance of the study, limitation of the study and scope of the study. Chapter two review of relevant scholarly works, situating this research within the broader academic discourse. Chapter three details the study area and delineates the methodology and materials used in the research. Chapter four encompasses the results, with a thorough discussion, and Chapter five provides the conclusion, and recommendations.

CHAPTER TWO

2. LITERATURE REVIEW

2.1. Concepts of Evapotranspiration

Evapotranspiration classified evapotranspiration as the overall term for all the processes by which water is changed from liquid or solid to a gaseous state (Pereira et al., 1999). The term, therefore, includes evaporation from open water, transpiration from vegetation leaves, sublimation from ice and snow, and bare soil (Dingman, 2002; Bahadur Roy, 2002). This phase shift is mainly caused by the availability of solar energy on the transpiring and evaporating surfaces. Because they occur simultaneously in influencing the environment, these two processes are virtually impossible to define separately.

Moreover, it is the quantity of water lost through transpiration and evaporation from vegetation and land surface and hence it is a key parameter in irrigation and agricultural systems (Hammer, 2020). In order for irrigation techniques and water control to be practical, evapotranspiration must be estimated carefully (Wanniarachchi & Sarukkalige, 2022). Evapotranspiration is influenced by several factors, including air temperature, speed of the wind, daylight hours, soil moisture content, and air humidity. It then follows that sensors to track these conditions must form part of any automated irrigation system in order to provide efficient irrigation. One of the main concepts in hydrology is evapotranspiration, which is the process through which water moves from the Earth's surface to the atmosphere through evaporation and plant transpiration. Evapotranspiration plays a significant role in balancing the water supplies in an ecosystem, consequently affecting the availability and distribution of water supplies (Chu et.al, 2017).

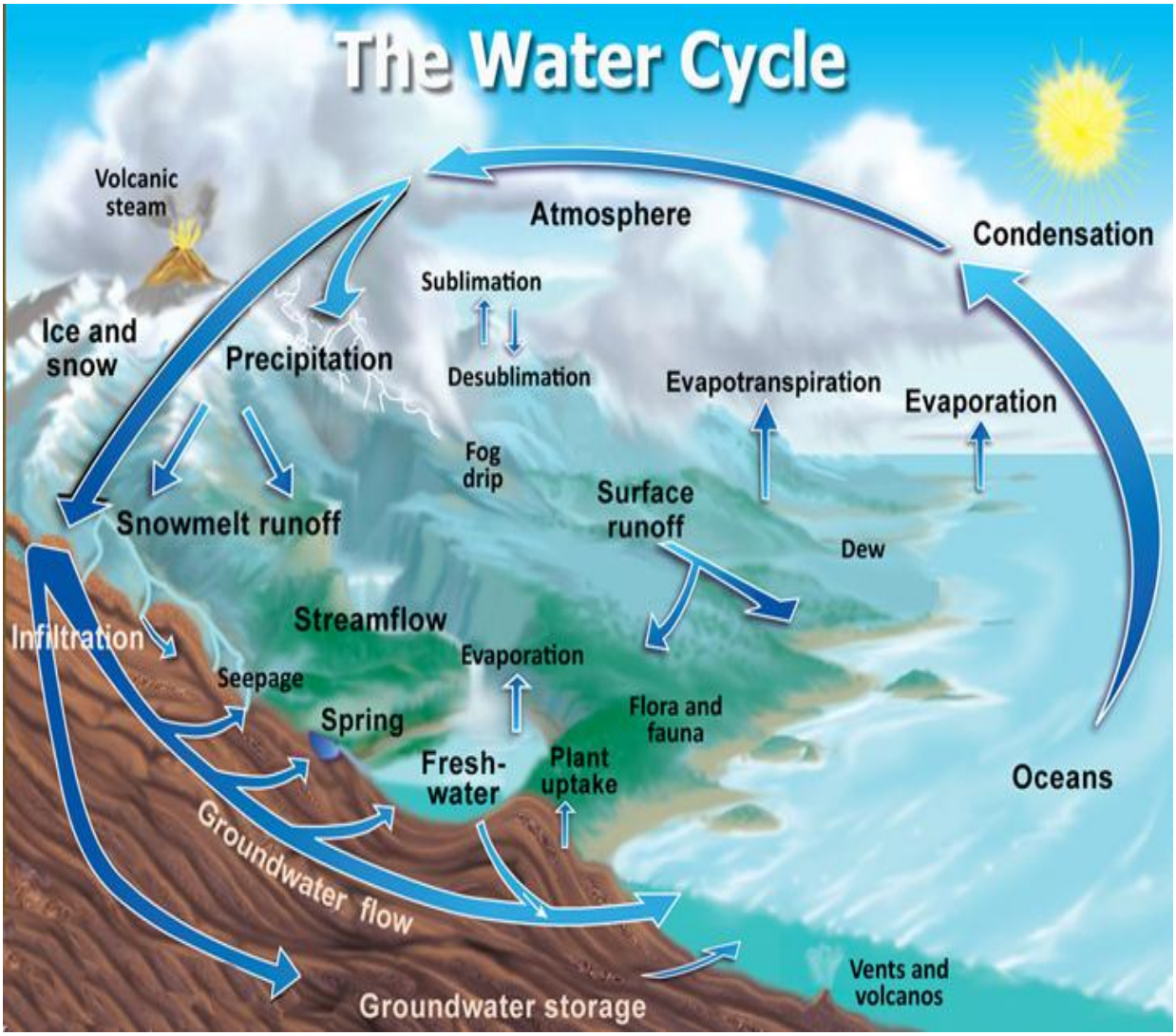

Figure 1 water cycle Source: (APEC water)

2.2. Evapotranspiration in Africa

African continent has profound location differences driven by variability in vegetation, climate, and land use, all of which are a product of the hydrological processes of the continent. ET values can fall to ranges of 200-600 mm per year in desert areas, including the Sahara Desert and the Sahel, primarily as a result of high temperatures, high solar radiation, and sparse vegetation cover that restricts transpiration (Zhao et al., 2018). Conversely, dense tropical rainforests in Central Africa, like the Congo Basin, possess the highest ET rates on the continent, typically in excess of 1500 mm a year, since such systems take advantage of high precipitation and well-vegetated

conditions that maximize transpiration (Saatchi et al., 2011). Traveling to the West and East African savannas, ET levels increase significantly, from 600 to 800 mm annually, because of seasonal rains that maintain high agricultural productivity and heterogenous vegetative cover (Awotwi et al., 2020). Conversely, Southern Africa is not uniform; while some of the semi-arid zones have ET values below 500 mm, temperate zones have the potential to reach up to nearly 1200 mm, thus impacting water availability as well as agriculture within the region (Thomas et al., 2011). These local ET differences are critical to inform water resource management, crop practice, and adaptation response to climate change, particularly since changing weather patterns will exacerbate existing vulnerabilities (Fischer et al., 2012; Hoffman et al., 2018).

2.3. Evapotranspiration in Ethiopia

In Ethiopia is characterized by great regional variation, which is decided by the country's diverse topography, climatic regions, and land use, all of which play important roles in hydrological processes. In the highland areas, such as the Ethiopian Highlands, ET rates can range from approximately 800 to 1200 mm per annum with benefit of cooler temperatures and adequate rain that favor rich vegetation, hence being very important for agriculture and water resources (Mekonnen & Hoekstra, 2016; Awulachew et al., 2010). Conversely, in the arid and semi-arid low-land conditions, such as sections of the Afar and Somali territories, rates of ET could drop to between 300 and 600 mm per year, primarily due to high temperatures, low precipitation, and infrequent vegetation that restricts transpiration (Hurni et al., 2010).

The southern and central regions, which enjoy a mix of agropastoral systems and grasslands, possess an average ET rate of between approximately 600 and 900 mm per year that relies significantly on the rainy season climatic patterns that predominate the Ethiopian climate (Zhang et al., 2018). The complexity of ET dynamics in Ethiopia is also compounded by the variable land use activities, including deforestation, agricultural expansion, and irrigation, which can have the potential to alter local microclimates and water supply (Beyene et al., 2018). Knowledge of these ET regional differences is crucial in designing water resource management, enhancing agricultural productivity, and combating climate change impacts, especially considering that Ethiopia is confronted with challenges such as increasing variability in the pattern of rainfall and water scarcity (Mastrorillo et al., 2016; Deressa et al., 2009).

2.4. The Relationship between Water Resources and Evapotranspiration

Evapotranspiration is one of the many processes in the hydrologic cycle that have the potential to impact the available water resources being released. Common restraints on evapotranspiration include existing open water availability and characteristics of soil and vegetation cover (Abate & Melesse, 2013). It is a basic part of the water cycle and of sustainable water resource management. (Gordon et al., 2005) It is the process by which water is evaporated from the Earth's surface and lost by transpiration by plants (Zeng et al., 2018). Accurate estimation of evapotranspiration is essential for effective water management practices, particularly for agriculture (Jung et al., 2010). Accurate estimation of evapotranspiration enables improved understanding of crop water needs, and it is vital in determining irrigation schedules and optimizing application of water. Additionally, understanding of the component's evapotranspiration can enable analysis whether irrigation practices can be improved and available water supplies can be used more effectively (Passioura & Angus, 2010). Also, differences in evapotranspiration rates arise from differences in water supply and atmospheric evaporative demand (Donohue et al., 2010). The differences bear enormous significance in terms of water availability and contribute to the overall water balance in a region.

While water is being evaporated from the surfaces of rivers, lakes, and soil, it is being carried into the atmosphere (Mendicino & Senatore, 2012). This leads to atmospheric moisture accumulation and the formation of water vapor (Sherwood et.al., 2010). Water vapor is an essential component for cloud and precipitation formation. As evapotranspiration returns a substantial amount of precipitation back to the atmosphere, it is the origin of future precipitation. Therefore, any fluctuation or alteration in the availability and distribution of surface water will directly affect evapotranspiration rates and thereby the overall water resources of an area. For example, when surface water is diminished, either due to drought or overuse, it will de-crease the amount of water available for evapotranspiration. This can lead to lower levels of atmospheric moisture, which affects cloud and precipitation development.

2.5. The Relationship between Anthropogenic Activity and Evapotranspiration

Evapotranspiration plays a vital role in the Earth's water cycle, with drastic consequences for climate and water resources (Lambin et al., 2003; Coe et al., 2009). To affect human activity on evapotranspiration, several steps can be taken. Sustainable land management can slow down the negative impacts of human actions on evapotranspiration. This can include activities such as afforestation, reforestation and conservation of natural vegetation, and these can enhance evapotranspiration rates and encourage healthy Implement water management practices: Proper water management could have a significant role in shaping anthropogenic impact on evapotranspiration(Morid & Bavani, 2008;Liu & Gao, 2018).This can include strategies such as optimizing irrigation to reduce excessive water consumption, implementing water-saving technologies, and promoting efficient use of water in agriculture, industry, and urban sectors. By adopting these measures, we can help mitigate the negative impacts of human activities on evapotranspiration and promote a more sustainable and balanced water cycle.

It is an important part of the hydrological cycle, and its accurate estimation is crucial for hydrological studies. Evapotranspiration rates can be significantly impacted by human activity, such as land use change and dam construction. These activities can alter the availability and distribution of water and thus affect the timing and amount of evapotranspiration in an area. For example, the construction of dams can lead to increased evapotranspiration due to the big water surface areas formed. Similarly, changes in land use patterns can lead to clearance of vegetation or planting of new crops, which alter the evapotranspiration rates (Ekka et al., 2020). This can affect local climatic conditions as well as the general availability of water. Moreover, anthropogenic processes that modify the hydrological characteristics of river landscapes, such as inter-basin water transfer and stream channelization, also influence evapotranspiration. These changes can potentially disrupt the natural flow of water and modify the distribution of moisture within a region, leading to changes in the rates of evapotranspiration (Ekka et al., 2004)

2 .6. The Effect of Climate Change on Evapotranspiration

One of the severe global issues that need to be addressed right away is climate change. One way of slowing down the effect of climate change is through increasing evapotranspiration. Evapotranspiration is the transportation of water from Earth's surface to the atmosphere via plant transpiration and soil evaporation (Novák, 2012). There are different ways through which the function of evapotranspiration in climate change can be controlled:

1. Implementation of water conservation measures: it has the potential to lower the volume of water lost as a result of evapotranspiration and help it be used more effectively for plant development and ecological processes by preventing wastage of water and implementing proper irrigation systems into operation (Liu et al., 2019).

2. Promoting afforestation and reforestation; Trees have a significant function in the regulation of evapotranspiration. They send the water drawn by them from the ground to the atmosphere through transpiration. By increasing wooded cover through afforestation and reforestation activities, we can promote evapotranspiration rates and decrease the amount of water available for applications other than evapotranspiration, i.e., agricultural use or human use (Zou et al., 2019).

3. Use of climate-smart water technologies in agriculture: Those practices like re-source conservation farming, micro-irrigation, and water harvesting have the potential to enhance agricultural water efficiency and lower evapotranspiration rates (Kang et al., 2021)

2.7. Factor Affecting Evapotranspiration

In the hydrological cycle that affects the availability and distribution of water resources is evapotranspiration (Singh et al., 2021). The following variables influence evapotranspiration:

2.7.1. The impact of temperature on evapotranspiration

Temperature plays a major role in evapotranspiration, a key component of the horo-logical cycle that helps to transport water from the land surface to the atmosphere. (Rahayuningsih et al., 2019) This intricate process, where both the evaporation from surfaces like soil, water bodies,

and vegetation and the transpiration from plant cells is greatly influenced by a change in thermal energy. As temperature increases, the intensity of the kinetic energy of water molecules is also intensified, thereby increasing their process of evaporation from liquid to gas (Rahayuningsih et al., 2019).

2.7.2. The impact rainfall on evapotranspiration

It impacts considerably on evapotranspiration (ET) control, which includes water body evaporation and plant transpiration and soil evaporation. Soils' water content directly relates to rainfall-supplied water, which determines the rate at which plants can transpire and the extent of evaporation from the soil surface (Daly & Porporato, 2005). After a rain event, soil moisture tends to increase, providing plants with the water needed for transpiration. Thus, evapotranspiration rates rise, especially in areas of high vegetation or agricultural plantings (Wang et al., 2012). Plant water availability rises as well, not only improving higher transpiration but assisting in the growth of the plant to form an increase in leaf area, enhancing transpiration capacity (Ozdogan et al., 2006). Moreover, enhanced soil moisture increases evaporation from the soil, contributing to the overall rise in evapotranspiration following rain (Brutsaert, 2005).

However, rainfall evapotranspiration relationship is not always linear, Prolonged rainfall may saturate the soil, reducing oxygen content in the root zone, and thereby negatively impact plant performance and limit transpiration despite sufficient water (Tardieu et al., 2015). In such a situation, evaporation is generally the predominant way of soil water loss from the soil surface (Baldocchi, 2008). In addition, the intensity, frequency, and timing of rain showers are major factors that regulate evapotranspiration processes. Intensive, infrequent rain events can cause rapid evaporation, while frequent, light rain showers can yield a regular water input that can support higher transpiration in the long run (Trenberth, 2011). Rain's impact on evapotranspiration also heavily depends on local vegetation and climate. In arid and semi-arid areas, quite low amounts of rainfall may enhance evapotranspiration strongly, but in temperate regions, the effect might be less severe (Dai et al., 2013). In addition, the interception from the canopy in forest areas may create a more complicated relationship in a way that some of the rainfall evaporates directly off the canopy surface before reaching the ground (Herbst et al., 2008). In brief, rainfall is a dominant driver of evapotranspiration, influencing the levels of soil moisture and plant rates of

transpiration, the effects of which vary with the different climates, vegetation, and soils. An understanding of the relationship is essential in the correct modeling and management of the water cycle, particularly in agriculture and water resource planning (Jackson et al., 2000).

2.7.3. The impact of land use land cover on evapotranspiration

Importantly influence evapotranspiration (ET), a critical component of the hydrological cycle and a determinant of local climate conditions. Different vegetation types display varying ET rates due to differences in leaf area index (LAI), rooting depth, and physiological traits. For instance, forests generally have higher ET rates compared to grasslands or agricultural areas because of their greater leaf area and ability to extract moisture from deeper soil layers (Zhang et al., 2016; Weng et al., 2019).

Additional, urban areas characterized by impervious surfaces and reduced vegetation typically exhibit much lower ET rates, which can lead to increased surface runoff and decreased groundwater recharge (Zhou et al., 2018). This alteration in local hydrology may heighten the likelihood of flooding, while urban heat islands can further influence ET dynamics through increased temperatures. Agricultural practices also play a role; land cover conversion from natural ecosystems to agricultural fields can either increase or decrease ET depending on the types of crops cultivated and management practices employed (Irmak et al., 2011). Additionally, the impact of LULC on ET is not static and can vary by season, as changes in land cover can modify soil moisture availability throughout the year (Mu et al., 2013). Overall, understanding the complex relationships between LULC and ET is essential for effective water resource management, climate change adaptation, and sustainable land use planning (Shah et al., 2021).

2.8. Purpose of Land Use Land Cover Information

According to Basudeb (2011) Land use application involves both baseline mapping and subsequent monitoring, since timely information is required to have knowledge on the state of use of current quantity of land and to identify the land use changes time to time. This knowledge helps to developing strategies to balance conservation, conflicting uses, and developmental pressure. Knowledge of land use and land cover is important for many monitoring and evaluate.

The most dangerous shift in land use was found to be the development of agricultural land at the expense of grassland and shrub lands, which resulted in the greatest change in soil erosion inten-

sity. Change detection is valuable in many applications related to land use and land cover (LULC) changes detection including cultivation, urban expansion and landscape changes (Tewabe & Fentahun, 2020). Change detection has emerged as a significant process in managing and monitoring natural resources and urban development mainly due to provision of quantitative analysis of the spatial distribution of the population of interest. There are a lot of available Techniques that serve purpose of detecting and recording differences and might also be attributable to change (Hassan et al., 2016). Remote sensing and GIS offer a powerful tool for LULC changes analysis; however, studies of LULC changes based solely on remote sensing and GIS may not be relevant or dependable for Specific environmental application at local level.

2.9. Land Use Land Cover Mapping

Land cover maps are presently being developed from local to national to global scales. The use of panchromatic, medium-scale aerial photographs to map land use has been an accepted practice since the 1940s. More recently, small-scale aerial photographs and satellite images have been utilized for land use/land cover mapping (Yeshaneh et al.,2013). Land cover Mapping serves as a basic inventory of land resources for all levels of government environmental agencies, and private industry throughout the world Remote sensing techniques are the most practical and cost efficiently system for obtaining a timely regional overview of land cover. Different Land cover classes are typically mapped from digital remotely sensed data through the processes of image classification of development, planning and management activities concerning the surface of the earth (Basudeb. 2004).

2.10. Geographic Information System for Evapotranspiration

A GIS is computer-based tool used to capture, store, query, manage, visualize, question, analyze, and interpret both the locations and attributes of spatial features (geospatial data) to understand relationships, patterns, and trends. GIS technology integrates common database operations such as query and statistical analysis with the unique visualization and geographic analysis benefits offered by maps. These abilities distinguish GIS from other information systems and make it valuable to a wide range of public and private enterprises for explaining events, predicting outcomes, and planning strategies. The role of GIS technology is employed to assist decision-makers by indicating various alternatives in development and conservation planning and by

modeling the potential outcomes of a series of scenarios. Data are collected about the real world and after those data are analyzed, information is compiled for decision-makers. Based on this information, actions are taken and plans implemented in the real world (Daniel et al, 2002). Map making and geographic analysis are not new, but a GIS performs these tasks faster and with more sophistication than manually.

Remote sensing plays a crucial role in estimating and monitoring evapotranspiration (ET) by providing valuable data that can enhance our understanding of hydrological processes over large and often inaccessible areas. The application of remote sensing technology allows researchers and policymakers to obtain spatially and temporally continuous information on land surface temperature, vegetation indices, and soil moisture, which are essential for ET estimation (Anderson et al., 2012). Several remote sensing-based methods, including the Surface Energy Balance Algorithm for Land (SEBAL) and the Moderate Resolution Imaging Spectroradiometer (MODIS) ET product, have been developed to estimate ET across various landscapes. These methods utilize satellite imagery to calculate energy balance components and derive ET from the energy available for evaporation and plant transpiration (Bastiaanssen et al., 1998; Mu et al., 2011).

2.11. The Role of Remote Sensing for Evapotranspiration

It is especially advantageous in areas where ground-based measurements are sparse or difficult to obtain, such as in Ethiopia's diverse and rugged terrain. It facilitates the monitoring of changes in ET over time, allowing for better assessments of water availability, and agricultural productivity (Gao et al., 2019; Sinha et al., 2019). Integrating remote sensing data with geographic information systems (GIS) and hydrological models significantly improves the accuracy of ET computation and water resource management (Franchini et al., 2018). As climate change continues to impact hydrological cycles, the role of remote sensing in ensuring sustainable water resource management is increasingly becoming vital, particularly in developing countries like Ethiopia, where agricultural productivity is heavily dependent on water resources (Mastrorillo et al., 2016)

2.12. Estimating Evapotranspiration

Estimating evapotranspiration, the process of water loss from the earth's surface due to evaporation and plant transpiration is crucial for various applications such as agricultural water man-

agement, hydrological modeling, and climate studies (Irmak & Kukal, 2022) Several models are commonly used to estimate evapotranspiration. These models include the Penman-Monteith equation, the Blaney-Criddle method, the Priestley-Taylor equation, and the Hargreaves equation, among others (Yeh, 2017). These models take into account various climatic variables such as temperature, humidity, wind speed, solar radiation, and vegetation characteristics to estimate evapotranspiration rates accurately. Additionally, advanced numerical models, such as the Soil Water Atmosphere Plant model or the Surface Energy Balance System for Land, incorporate more complex processes and factors to provide more detailed estimations of evapotranspiration. Some other sources that can be used for further information on evapotranspiration models include: - The Food and Agriculture Organization of the United Nations, which provides guidelines and methodologies for estimating evapotranspiration using different models. The American Society of Civil Engineers, which offers resources and publications related to evapotranspiration modeling.

Estimating evapotranspiration (ET) using remote sensing techniques is a topic of extensive research, and various classification methods have been proposed. Here, we discuss some important aspects of different classifications of ET estimation methods. The choice of remote sensing data sources is crucial. Different satellites, such as MODIS, Landsat, and Sentinel, provide data at various spatial and temporal resolutions, and the selection depends on the specific research or application needs (Zhang et al., 2018). Evapotranspiration, or ET, is an essential hydrological cycle activity that is also important for land climate monitoring and agricultural practice optimization. For effective water resource management, irrigation scheduling, and comprehension of the energy-water-food nexus, accurate ET estimate is crucial (Ahmad et al., 2017; Hamad Bin Khalifa University, 2021). Numerous techniques, such as radiation- and temperature-based methods, have been devised to measure ET.

2.12.1. Surface Energy Balance Algorithm for Land

It is developed by Bastiaanssen et al. (1998), has emerged as a prominent remote sensing method for accurately estimating ET by utilizing satellite data to analyze surface energy components. SEBAL operates on the concept that the available energy at the land surface can be partitioned into different components, specifically sensible heat, latent heat, and ground heat flux. Gao et al.

(2019) emphasize SEBAL's capability to provide spatially distributed ET estimates, allowing researchers and practitioners to understand the complexities of water use in diverse agricultural landscapes.

One of SEBAL essential applications is in agricultural water management, where it aids in assessing crop water consumption and optimizing irrigation practices. Allen et al. (2020) illustrate how SEBAL can support precise irrigation scheduling by comparing the water use patterns across various crops, effectively identifying areas requiring supplemental irrigation. Additionally, SEBAL's ability to monitor changes in ET over time positions it as an effective tool for drought assessment. According to Zhang et al. (2020), SEBAL can capture variations in ET linked to drought conditions, thereby providing essential data for timely agricultural interventions and resource management. Furthermore, researchers like Bastiaanssen et al. (2019) have employed SEBAL to explore the effects of climate variability on water resources, helping stakeholders develop informed regional water management strategies.

2.12.2. Preceding studies made on evapotranspiration by using combined Penman-Monteith and Hargreaves Methods

Potential evapotranspiration (PET) has been estimated using temperature-based techniques, such as the Hargreaves approach (Liu, 2022). These techniques are quite easy to use and rely on temperature data as the primary input parameter. Nonetheless, research indicates that radiation-based techniques, including the Jensen-Haise and Hargreaves approaches, outperform temperature-based techniques in PET estimation (Ahmad et al., 2017). Radiation-based techniques provide a more thorough estimate of ET by accounting for solar radiation and other atmospheric variables.

For instance, a study carried out in the Rogerm Basin examined several PET estimating techniques and discovered that the radiation-based Hargreaves approach was superior for PET calculation (Hamad Bin Khalifa University, 2021). When it comes to capturing the variability of ET, the Hargreaves technique performed better than temperature-based methods, which makes it a good option for areas with little access to meteorological data. To maximize the energy, water, and food nexus, precise ET calculation is also essential in addition to PET estimation (Hamad Bin Khalifa University, 2021). As an alternative to data-rich models, models based on remote sensing have been put out to estimate ET (Srivastava et al., 2016). In areas where data is poor,

these models use satellite data to predict ET, giving useful information for managing water resources (Hamad Bin Khalifa University, 2021). A more thorough knowledge of water consumption patterns is made possible by the ability of remote sensing-based models to incorporate both temporal and geographical fluctuations in ET.

However, the research region and the accessibility of meteorological data may have an impact on how accurate remote sensing-based models are (Srivastava et al., 2016). For these models to produce accurate findings, ground-based validation and calibration are frequently necessary. In addition, the particular research region and the required degree of precision should be taken into account when choosing suitable remote sensing-based models.

To determine their performance, several ET estimate techniques have been examined in a number of researches. In their evaluation of six PET techniques, Lu et al., (2011) discovered that, in comparison to other models, the Thornthwaite approach fared the poorest. In some climate situations, the Thornthwaite technique overestimates ET. Comparing several PET models, Li et al. (2021) discovered that the Shuttle worth-Wallace model had the most association with the FAO Penman-Monteith technique. ET estimate accuracy was higher for the Shuttleworth-Wallace model, a more intricate model with more variables.

In recent years, machine learning algorithms have been applied to improve ET estimation. These algorithms use historical data and other environmental variables to develop models that can accurately estimate ET (Srivastava et al., 2016). For example, neural network models have been used to estimate ET based on meteorological and satellite data (Adamala et al., 2014). These models have shown promising results in capturing the complex relationships between environmental variables and ET.

Furthermore, the use of ensemble models, which combine multiple ET estimation methods, has gained attention in recent years. Ensemble models can provide more robust and accurate ET estimates by leveraging the strengths of different methods and reducing uncertainties (Ngongondo et al., 2013). For example, a study conducted in southern Malawi compared the performance of the FAO Penman-Monteith, Priestley-Taylor, and Hargreaves methods individually and in an

ensemble model. The results showed that the ensemble model outperformed the individual methods, providing more accurate ET estimates.

2.12.3. Preceding Studies Made on Evapotranspiration by Hargreaves Samini Method

Investigators have made more progress in the last decade in enhancing the application and accuracy of the Hargreaves technique for evapotranspiration (ET) estimation. These developments include the creation of regional calibration techniques, the incorporation of data from remote sensing, and the assessment of the effects of climate change on ET estimate.

To further enhance the Hargreaves method's effectiveness by taking into consideration regional differences in vegetation and climate, regional calibration techniques have been put forward. For instance, in the Chinese Yellow River Basin, Wang, & Zhang (2017) carried out a regional calibration of the Hargreaves approach. Their research showed that, in comparison to the original Hargreaves equation, region-specific calibration factors increased the accuracy of ET estimate.
The integration of remote sensing data, such as satellite-derived vegetation indices, has also been explored to refine the Hargreaves method. Huang, & Su (2018) incorporated the Normalized Difference Vegetation Index (NDVI) into the Hargreaves equation to consider the vegetation effect on ET. Their study showed that the NDVI-based Hargreaves method provided more accurate ET estimates, especially in areas with significant vegetation cover. Furthermore, utilizing the Hargreaves technique, researchers have looked at how climate change affects ET estimation. According to Moradkhani &Hsu (2018) assessed the Hargreaves method's effectiveness in the US under several climate change scenarios. In order to ensure accurate ET calculation in a changing environment, their work demonstrated the necessity of modifying the Hargreaves coefficients to account for variations in temperature and precipitation patterns.

Apart from these developments, a number of researches have concentrated on validating and contrasting the Hargreaves technique with alternative ways for estimating ET. For example, according to Kisi &Shiri (2019) examined how well the Penman-Monteith approach and the Hargreaves method performed in various climatic zones. According to their research, the Hargreaves technique produced accurate estimations of ET, especially in areas with a lack of data availability.

Overall, these advancements in the Hargreaves method have contributed to improving the accuracy and applicability of ET estimation. Regional calibration approaches, the integration of remote sensing data, and the consideration of climate change impacts have enhanced the performance of the Hargreaves method in various climatic regions. Future research should continue to explore these advancements and further refine the Hargreaves method to ensure reliable and accurate ET estimation in different contexts.

2.12.4. Priestley and Taylor Method Explanation

The Priestley and Taylor Method, also known as the Penman-Monteith equation, is a widely-used method for estimating evapotranspiration rates. It takes into account various meteorological factors such as radiation, air temperature, humidity, and wind speed to calculate the evapotranspiration rate from area reference surface (Cordova et al., 2015). This method is considered the standard for calculating reference evapotranspiration and is recommended by the Food and Agriculture Organization.

2.12.5. Blaney-Criddle Method of Evapotranspiration Determination Explanation

The Blaney-Criddle method is a widely-used approach for estimating potential evapotranspiration, which is a key parameter in various water resource management applications such as irrigation scheduling and water balance calculations (Zhan & Lin Shelp, 2009). This method relies on standard meteorological data, such as temperature and precipitation, to estimate the amount of water that could potentially evaporate from a given landscape or crop. The method takes into account the climatic conditions of the specific region to provide a more accurate estimation (Xu & Singh, 2001).

2.13. Conceptual Framework

The conceptual framework illustrates the interplay between Temperature and Rainfall, which serve as key environmental components influencing Evapotranspiration, a dependent variable that is affected by these climatic factors. Evapotranspiration further correlates with various land cover types, which include Water Bodies, Forest, Shrubland, Agricultural Areas, and Built-up Areas. The changes in evapotranspiration rates, driven by fluctuations in temperature and rain-

fall, subsequently impact the distribution and health of these land cover types. Each land cover type interacts distinctly with evapotranspiration, reflecting its unique ecological characteristics and contributions to the overall ecosystem dynamics. The framework emphasizes that while Evapotranspiration is dependent on the independent variables of temperature and rainfall, the resultant land cover types play a critical role in shaping the ecological landscape of the area.

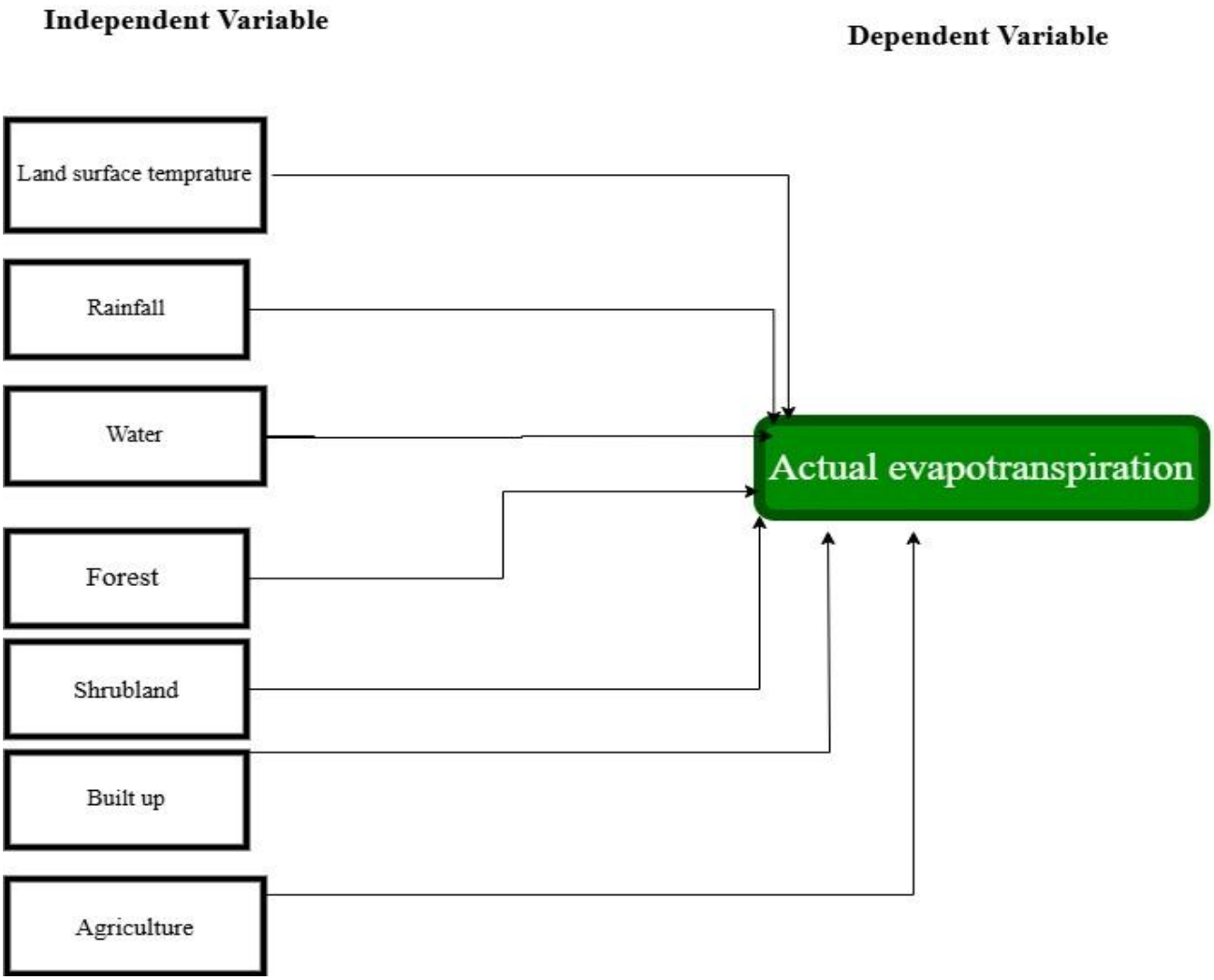

Figure 2 Conceptual framework of the study

CHAPTER THREE

3. MATERIAL AND RESEARCH METHOD

3.1. Description of the Study Area

3.1.1 Location

The research was conducted in the vicinity of the Grand Ethiopian Renaissance Dam (GERD), located near the Ethiopia Sudan border, approximately 620 kilometers northwest of Addis Ababa. The main dam is situated about 14 kilometers from the border with Sudan, while the saddle dam lies even closer, at a distance of approximately 3.3 to 3.5 kilometers from the border. Geographically, the study area extends between 10°00′00″ N to 11°00′00″ N latitude and 35°00′00″ E to 36°00′00″ E longitude. The GERD itself spans roughly 2,572 meters in length and 483 meters in height. The total study area covers approximately 1,409,397.44 hectares, encompassing the GERD project and its surrounding environment. Hydrologically, the area falls within the Blue Nile (Abay) Basin and includes parts of four major sub-basins: the Lower Abay Sub-basin, which contains the GERD site and the main course of the Blue Nile River; the Didessa Sub-basin; the Dabus Sub-basin; and the Beles Sub-basin. These sub-basins represent the key hydrological zones influencing the water resources and catchment dynamics of the GERD area.

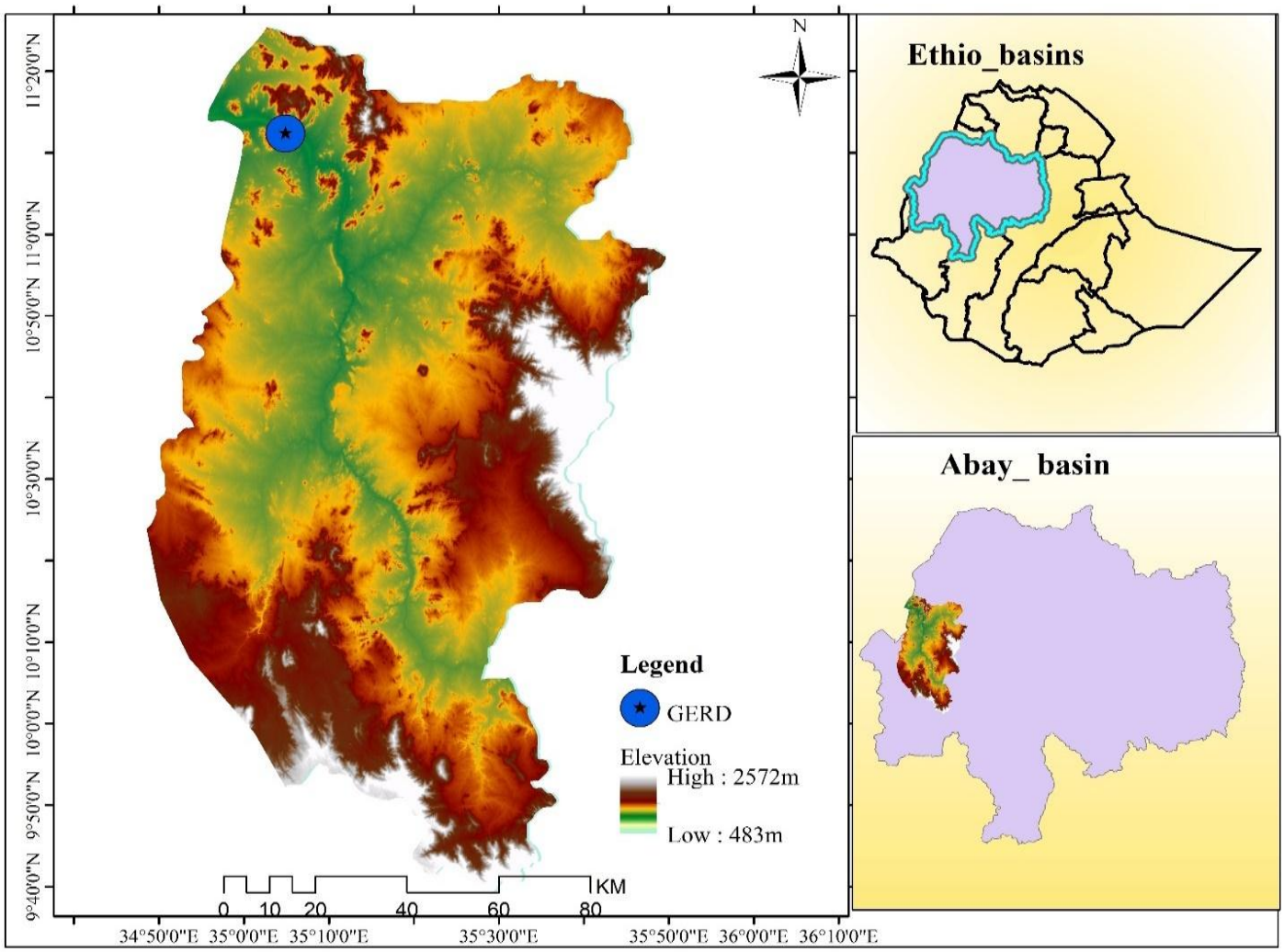

Figure 3 Study area

3.1.2 Land use land cover

The area surrounding the Grand Ethiopian Renaissance Dam (GERD) discover a diverse landscape characterized by various land cover types. Among those 24.5% are covered by forests, highlighting the ecological importance of these areas in terms of biodiversity and carbon sequestration. Water bodies account for 10% of the region, providing essential resources for irrigation and local communities. Shrub land, covers about 46%, the remaining land built-up areas and Agriculture, with built-up areas occupying around hectares (3.65%) and Agriculture extending over (15.3%) (Figure3).

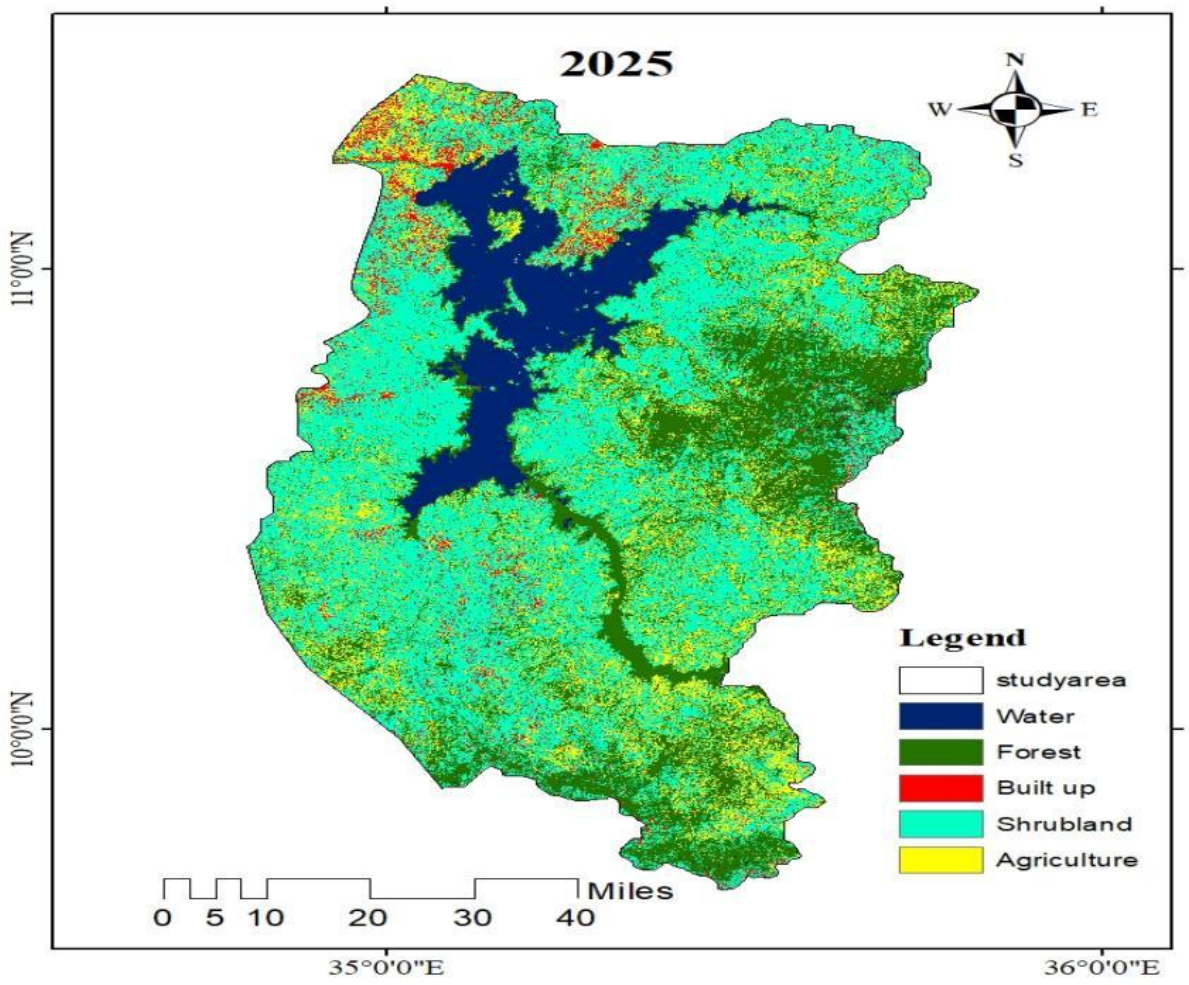

Figure 4 LULC map the study area

(Source: Aouther,2025)

3.1.3. Climate

The annual average precipitation in the GERD and its vicinity is typically around 970.4 mm, and the average annual temperature is approximately 30°C. The highest monthly precipitation was recorded in May, June, July and August. The highest monthly temperature was recorded in January, February, March, and April. The figure below (Figure 5) data the average monthly precipitation and temperature of the study area.

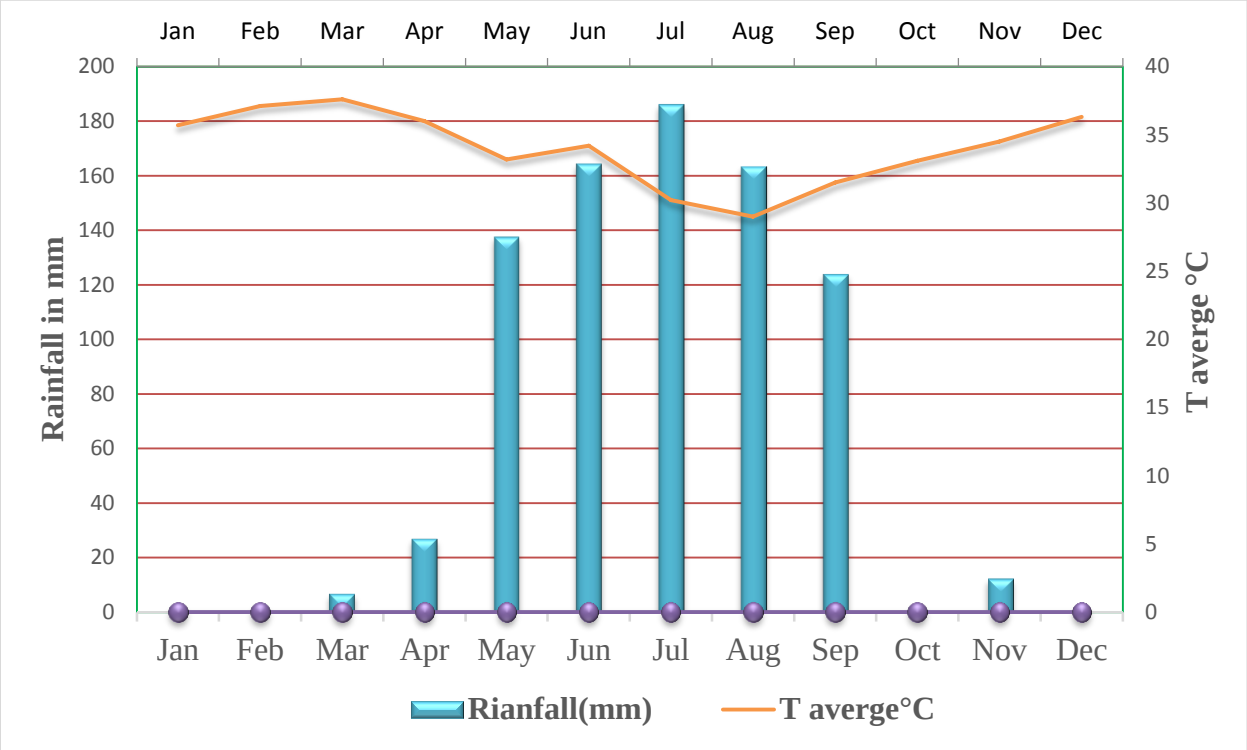

Figure 5 Annual average precipitation and average temperature from 2001 to 2023

Source: National meteorological agency

3.1.4. Drainage pattern

The Grand Ethiopian Renaissance Dam (GERD) and its surrounding drainage system demonstrate a complex network of flow directions, with streams traversing the region in diverse patterns (figure 2). This complex hydraulic system plays a crucial role in shaping the hydrological dynamics of the area. The GERD, positioned on the Blue Nile River in Ethiopia, has the potential to influence the flow patterns of rivers and streams within its vicinity (Figure 2)

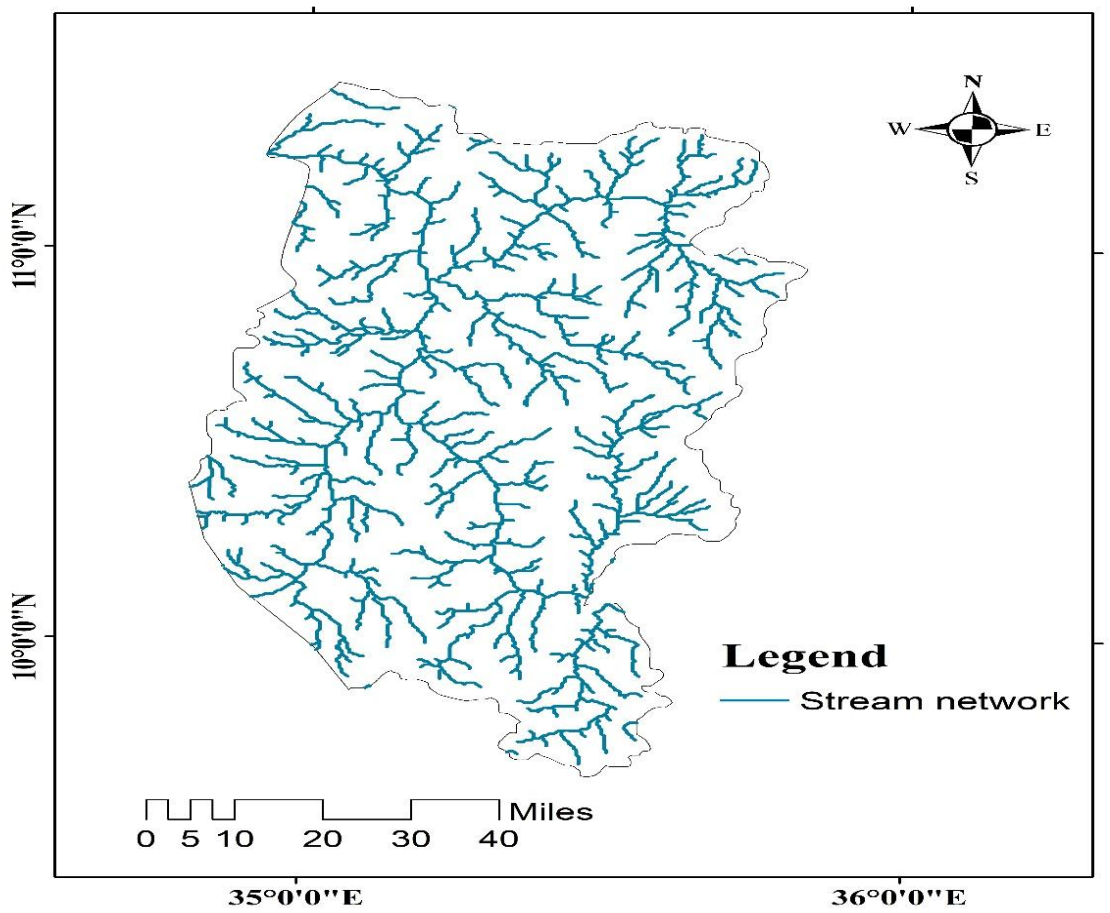

Figure 6 Drainage pattern (source: hydro shade)

3.1.5. Soil

The main soil types within the dataset for the study area encompassing the Grand Ethiopian Renaissance Dam (GERD) and its surroundings were identified Calcic Xerosols and Leptosols are also recognized as prevalent soil types in the region. highlighted the diverse soil composition found in the study area (Figure 5). This analysis forms the basis for understanding the soil characteristics of the region, providing valuable insights for land management strategies, agricultural practices, and environmental conservation efforts surrounding the GERD.

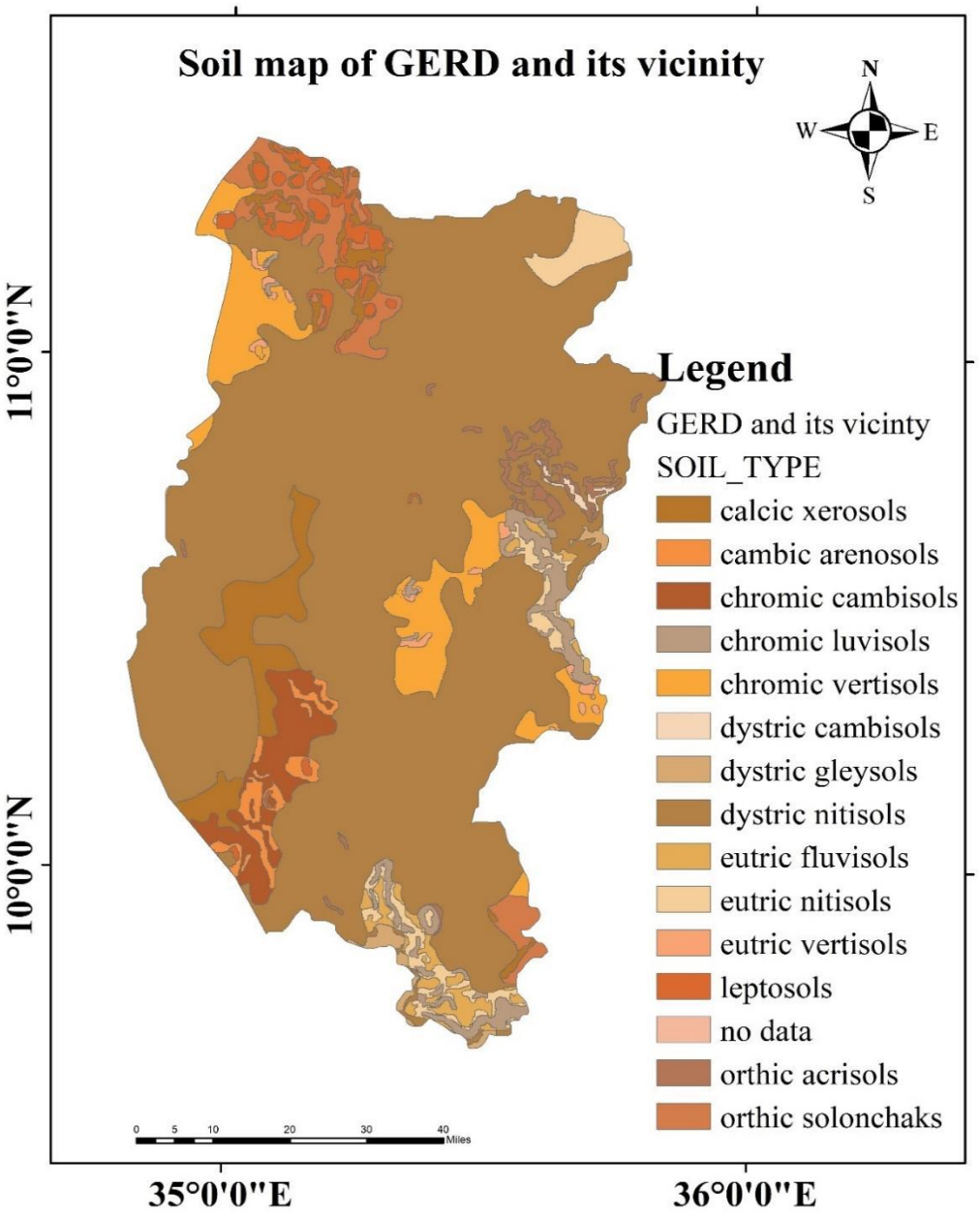

Figure 7 Soil map of the Study area

(Source: FAO)

3.1.6. Slope

According to the FAO slope classification, slopes are categorized based on their degree of steepness as follows: flat to very gentle slopes range from 0 to 2 degrees, indicating nearly level ter-

rain; gentle slopes fall between 2 and 5 degrees, showing a slight incline; sloping terrain is defined by slopes from 5 to 10 degrees, where the incline becomes more noticeable; moderately sloping land ranges from 10 to 15 degrees, representing a moderate incline; strongly sloping areas have slopes between 15 and 30 degrees, indicating steep terrain; and steep slopes are those greater than 30 degrees, characterized by very steep or rugged landforms. This classification provides a standardized framework for describing land surface gradients, which is essential for soil description, land use planning, and understanding erosion potential, as detailed in FAO guidelines on soil and landform.

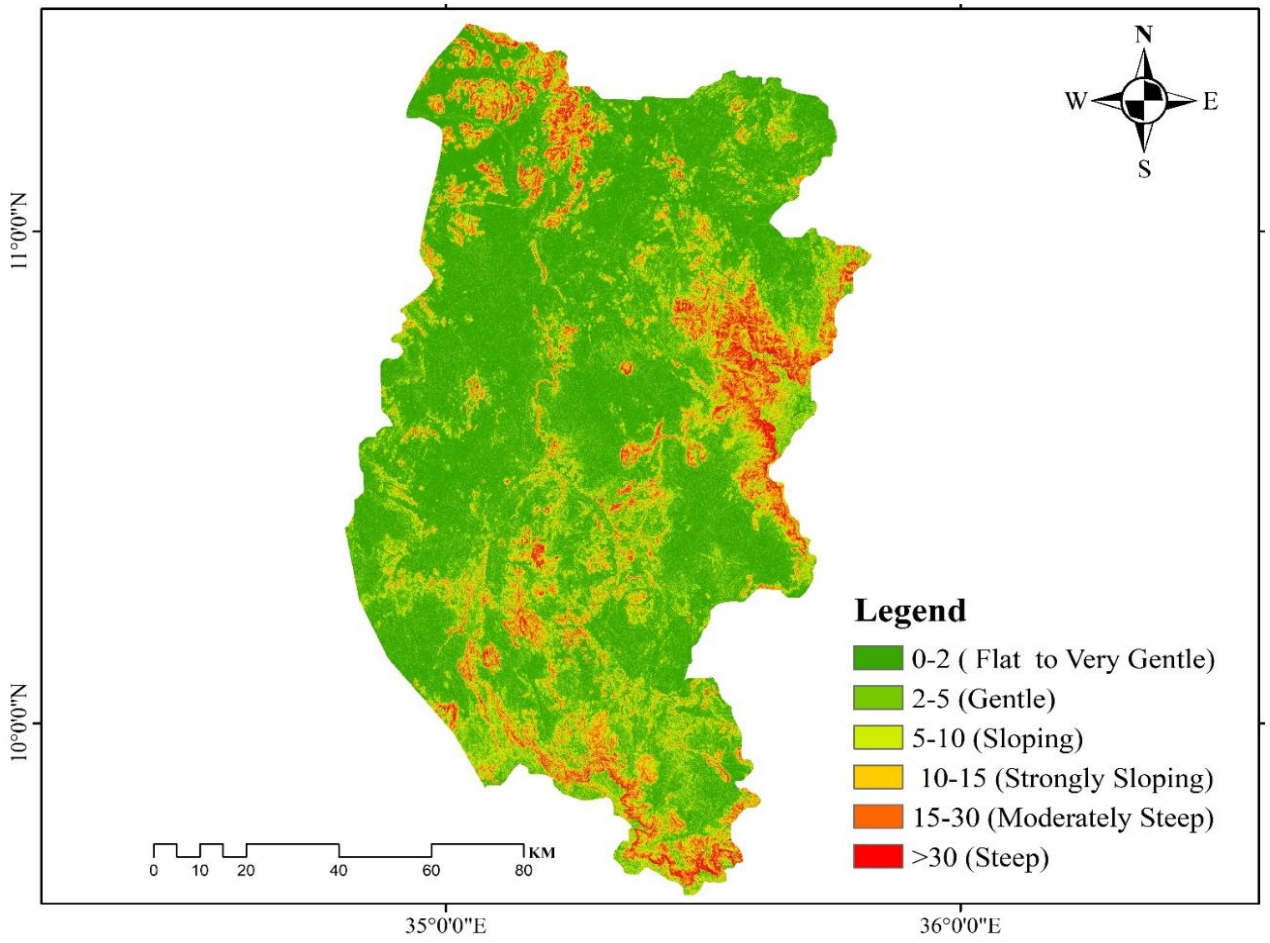

Figure 8 Slope of the study area (Source: Aouther,2025)

3.1.7. Agro _ecological zone

The Grand Ethiopian Renaissance Dam (GERD) and its surrounding area are characterized by distinct elevation zones that influence the local climate, hydrology, and land use. According to common Ethiopian agro-ecological classifications, the region can be divided into three main elevation belts: the Kolla (lowland) zone ranging from approximately 500 to 1500 meters above sea level, the Woina Dega (midland) zone from 1500 to 2300 meters, and the Dega (highland) zone from 2300 to 3200 meters. The GERD reservoir itself is situated primarily within the Kolla and lower Woina Dega zones, with reservoir water levels reaching around 640 meters elevation at full supply level, which places much of the dam and immediate vicinity in the lowland Kolla zone (Ministry of Water and Energy Ethiopia, 2023; Hydropower.org, 2023).

These elevation zones correspond to significant climatic and ecological differences: the Kolla zone is typically warmer and drier, the Woina Dega zone has moderate temperatures and rainfall, and the Dega zone is cooler with higher precipitation. The presence of the GERD reservoir in the Kolla and Woina Dega belts thus influences local microclimates by increasing humidity and altering evapotranspiration patterns in these elevation ranges. This elevational context is critical for understanding the hydrological impacts of the dam on surrounding ecosystems and agricultural practices, as well as for planning water resource management in the Nile Basin (EEP, 2024; Vajiram & Ravi, 2023).

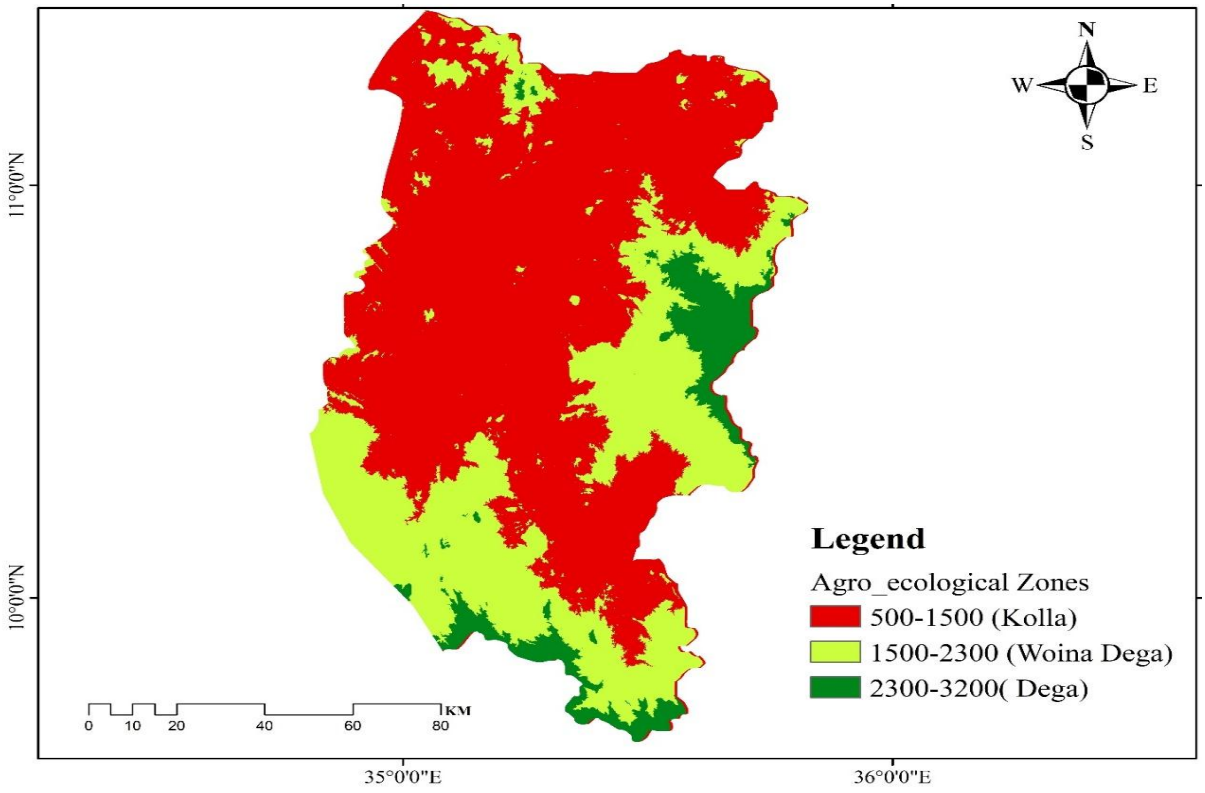

Figure 9 Agroecological of the study area (Source: Aouther,2025)

3.2. Methodology

3.2.1. Research design and approach

This research employs a quantitative research approach within an explanatory design framework to comprehensively address its objectives regarding land use/land cover (LULC) changes, climate variability, and evapotranspiration in the study area. By prioritizing quantitative data collection and analysis, the study aims to systematically identify patterns, relationships, and cause-and-effect linkages among these variables

3.2.2. Sampling technique

The researchers organized the land into different categories or groups based on land use and cover types of LULC such as forests, bulitup, agriculture, water and shrubland. To accurately study these diverse areas, they randomly selected specific fields within each category. This approach helps ensure that the sample accurately reflects the variety and characteristics of the entire land

area, reducing the risk of bias and making the findings more reliable and representative of the overall landscape.

3.2.3. Types and sources of data

To achieve the study's objectives, both primary and secondary data sources were utilized. Primary data were collected through remote sensing image and metrological station data, while secondary data were sourced from, of published and unpublished materials, including books, journals, articles, and websites.

3.2.5. Meteorological data

Meteorological data, specifically maximum and minimum temperatures, were collected for the study area., Which is crucial for determining the heat energy available to drive the evapotranspiration processes.

Table 1 Meteorological station

Station name	Record length	Class	Lat	Long	Elevation
Assosa station	1957	Class1	10.0634° N	34.5° E	1,570m
Sherkole gizen	2000	Class2	10°41'33"N	34°47'20"E	729 m

Source: National meteorology

3.2.6. Remote sensing data

3.2.6.1. Landsat image

Landsat 7 and Landsat 8 are Earth-observing satellites that capture detailed images of the land surface across different parts of the light spectrum, including visible, infrared, and thermal wavelengths. Launched in 1999 and 2013 respectively, these satellites provide high-resolution data typically at 30 meters per pixel that allow scientists to analyze various land surface parameters (Irons et al., 2012). Landsat 7, equipped with the Enhanced Thematic Mapper Plus (ETM+), offers valuable information for assessing land cover, vegetation health, and surface temperature, although its thermal infrared band has slightly lower resolution (Chander et al., 2009). Landsat 8, with its more advanced sensors the Operational Land Imager (OLI) and Thermal Infrared Sensor (TIRS) delivers improved image quality, higher radiometric resolution, and additional spectral bands, including two thermal bands that enable more precise measurements of land surface tem-

perature (Roy et al., 2014). This detailed information is crucial for estimating evapotranspiration (ET), as it provides key inputs such as surface temperature, vegetation vigor, and land cover type. By analyzing these parameters, scientists can better understand how much water is evaporating from the land and transpiring through plants (McVicar et al., 2012). The enhancements in Landsat 8 make it particularly valuable for monitoring environmental changes and supporting water resource management through more accurate ET modeling. Landsat images, in general, are multispectral aerial photographs that serve as a vital resource for land use planning, environmental monitoring, and resource management. They capture reflectance across multiple spectral bands, enabling the identification of different land cover types and dynamic environmental processes over time, and their long-term, consistent record makes them particularly useful for detecting change and assessing land degradation (Wulder et al., 2012; Roy et al., 2014).

3.2.6.2. Moderate Resolution Imaging Spectroradiometer data

These datasets provide estimates of frictional velocity, which is a key parameter in surface energy flux calculations. Using frictional velocity as a proxy, the model can effectively account for wind influences on evapotranspiration, particularly in regions where ground-based measurements are scarce. This approach ensures that the wind component's effect on the energy balance is incorporated indirectly, enhancing the accuracy of ET estimations within the SEBAL framework (Su et al., 2015).

3.6.2.3. Climate Hazards Group InfraRed Precipitation with Station data

While CHIRPS (Climate Hazards Group InfraRed Precipitation with Station data) is widely used for high-resolution rainfall monitoring at approximately 5 km spatial resolution, there are other datasets capable of providing rainfall estimates at 1 km resolution. For instance, the GPM IMERG (Global Precipitation Measurement Integrated Multi-Satellite Retrievals) product offers precipitation estimates at a near 1 km resolution, providing finer spatial detail suitable for localized studies. These higher-resolution datasets are particularly valuable for detailed hydrological, agricultural, and climate analyses during rainy seasons such as the fall, where localized precipitation patterns are critical. GPM IMERG, in particular, combines satellite microwave and infrared observations with ground-based data to produce daily and half-hourly rainfall estimates at approximately 0.1 to 1 km resolution, making it an excellent choice for regional- and local-scale precipitation monitoring (Huffman et al., 2019).

CHIRPS (Climate Hazards Group InfraRed Precipitation with Station data) is a high-resolution satellite-based rainfall dataset that integrates infrared satellite imagery with in-situ station data to monitor and analyze precipitation patterns globally. Its temporal coverage, spanning several decades, coupled with its high spatial resolution (~5 km), makes it an invaluable tool for investigating climate variability over various timescales. CHIRPS is particularly effective in detecting anomalies and trends in precipitation associated with climate phenomena such as El Niño, La Niña, and regional droughts or floods. By providing accurate and consistent rainfall data, CHIRPS enables researchers to assess the impacts of climate variability on water resources, agriculture, and ecosystems, especially in regions where ground-based measurements are sparse or unreliable. Its long-term record facilitates climate trend analysis and enhances understanding of how precipitation patterns are changing in response to global climate change (Funk et al., 2015)

Table 2 Satellite imagery

Input Parameter	**Description**	**Source / Notes**
Satellite Image Bands	Multispectral bands (visible, NIR, SWIR) and thermal infrared bands	Landsat TM/ETM+ bands 1-5,7 (30m), band 6 thermal (60m/120m); Landsat 8 OLI/TIRS bands
Surface Reflectance (ρλ)	Reflectance in individual spectral bands	Derived from satellite DN after radiometric calibration and atmospheric correction
Surface Albedo (α)	Fraction of incoming shortwave radiation reflected by surface	Calculated from weighted sum of reflectance bands (visible + NIR + SWIR)
Normalized Difference Vegetation Index (NDVI)	Indicator of vegetation amount and condition	Computed as (ρ4 - ρ3) / (ρ4 + ρ3) from NIR and red bands
Land Surface Temperature (Ts or LST)	Surface temperature from thermal infrared band	From thermal bands of Landsat
Incoming Shortwave Radiation (RS↓)	Solar radiation reaching the surface (W/m^2)	From landsat 7 and landsat 8
Outgoing Longwave Radi-	Thermal radiation emitted by	Calculated using Stefan-Boltzmann law

ation (RL↑)	surface (W/m²)	with Ts and surface emissivity
Incoming Longwave Radiation (RL↓)	Atmospheric longwave radiation reaching surface (W/m²)	From landsat 7 and landsat 8
Surface Emissivity (ε_0)	Efficiency of surface in emitting thermal radiation	Estimated from vegetation indices
Soil Heat Flux (G)	Heat flux into soil	Estimated as fraction of net radiation (Rn), typically $G = \gamma \times Rn$, with $\gamma \sim 0.1–0.2$ depending on vegetation cover
Net Radiation (Rn)	Net available radiation at surface (W/m²)	Calculated as $Rn = (1 - \alpha) \times RS\downarrow + RL\downarrow - RL\uparrow - (1 - \varepsilon_0) \times RL\downarrow$
Air Temperature (Ta)	Near-surface air temperature (K)	From meteorological stations
Wind Speed (U)	Near-surface wind speed (m/s)	From MOD13Q1
Air Density (ρ)	Density of air (kg/m³)	Calculated from air pressure and temperature
Specific Heat of Air (Cp)	Heat capacity of air at constant pressure (~1005 J/kg·K)	Constant
Aerodynamic Roughness Length (z_0)	Characterizes surface roughness affecting momentum transfer	Derived from vegetation parameters
Zero-plane Displacement Height (d)	Height at which wind speed theoretically drops to zero due to vegetation canopy	Estimated as fraction (~2/3) of vegetation height
Psychrometric Constant (γ)	Relates partial pressure of water vapor to temperature	Calculated from atmospheric pressure and temperature
Satellite Overpass Time and Sun Elevation Angle (β)	Needed for solar geometry calculations	From satellite metadata (header files)

Land Use / Land Cover (LULC)	Classification of surface types (Forest, Agriculture, water, Shrubland, and Built up.)	Derived from multispectral bands using classification algorithms

The researcher selected time intervals 2001, 2012, and 2023 allowed for a comprehensive analysis of land use land cover dynamics over 11-year gaps, a period deemed appropriate given the gradual nature of changes in hydrological processes. The researcher initially selected 2001 as the baseline year for the study to evaluate evapotranspiration conditions before the dam's construction, which began in 2012. This baseline data was crucial for understanding the impacts of the dam on evapotranspiration dynamics. To analyze the changes over time, the year 2023 was later chosen to assess current conditions, providing a comprehensive view of the long-term effects on evapotranspiration resulting from the dam's construction.

3.2.7. Image per-processing

The satellite images were prepared for analysis by undergone The Landsat time series data used in this study have undergone several pre-processing steps, including cloud-masking, georeferencing, resampled, and clipping to the study area boundary, all performed within the Google Earth Engine platform (https://earthengine.google.com/). The satellite images were further prepared for analysis by undergoing radiometric corrections, such as atmospheric correction and cloud masking, to improve their quality and enhance the images for better interpretation. Image enhancement refers to the process of improving the quality and interpretability of remote sensing images captured by satellites, aircraft, drones, or other platforms (Lillesand et al., 2015).

Additionally, MODIS data was resampled to the appropriate spatial resolution using bilinear interpolation to serve as input for the SEBAL model, enabling the estimation of wind speed indirectly. The panchromatic bands were also resampled within Google Earth Engine using bilinear interpolation to ensure consistency in spatial resolution and improve the accuracy of the analysis. Bilinear resampling was chosen because it provides a good balance between preserving data quality and enhancing the spatial detail, especially when working with continuous data like MODIS and panchromatic bands.

3.2.8. Software used

Multiple software tools were employed to analyze the study area, each serving a specific function to ensure accurate results. All pre-processing, classification, and analysis of the Land Use/Land Cover (LULC) information were performed on the Google Earth Engine (GEE) platform, which facilitated the processing of multispectral imagery and provided a robust environment for the extraction of LULC data. Evapotranspiration calculations, including Actual Evapotranspiration (AET), were also conducted within GEE, enabling the modeling of water loss through evaporation and plant transpiration. Excel was used to generate graphs. ArcGIS 10.8.2 was employed for the display and visualization of maps, enabling effective spatial analysis and presentation of results. In addition, R software was utilized for Random Forest regression, a machine learning technique used to model relationships and make predictions based on the study's environmental data, including temperature, rainfall, and AET. This approach is particularly useful for handling large datasets and complex patterns, ensuring robust and accurate results in the analysis. Furthermore, the Mann-Kendall trend test was applied to detect significant trends in temperature and rainfall data, providing insights into temporal changes in these variables. The Random Forest regression model was used to explore and predict relationships between temperature, rainfall, and AET.

3.3. Data Analysis Techniques

3.3.1 Computing of evapotranspiration

To calculate actual evapotranspiration this study was used b surface energy balance algorithm for land.

3.3.1.1. Surface energy balance algorithm for land

Evapotranspiration (ET) using remote sensing techniques is a topic of extensive research, and various classification methods have been proposed. The choice of remote sensing data sources is crucial. Different satellites, such as MODIS, Landsat, and Sentinel, provide data at various spatial and temporal resolutions, and the selection depends on the specific research or application needs (Zhang et al., 2018). Energy balance methods are widely used in remote sensing-based ET estimation. These methods leverage remote sensing data to estimate energy components like net

radiation, sensible heat flux, and latent heat flux (Bastiaanssen, 2000). Surface Energy Balance Models consider the energy balance at the Earth's surface, accounting for heat fluxes, heat storage, and changes in surface temperature. They often rely on remote sensing data, such as land surface temperature and vegetation characteristics (Allen et al., 2007).

Among these energy balance methods in this research, the SEBAL algorithm-based model was applied for the dynamics of actual evapotranspiration over the study region. SEBAL utilizes digital images produced by sensors such as Landsat that can capture radiation throughout the visible, near-infrared, and thermal infrared bands. Developed by Bastiaanssen et al. (1998), the SEBAL model has become a valuable tool in various fields, such as agriculture, hydrology, and environmental studies. It operates on the basic principle of energy balance at the land surface. SEBAL model is the most widely used algorithm for estimating ET throughout the world that involves application for and water resources management and water balances

The SEBAL model offers precise information that can be determined remotely over a large spatial scale and aggregated across time and space, making it practically relevant in the absence of ground data and beneficial for research pertaining to irrigation water use. It is easy to utilize and may find widespread application in diverse habitats and climates. For this reason, the SEBAL model is a helpful tool for studies pertaining to hydrology.

$$\mathrm{ETa} = \mathrm{Rn} - \mathrm{G} - \mathrm{H} \quad (1)$$

$$\mathrm{Rn} = (1-\alpha) \cdot \mathrm{Rshort} - \mathrm{Rlong} \quad (2)$$

$$\mathrm{H} = \rho \cdot \mathrm{Cp} \cdot (\mathrm{Ts} - \mathrm{Ta}) \cdot \mathrm{u} \quad (3)$$

$$\mathrm{G} = \gamma \cdot \mathrm{LST4} \quad (4)$$

Where're: Net radiation: soil heat flux ;Sensible heat flux; *a*: Albedo, which is a measure of reflectivity of the surface ;R short: Incoming shortwave radiation long: Outgoing long wave radiation ; ρ: Air density ;Cp: Specific heat of air (approximately 1005 J/(kg•K)) ; Ts: Surface temperature ;Ta: Air temperature ; U: Wind Speedle\gamma$\gamma$: A coefficient (often taken as a fraction of net radiation, typically around 0.1 or 0.2, depending on vegetation cover);LST: Land Surface Temperature .

3.3.2. Computing of Climate Variability

3.3.2.1. Mann-Kendall test

The trend analysis for rainfall and temperature from 2001 to 2023 was conducted using the Mann-Kendall test statistic (S) alongside Sen's slope (Q). The Mann-Kendall test, introduced by Mann in 1945, is a widely used nonparametric statistical method for analyzing trends in environmental time series data (Frimpong et al., 2022; Nkiaka et al., 2017a). This test offers two main advantages: it does not require the data to follow a normal distribution, and it is robust against abrupt changes in inhomogeneous time series. To estimate the trend's magnitude, Sen's estimator a nonparametric method introduced by Sen in 1968 and referenced by Mustapha (2013) and Nkiaka et al. (2017b) is applied. This method calculates the slope of the trend and indicating annual changes A positive value for Sen's slope indicates an increasing trend in the time series, whereas a negative value signifies a decreasing trend. Two types of statistics depend upon the number of data values i.e.; S is the statistics used if several data values are less than 10 while Z is the statistics (normal approximation/distribution) for data values greater than or equal to 10. S is calculated based on total signs (it is always between −1, 0, and 1). In cases in which N > 10, the standard Z is calculated as follows:

$$S = \sum_{i=1}^{n-1} \sum_{j=i+1}^{n} \mathrm{sgn}(xj - xi) \quad (5)$$

where the Xi is the actual time data for the time series of i = 1, 2, 3, …, n, and n is the sample size.

The value of sgn (Xj − Xi) is calculated as follows

$$\mathrm{sgn}(xj - xi) = 1 \text{ if } xj - xi > 0$$

$$= 0 \text{ if } xj - xi = 0$$

$$= -1 \text{ if } xj - xi < 1$$

The S-statistics approximately behave as normally distributed, and the test is performed with normal distribution with the mean and variation as given in the below equations:

$$\text{var(S)} = \frac{n(n-1)(2n+5)-\sum_{i=1}^{m} t(t-1)(2t+5)}{18} \quad (6)$$

Standard Z for one limit test is as shown below in Equation the positive value of Z shows an increasing trend and the negative value shows a decreasing trend.

$$f(x) = \begin{cases} (s-1)/\sqrt{var(s)} & S > 0 \\ 0, & S = 0 \\ & = \frac{s+1}{\sqrt{var(S)}} \end{cases} \quad (7)$$

Then, the MK test from the Z value was computed annual land surface temperature and annual rainfall time series data.

$$\beta = \left(\frac{\text{xj}-\text{xi}}{\text{j}-\text{i}}\right) \quad (8)$$

where β represents the median value of the slope values between data measurements xi and xj at the time steps i and j (i, j), respectively. A positive value of Sen's slope (β) indicates an increasing trend and a negative value suggests a decreasing trend in the time series. The trend from Sen's slope (β) estimation was computed based annual rainfall and temperature time series data.

3.3.3. Computing of Land Use Land Cover

3.3.3.1. Image Classification

The adoption of supervised image classification methods, particularly employing the Random Forest Classifier, is warranted due to their efficacy when sample training data is available for the study area. This approach is selected for its ability to accurately categorize pixels into different land cover classes. The Random Forest algorithm, developed by Leo Breiman and Adele Cutler, is a popular machine learning method that combines the outputs of multiple decision trees to yield a single, more robust result. The approach is widely adopted due to its ease of implementation and its capacity to handle both classification and regression problems effectively. The strength of Random Forest lies in its ability to improve accuracy and manage complex datasets by leveraging the collective predictions of the ensemble of decision trees. The versatility and effectiveness of the Random Forest algorithm have contributed to its widespread adoption across various domains. For this land use/land cover (LULC) mapping task, the study classified the land

cover into five broad classes: Water, Forest, Shrubland, Built-up, and Agriculture. These classes were identified and mapped to analyze land use/land cover changes over time.

The supervised classification method utilized in this study was implemented within the Google Earth Engine platform, which allows for efficient processing of large remote sensing datasets. The process of supervised classification generally includes four main steps: preprocessing the image, selecting features based on specific criteria to define patterns, choosing a classifier (in this case, the Random Forest algorithm), and evaluating the accuracy of the classification. This method was chosen for its ability to handle complex and diverse datasets, which is crucial for accurately mapping and analyzing land cover changes in the study area (Belay & Mengistu, 2019; Yesuph & Dagnew, 2019).

Image classification methods, like supervised classification, have been widely used to classify data based on established input features (Abburu & Golla, 2015). Furthermore, machine learning techniques, such as Random Forest, are increasingly used in remote sensing for improved classification and interpretation of satellite data (Alpaydin, 2020). This aligns with previous research that emphasizes the importance of these algorithms in producing more accurate thematic maps of Earth's surface elements, such as vegetation, buildings, and highways (Mahmon et al., 2015). Among various machine learning classifiers such as support vector machine, classification and regression tree, and RF available for classification, the RF classifier outperforms others (Pelletier et al. 2016). The RF classifier was employed as the classification method due to its robustness and its ability to handle multi-dimensional datasets. The RF classifier has shown convincing results in LULC classification in various studies (Pelletier et al. 2016). A total of 100 trees per node were selected for the present study.

Table 3: Description of the LULC classes

Land use land cover classes	Description
Forest	The area comprises natural and manmade forests and vegetation of different types
Agricultural area	The land covered by farmlands, crop lands and range lands
Water body	The area covered by rivers, ponds and reservoirs.
Built up area	The land area used for settlement, urban areas, transportation and construction services
Shrub land	Land covered by short trees, grasses and bush lands

Source: FAO

3.3.3.2. Change Detection Analysis

Change detection analysis was conducted to assess and visualize the spatial and temporal patterns of land use and land cover (LULC) changes throughout the study period. This process entails comparing classified images from different periods to identify areas where land cover has undergone modifications. Post-classification comparison techniques were employed for change detection, with the utilization of Delta Cue, an application tailored for identifying changes in remotely sensed imagery acquired at two different dates (Thambawita et al., 2023). Delta Cue operates on co-registered image data and employs differentiating as its primary change detection method. To quantify the total extent of LULC change between 2001 and 2023.

3.3.3.3. Accuracy assessments of land use land cover

The accuracy assessment of the Land Use and Land Cover (LULC) classification was conducted using a confusion matrix to evaluate the correctness of the classification results. Confusion matrices were generated to compare the LULC classifications for the years 2001, 2012, and 2023, using training data collected within Google Earth Engine. For each LULC class, at least 50 training points were gathered, and the dataset was split into 80% for training and 20% for testing, in accordance with best practices for classification accuracy evaluation when fewer than 100 samples are available. The Random Forest Classifier was employed in Google Earth Engine to perform the classification, and the confusion matrix was used to assess the classification accuracy.

3.3.4. Random forest regression

It is the most frequently utilized non parametric machine learning algorithm for identifying non-linear relationships for classification and regression (Cohen et al., 2003). In this study, non-parametric machine learning algorithm (random forest regression algorithm) was tested to climate variability to predict the actual evapotranspiration outcomes and to measure each variable importance during prediction.

To build the model, it is generally advised that datasets with fewer than 100 observations use an 80/20 split, allocating 80% for training and 20% for testing. This approach ensures there is enough training data for effective learning (Cutler et al., 2007). For datasets containing between 100 and 500 observations, a 70/30 split is commonly accepted, providing a significant amount of data for training while still having sufficient data for testing (Liaw & Wiener, 2002).

3.4. Methodology Flow Chart of the Study

Below the figure 6 the overall flowchart of the study.

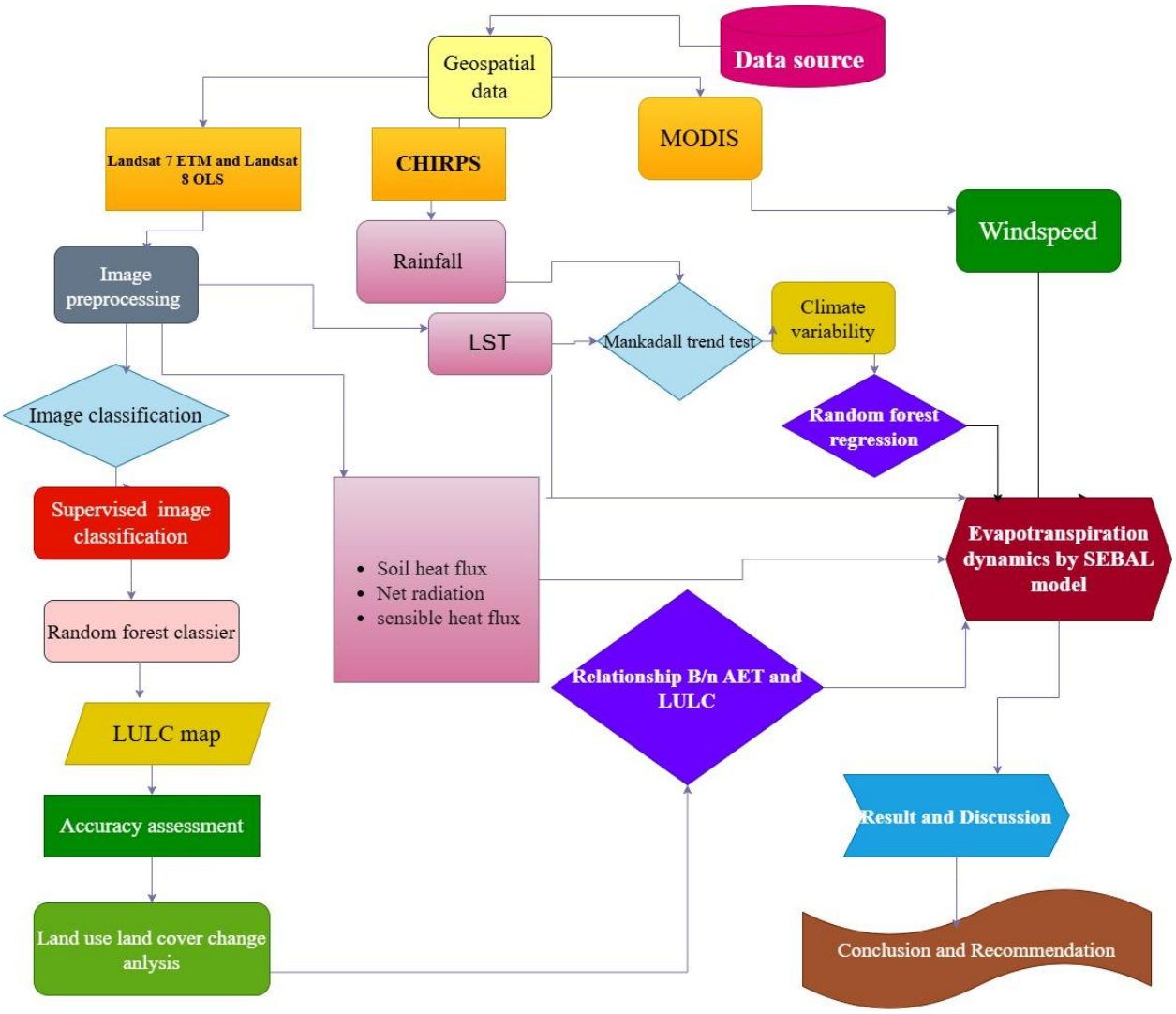

Figure 10 Methodology flowchart

CHAPTER FOUR

4.RESULAT AND DISSCUSSION

This chapter covers the results and discussions analyzing data that were obtained from primary and secondary data to answer. To analyses the collected data in line with the overall objective of the research undertaking.

4.1. Spatiotemporal Variations of Evapotranspiration in the GERD and its vicinity for the period of 2001 to 2023

From 2001 to 2012, the maps show progressive intensification of high evapotranspiration regions, mainly in the central and southern regions, as a result of vegetation growth and land use changes. After 2020, the areas of high evapotranspiration in the south and south-west, differentiated by yellow and red colors (up to 12 mm/day), corroborate that dam management and water handling play a major role in shaping regional hydrological cycles, Overall, the evidence verify that filling of the GERD has accelerated evapotranspiration in affected regions substantially, again pointing towards ongoing hydrological observation.

Spatial pattern of mean AET (actual evapotranspiration) of 2001-2023 study period, as shown in figure (11), shows a clear rise in evapotranspiration, particularly after impounding GERD reservoir in 2020. This trend agrees with earlier work by Ahmed et al. (2020), who found that grand dam impoundments significantly influence regional evapotranspiration by changing local microclimates and adding to surface moisture availability, particularly in riparian and adjacent regions. Other similar dam construction leads to an increase in water surface area, which in turn increases evaporation and can also affect transpiration rates from vegetation around the reservoir (New & Xie, 2008).

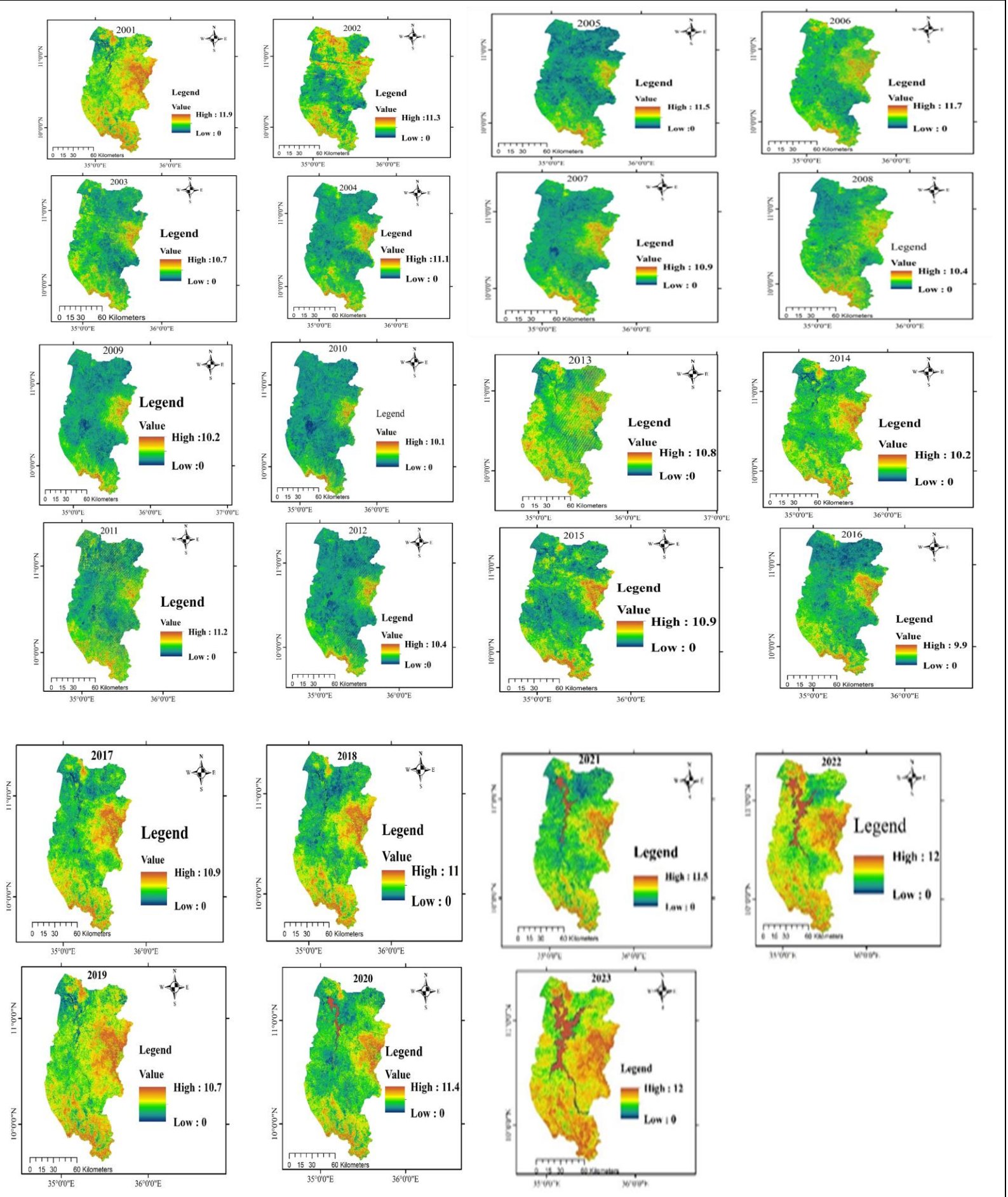

Figure 11 Actual evapotranspiration map from 2001 to 2023

The spatiotemporal analysis of actual evapotranspiration (AET) in the study area from 2001 to 2023 reveals a significant increase following the impoundment of the Grand Ethiopian Renaissance Dam (GERD) reservoir beginning in 2020. Prior to reservoir filling, AET ranged between 9.9 and 11.9 mm/day, primarily governed by natural seasonal variations, temperature, and precipitation. However, since the first filling phase in July 2020, AET has steadily increased, reaching approximately 12 mm/day by 2023, demonstrating the reservoir's substantial hydrological influence. This rise aligns with findings by Yihdego et al. (2019), who noted that large reservoirs expand surface water area and alter vegetation, thereby enhancing local evapotranspiration rates. Similar phenomena have been observed at other major reservoirs worldwide, such as China's Three Gorges Dam, where increased surface evaporation altered microclimates, elevating humidity and modifying rainfall patterns (Wu et al., 2020; Mengistu et al., 2023). Furthermore, studies by Azagegn et al. (2024) and assessments published in Tawfik & Dombrowsky (2017) confirm that GERD's filling and operation have increased evaporation losses and altered downstream hydrology and flow regimes.

The reservoir's large volume holding up to 74 billion m^3 of water results in estimated evaporation losses around 1.5 to 1.7 km^3 annually, which, although lower than losses from downstream reservoirs like Lake Nasser, still represent a significant water volume (MDPI Water, 2022). While these changes may enhance agricultural productivity through improved soil moisture recharge as noted by Kamble et al. (2021), the increased AET raises serious concerns for downstream water availability in the Nile Basin. Evaporative losses reduce river flow to downstream countries such as Sudan and Egypt, complicating water-sharing agreements and heightening geopolitical tensions as highlighted by Hirsch & Johnson (2020). However, coordinated management among the Nile Basin countries could mitigate some negative impacts by spreading reservoir filling over several years and optimizing releases. Overall, the GERD reservoir's construction has transformed local and regional hydrology, affecting climate, agriculture, and transboundary water resource management in the Nile Basin Azagegn et al., 2024; Zulkifli et al., 2022).

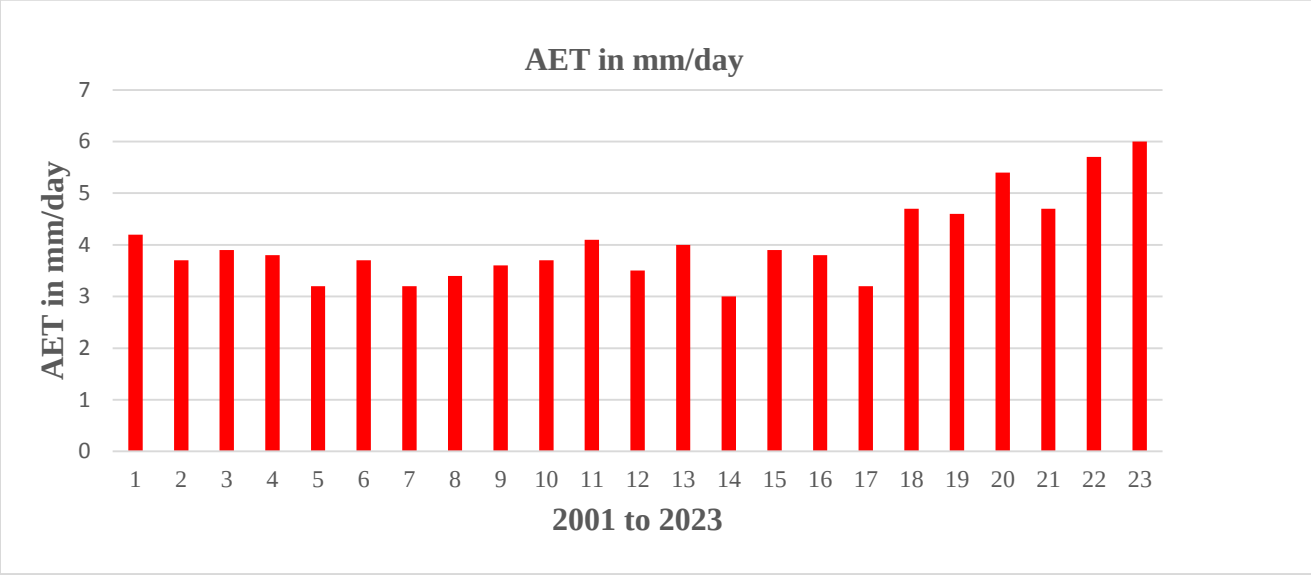

Figure 12 AET annual from 2001 to 2023

The analysis of evapotranspiration (AET) from 2001 to 2019 in the study area shows relatively stable values, with limited variability likely maintained by natural inter-annual climatic fluctuations, indicating consistent land surface and hydrological conditions before the GERD reservoir construction. However, since the dam filling began in 2020, there has been a rapid and sustained increase in AET, rising from approximately 5.4 mm/day in 2020 to a peak of 6 mm/day by 2023. This sharp increase strongly suggests that the reservoir impoundment has significantly influenced local evapotranspiration processes.

The expansion of the reservoir's surface water area has increased surface dampness and altered the local microclimate, raising humidity and contributing to enhanced evapotranspiration, as supported by Smith et al. (2018), who demonstrated that large reservoirs intensify evapotranspiration through microclimate modification and increased surface moisture. Such hydrological and climatic changes are consistent with observations from other large reservoirs worldwide, including the Three Gorges Dam in China, where increased evaporation and microclimate shifts have been documented (Wu et al., 2020; Mengistu et al., 2023). While the connection between dam filling and increased AET is clear, it is important to consider other factors such as climate variability and land use changes that may also contribute. Overall, the GERD reservoir has not only transformed local evapotranspiration dynamics but has also altered broader hydrological and

climatic conditions in the region, impacting downstream water resources, groundwater recharge, vegetation health, and regional temperature patterns (Aty, 2022).

This comprehensive impact underscores the critical role of large reservoirs in modifying local environments and highlights the need for integrated water and climate management strategies in the Nile Basin. Dam construction significantly increases the surface area of water, leading to a substantial rise in evaporation (Tian et al., 2021). A study in the Shiyang River Basin found that cascade dams significantly increased evaporation and altered isotope composition in landscape water, highlighting the potential for water loss in arid regions (Zhu et al., 2021). Research on the Three Gorges Dam in China demonstrated that the dam's impoundment had both cooling and warming effects on the surrounding climate, impacting vegetation dynamics and evapotranspiration (Yang et al., 2024).

4.2. Climate Variability in the GERD and its Vicinity form the Period of 2001 to 2023

Below the graph of figure (13) shows the annual Land Surface Temperature (LST) around the Grand Ethiopian Renaissance Dam (GERD) from 2001 to 2023. From the findings, there is a general pattern of temperature decline year after year but with fluctuations. In most years, the temperature is 36°C with a variation from a high of 37.3°C in 2010 and a low of 33°C in 2023. The observed trend of decreasing temperature may be attributed to land use, vegetation, or the impact of the artificial lake of the dam after its impounding had commenced. To confirm such a decline is perceived, some studies indicate that big reservoirs like the artificial lake of the GERD influence nearby temperatures Similarly, Hwang et al. (2007), indicate that large reservoirs also have a cooling influence in adjacent areas via land use change and the moderation of the water body.

Water bodies take longer to heat and cool compared to land, yielding more equalized temperatures and, therefore, having the potential to be the source of the cooling effect observed in Figure (9).Similarly, Ahmad (2024), in their research study of the Aswan High Dam, observed that after the reservoir behind the dam was filled, there was a reduction in surface temperatures in comparison with the surrounding environment and attributed this to evaporative cooling effects from the water body. The cooling effect is also improved by Chen et al. (2020), which in their research

found that following the impoundment of the Three Gorges Dam in China, the local region exhibited a significant reduction in LST via evaporative cooling and local climate modification. Furthermore, Mase et al. (2015), found the same patterns in major reservoirs, noting that after construction and filling, moderating effect of the water body brings significant temperature drops. In line with the pattern seen in Figure (13), temperatures have been decreasing year on year, particularly after reservoir filling began. The GERD reservoirs lead to increased evapotranspiration, which can cool the surrounding air. The result shown that this cooling effect can be noticeable, especially near the reservoir. The dam construction can even lead to a decrease in average annual temperature in the reservoir area.

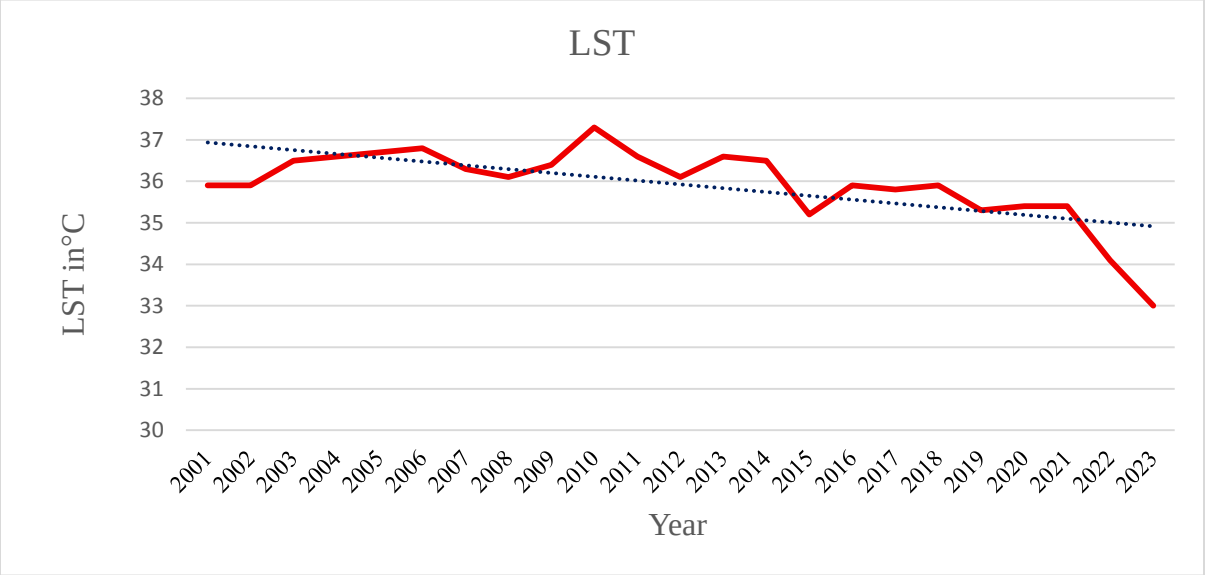

Figure 13 LST from 2001 to 2023

Below the figure (14) is the GERD catchment area annual rainfall record for the period between 2001-2023. The records show variability in rainfall with an increment between 2020-2023, The increased moisture from reservoir evaporation can contribute to changes in precipitation patterns. noted that surplus precipitation over decades in catchment areas upstream results in enhanced flow of water, causing the dam to be filled more rapidly. Mostafa et al. (2016), through their study on the Aswan High Dam, also concluded that inter seasonal variation in rainfall in the Nile Basin was directly influencing the reservoir water level and allowing the filling to occur more rapidly in wetter years. Muchuru et al. (2014), in case study of Kariba Dam in Southern Africa

had investigated the impact of season variation of rainfall on the reservoir level. The study found that increased rain in some seasons meant faster filling, and dry seasons meant slower filling. As much as the same can be noticed in the GERD as well where 2020-2023 with moderate additional rain may have caused faster filling of the reservoir. Further, Chen et al. (2020), in the case of the Three Gorges Dam in China, noted the implication of rain in relation to changing the rate at which gigantic reservoirs fill.

Their research indicated that excess rainfall translates to high water inflows, indicating a rapid filling rate and steady hydroelectric production. In the same way, the slight increase in rainfall throughout the filling period of GERD can be viewed as a factor in the provision of better conditions for water storage within the dam. In general, Figures (13) and (14) illustrate relationship between temperature and precipitation regimes across the GERD area.

The declining trend of temperatures of Figure (10) from 37.3°C in 2010 to 33°C in 2023 is consistent with the moderating effect of the GERD artificial lake. Parallel to this, the marginal increase in precipitation from 2020 to 2023 also indicated by Figure (10) had something to do with perhaps causing the reservoir filling to increase at a faster rate since there was an additional volume of water that had to be stored due to favorable climatic conditions, The joint impact of temperature change and changes in rainfall points to the overarching influence of GERD filling and construction in altering the regional climate and water supply.

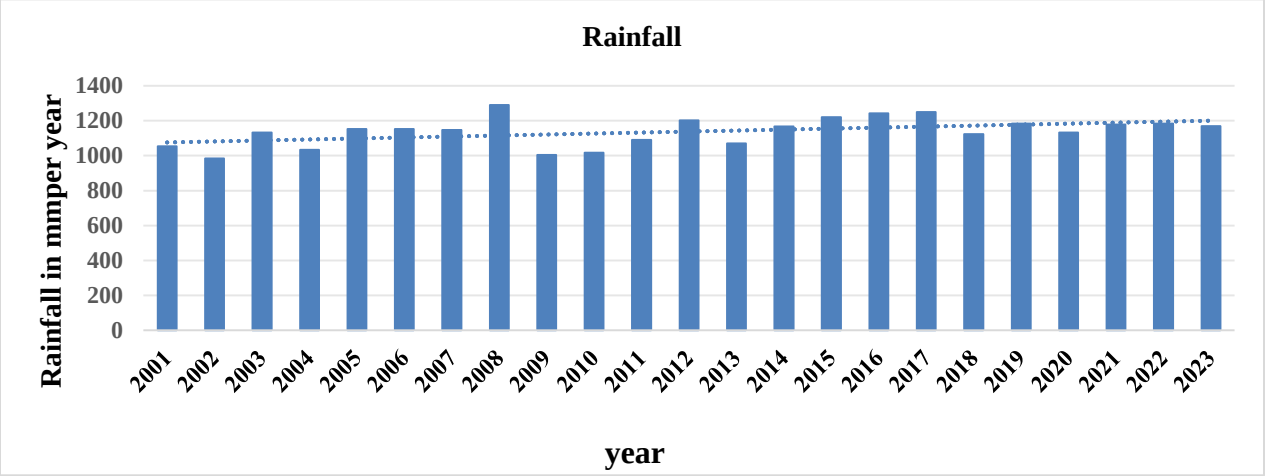

Figure 14 Rainfall from 2001 to 2023

Table 4 Man Kendall trend test of climate variability

	Rainfall	LST
Kendall's tau	0.047	0.27
S	12	69
Var(S)	1432.6	1433.6
p-value (Two-tailed)	0.77	0.073
Alpha	0.05	0.05
Sen's Slope	2.6	-0.07

Based on the above table 4 trend analysis for the GERD and its vicinity from 2001 to 2023 discover important patterns in local climatic variables, particularly annual rainfall and Land Surface Temperature (LST). The analysis shows no statistically significant trend in annual rainfall (Kendall's tau = 0.047, p = 0.77), although there is a slight increasing tendency reflected by the Sen's Slope value of 2.6 mm/year (Table 4). This suggests potential changes in precipitation that could be related to the presence of the GERD reservoir. Conversely, the analysis of LST indicates a weak decreasing trend (Kendall's tau = 0.27, p = 0.073), with a Sen's Slope of 0.07 °C/year, reflecting signs of localized cooling. Although these trends do not reach statistical significance at the 5% level, they align with early indications of microclimatic modifications associated with the filling of the GERD reservoir, which began in 2020. The filling of the reservoir is significant, as it introduces a substantial artificial lake into the landscape, likely impacting local climatic dynamics.

The observed contrasting trends of increasing rainfall and decreasing LST can be attributed to the newly formed reservoir. Research indicates that large water bodies, such as reservoirs, can significantly alter local climatic conditions by enhancing evapotranspiration, increasing atmospheric moisture availability, and moderating surface temperatures due to water's high thermal capacity (Yihdego et al., 2019; Mengistu et al., 2023).

This results in microclimatic cooling and localized increases in precipitation, a phenomenon also observed in other large dam environments. A study by Wu et al. (2020) on the Three Gorges Reservoir in China highlighted significant changes in local precipitation and temperature patterns due to the creation of the reservoir, leading to similar trends of increased rainfall and moderated temperatures. Similarly study by, Kamble et al. (2021) found that the presence of the Sardar Sarovar Dam in India caused localized rainfall increases and a cooling effect in the surrounding areas. Additionally, the Three Gorges Reservoir has been shown to cool nearby land surface temperatures by approximately 0.1 to 1.5°C, as reported by Song et al. (2017), along with an increasing trend in annual precipitation. Likewise, Chen et al. (2022) highlighted that dam construction caused a decrease of about 0.12 °C in temperature in the reservoir area.

The GERD, being one of Africa's largest hydroelectric projects, has created a notable new water body, and its presence is likely contributing to these observed trends. While the statistical significance of the identified trends is marginal, the general direction of change aligns with the expected climatic influence of large reservoirs. This alignment suggests that the filling of the GERD is beginning to exert its influence on local weather patterns, albeit subtly at this stage. As the reservoir stabilizes and reaches its full capacity, it is plausible that these microclimatic effects will intensify, further influencing precipitation and temperature trends in the region. The observed trends reflect not only the immediate impacts of the GERD on local climate but also the potential for longer-term changes as the ecosystem adapts to the new hydrological conditions.

Continued monitoring and the collection of long-term data are essential to confirm these initial signals of climate adjustment induced by the GERD project. A similar approach was used by Omran. (2019), who emphasized the need for ongoing assessment of climate impacts following dam construction to understand the broader ecological ramifications in the affected regions. Understanding these dynamics is vital for predicting future climatic patterns and for assessing the cumulative impacts of large-scale water infrastructure projects. While the current analysis indicates only marginal statistical significance in the observed trends, the direction of change aligns with findings from other studies that indicate large reservoirs can modify local climates. This underscores the importance of ongoing research and monitoring to fully comprehend the implications of the GERD on regional climate dynamics as it evolves.

4.3. Land Cover Change Dynamics in the Study Area form the Period of 2001, 2012 and 2023

Remote sensing data, particularly from Landsat satellites, plays a crucial role in understanding Earth's environmental processes. It helps analyze the impact of land cover on these processes (Huete et al., 2002; Lotsch et al., 2003). Landsat imagery, with its multispectral and multitemporal features, is commonly used for land use and land cover mapping. In the area the Grand Ethiopian Renaissance Dam (GERD) and its vicinity.

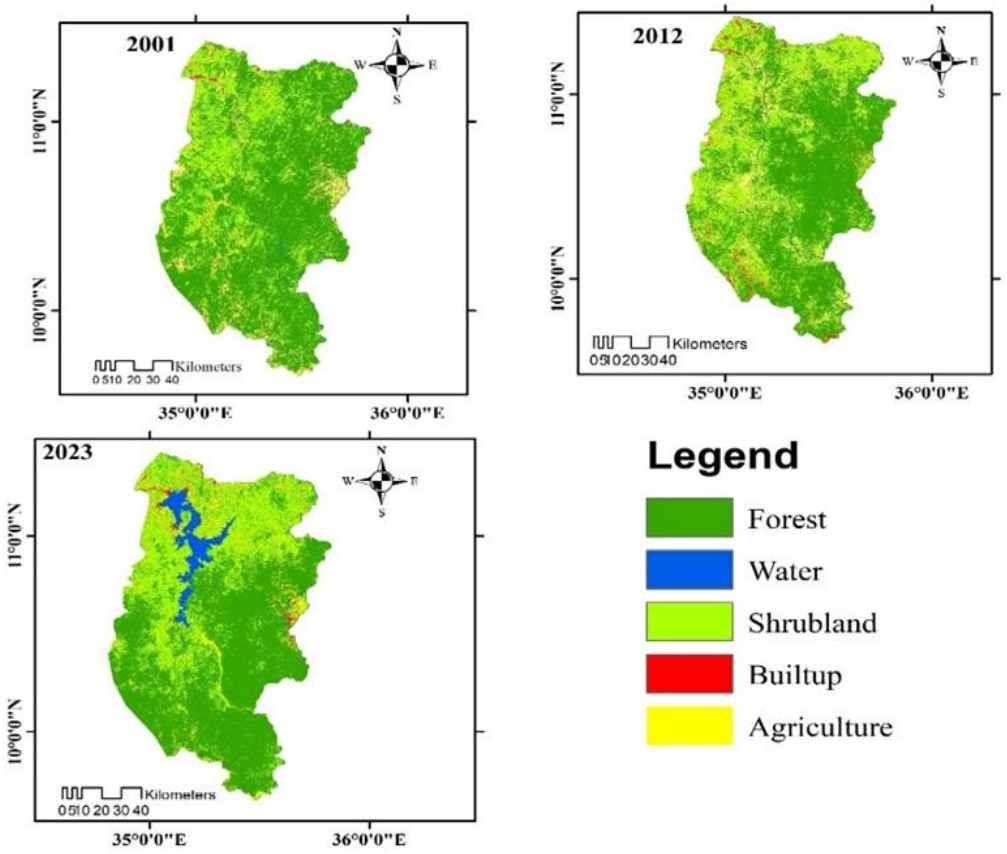

Figure 15 LULC map of the study area

Based on the above figure (15) the construction of the Grand Ethiopian Renaissance Dam (GERD) has led to significant in the land use and land cover (LULC) dynamics observed between 2001, 2012, and 2023. Due to the construction of the dam has displaced approximately 20,000 people (Elsanabary & Ahmed, 2018), a common consequence of large dam projects globally. Similar studies suggest that dam construction often results in decreased agricultural land

due to inundation or displacement of farming communities (Shuka et al., 2022), which aligns with observed patterns near GERD. Moreover, the case of China's Three Gorges Dam illustrates how such large infrastructure projects cause extensive hydrological disruptions and displacement of communities (Huang et al., 2019; Zhao et al., 2012). Conversely, some dam projects, as reported by Liu et al. (2021), can lead to increased vegetation cover over time, owing to ecological succession and land regeneration processes.

The LULC changes observed in the vicinity of GERD highlight these complex interactions. The sharp increase in water bodies from approximately 1,920 hectares in 2001 to over 51,240 hectares in 2023 is directly attributable to reservoir formation, inundating large areas and fundamentally altering the landscape (Seddon et al., 2020). This pattern is consistent with other dam impact studies, which have documented substantial landscape inundation and natural land cover changes (Fearnside, 2016). Over the same period, shrub land increased steadily. The sharp reduction in forest cover from 969,564 hectares in 2001 to 483,852 hectares in 2012 indicates significant deforestation linked to dam construction and related infrastructure development. This pattern is also observed in the Nashe watershed study, where dam construction similarly caused forest loss (Fikadu & Olika, 2023).

However, forest cover partially recovered to 746,210 hectares by 2023, likely due to natural regeneration or reforestation efforts (Raju et al., 2017). Agricultural land initially surged, potentially due to land redistribution or changing land use patterns, but eventually declined, likely impacted by inundation from the reservoir and resettlement of farming communities a trend consistent across other dam affected regions (Kumar et al., 2021). Built-up areas expanded significantly until 2012, driven by infrastructure development associated with the dam, but decreased by 2023, indicate due to ongoing displacement of people.

The land use and land cover (LULC) changes observed between 2001, 2012, and 2023 in the vicinity of the GERD reflect significant environmental transformations associated with large dam construction. The sharp increase in water bodies from approximately 1,920 hectares in 2001 to over 51,240 hectares in 2023 is directly attributable to the formation of the reservoir, which inundated extensive areas of land (Seddon et al., 2020). This phenomenon is consistent with other studies on dam impacts, highlighting how reservoirs lead to substantial change of land use land

cover (Fearnside, 2016). The initial decline in forest cover from 969,564 hectares in 2001 to 483,852 hectares in 2012 aligns with findings that dam construction often results in deforestation due to land clearing and infrastructure development (Raju et al., 2017). The partial recovery of forest cover to 746,210 hectares by 2023 could be linked to natural regeneration or reforestation efforts following initial disturbance. Meanwhile, agricultural land initially surged before declining likely impacted by inundation from the reservoir and the resettlement of farming communities parallelling patterns observed in other dam-affected regions (Kumar et al., 2021). The Nashe watershed study (Fikadu & Olika, 2023) exemplifies similar dynamics, due to the reason of dam construction decrease forests.

Research in other contexts underscores the significant impacts of large-scale infrastructure projects on LULC. Similar study, an assessment of the Three Gorges Dam in China revealed similar effects, such as substantial alterations in land cover and an increase in water bodies (Zhang et al., 2020). Similarly, studies conducted in Lake Victoria indicated comparable patterns of land cover change resulting from dam construction, emphasizing issues related to community displacement and shifts in land use (Nassali et al., 2020). Moreover, in Brazil has demonstrated that hydroelectric projects can cause considerable deforestation and alterations in local land use patterns (Barros et al., 2019).

Research in other contexts underscores the significant impacts of large-scale infrastructure projects on LULC. Similar study, an assessment of the Three Gorges Dam in China revealed similar effects, such as substantial alterations in land cover and an increase in water bodies, which resulted in the loss of arable land and disrupted local ecosystems (Zhang et al., 2020). Similarly, studies conducted in Lake Victoria indicated comparable patterns of land cover change resulting from dam construction, emphasizing issues related to community displacement and shifts in land use (Nassali & Fangninou, 2020). Moreover, in Brazil has demonstrated that hydroelectric projects can cause considerable deforestation and alterations in local land use patterns (Barros et al., 2019).

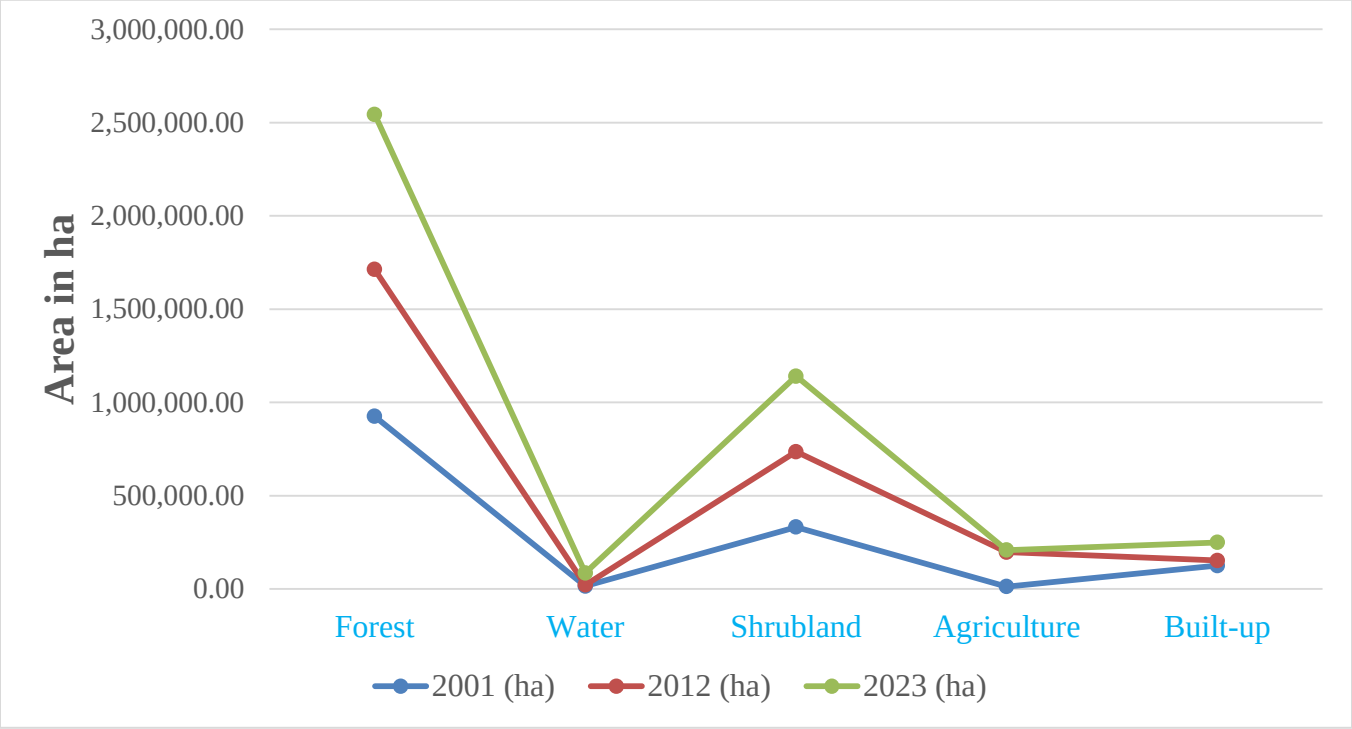

Figure 16 LULC in ha

In land cover classes surrounding the Grand Ethiopian Renaissance Dam (GERD) are closely linked to the construction and operational phases of the dam, which have significantly impacted land use and ecosystem dynamics in the region.

The initial decrease in forest cover from 925,572.15 hectares in 2001 to 787,459.32 hectares in 2012, followed by a slight increase to 831,211 hectares in 2023, may be attributed to the dam's construction activities, which often involve deforestation for infrastructure development, access roads, and other construction-related land clearing. During the early phases, large-scale land clearing to facilitate dam construction and related infrastructure likely caused substantial forest loss. Once the construction phase concluded and strategies for land management and reforestation were implemented, some forest regeneration might have occurred, contributing to the gradual increase in forest cover by 2023 (Zeleke & push, 2020).

The notable increase in water bodies from 14,902.47 hectares in 2001 to 64,788 hectares in 2023 reflects the dam's reservoir expansion and associated water management activities. The impoundment of water for hydroelectric power generation naturally expands water bodies in the

immediate vicinity, impacting local hydrology and surrounding ecosystems (Gebreegziabher et al., 2018).

Similarly, changes in shrubland, agriculture, and built-up areas indicate land use shifts driven by development activities related to dam construction, population displacement, and infrastructural development. The increase in shrubland area may be a result of land abandonment or secondary succession following initial disturbance, while the fluctuations in agricultural and built-up areas reflect ongoing land management and urbanization trends influenced by the dam project.

Figure 17 Dam sit (source: filed survey ,2024)

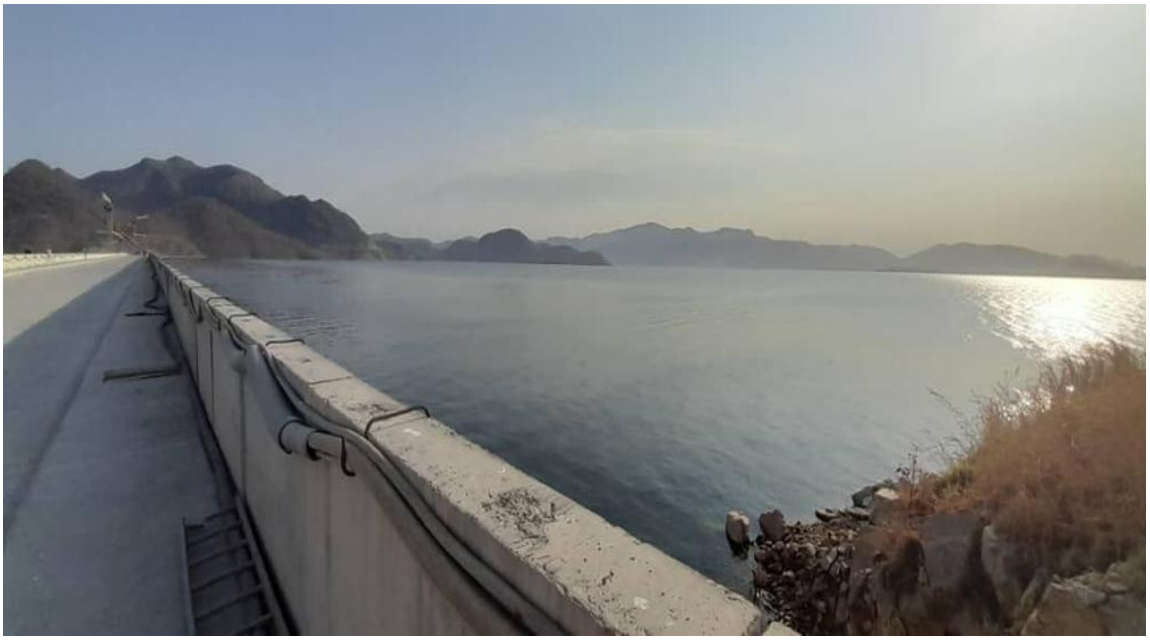

Figure 18 Artificial Lake (source: filed survey 2024)

In figure17 the GERD Dam Site as a bustling construction zone situated along the banks of the Blue Nile River in Ethiopia. This visualization captures the essence of ongoing construction activities, showcasing a plethora of workers, heavy machinery in operation, and the gradual development of the physical infrastructure of the Grand Ethiopian Renaissance Dam. Moving on to Figure 18, shifts to the GERD Artificial Lake, a consequential reservoir that is taking shape behind the dam structure. This depiction compresses the transformation of the once flowing river into a massive body of water, illustrating the reservoir's formation, the containment provided by the dam, and the surrounding landscape that will be influenced by the presence of this artificial lake.

4.3.1. Change detection analysis

4.3.1.1. Change detection

The transformation of land cover classes from 2001 to 2012, 2012 to 2023, and cumulatively from 2001 to 2023 around the Grand Ethiopian Renaissance Dam (GERD) construction site unveils a complex narrative of environmental dynamics and human interventions (Figure 19). The significant decline in forest cover between 2001 and 2012 by 138,112.83 hectares is likely attributable to infrastructure development, land clearing, and deforestation associated with dam

construction activities (Gebreegziabher et al., 2018). During this period, water bodies decreased by 9,028.17 hectares, possibly due to alterations in river flow, dam operation, or water resource management. Conversely, the expansion of shrubland by 72,797.49 hectares suggests ecological succession or land use change following initial disturbances. The notable increase in agricultural land by 171,933.97 hectares indicates land conversion driven by population growth and settlement expansion linked to the dam's development (Yami et al., 2020). The decrease in built-up areas by 97,590.33 hectares may reflect initial land clearing, with subsequent urban development occurring in later years.

Between 2012 and 2023, forest cover showed signs of recovery, increasing by 43,751.68 hectares, possibly due to reforestation or afforestation efforts. Water bodies expanded by 58,913.7 hectares, largely influenced by the reservoir filling and hydrological changes caused by the dam (Gebreegziabher et al., 2018). The stabilization of shrubland with marginal growth supports the idea of ecological resilience amidst ongoing land use shifts. Meanwhile, the significant reduction in agricultural land by 171,933.97 hectares suggests land abandonment, changes in land use policies, or environmental constraints on agriculture. The expansion of built-up areas by 70,280.84 hectares aligns with continued urbanization driven by dam-related infrastructure and population dynamics.

Cumulatively, from 2001 to 2023, these land cover changes depict a landscape shaped by the combined impact of human interventions and environmental factors. Forest cover decreased by 94,360.47 hectares, reflecting long-term deforestation pressures, while water bodies increased, possibly due to dam-induced hydrological regulation. Shrubland growth underscores ecological adaptation or secondary succession, and the decrease in agricultural and urban areas indicates ongoing land use restructuring (Zeleke & Push, 2020). These insights highlight the pressing need for sustainable land management and continuous environmental monitoring to mitigate adverse ecological effects stemming from dam construction (Yami et al., 2020).

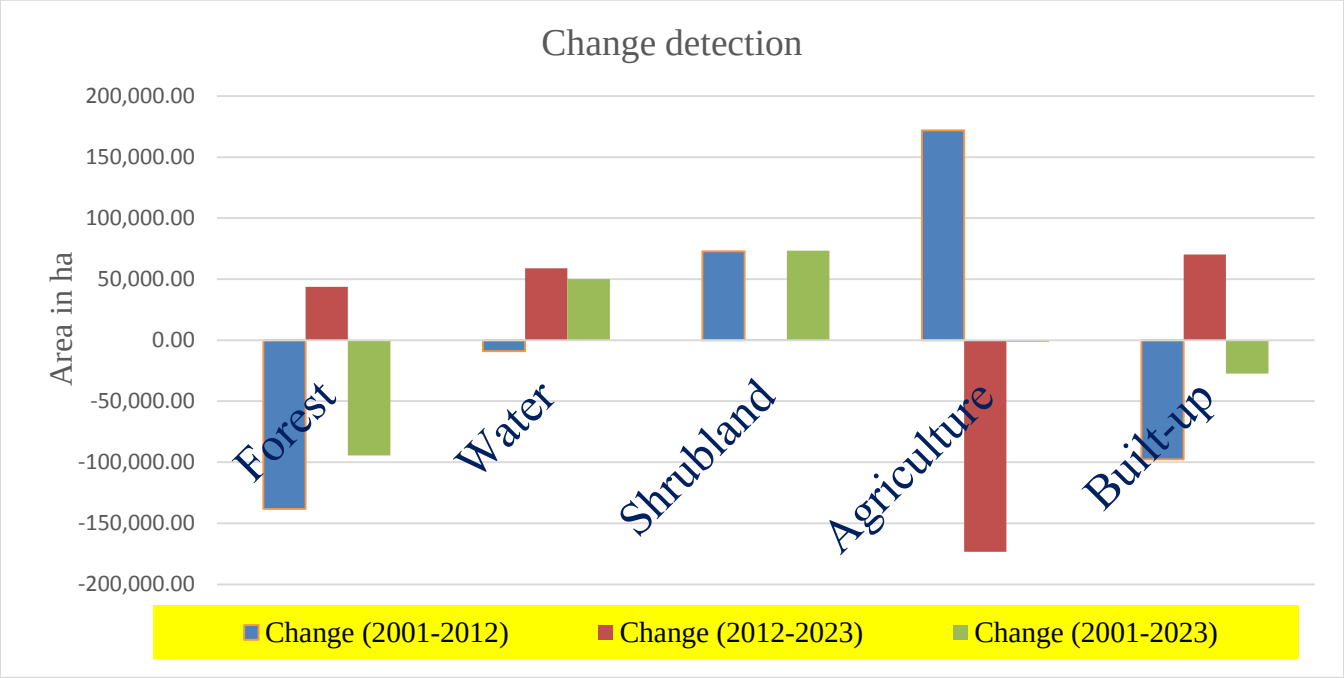

Figure 19 Change detection

4.3.1.2. Transition matrix

A Land Cover Change Matrix records that each land cover category will change to the other category (Peiman, 2011). comparing the land cover from respective years Comparing the land cover from the respective years 2001–2023 in the GERD (Grand Ethiopian Renaissance Dam) and its vicinity was informative, as it provided a better understanding of the changes.

Table 5 LULC transition area.

2023 \ 2001	Water	Forest	Agriculture	Built-up	Shrubland
Water	88.5	0.5	1.2	4.8	5
Forest	1	83	3.5	6.5	6
Agriculture	2.5	5	65	18	9.5
Built-up	5	8	15.	55	17
Shrubland	3	3.5	15.3	16.7	62

In the vicinity of the Grand Renaissance Dam in Ethiopia, land cover dynamics between 2001 and 2023 reveal a landscape with moderate stability as well as dramatic changes due to human interventions and development. Water bodies have also not changed much, with about 88.5% of the cover still in water, while part of the water areas about 4.8% has been developed to built-up land, an indication of infrastructural growth related to dam construction and expansion. Forest cover is also much intact, with about 83% remaining intact; however, part of it about 6.5% has been altered to built-up land, an indication of localized deforestation or clearance for developmental purposes. Agricultural land still dominated, with 65% of the land remaining under cultivation, but a significant portion (approximately 18%) has been transformed into built-up land, suggesting increasing human settlement and infrastructure near the dam. Built-up lands have increased hugely, with some 55% remaining as urban land, and some of it about17% has been converted to shrubland. Conversely, shrubland has been relatively more resilient, with 62% intact, although approximately 16.7% has been converted into urbanized land, and 15.3% into agriculture, indicating ongoing changes in land use due to urbanization and exploitation of resources. Overall, the evidence indicates both resistance of natural features of the landscape as well as the insidious impacts of development associated with the dam and the surrounding region.

4.3.2. Accuracy assessment land cover types

The LULC mapping was conducted using the Random Forest classifier within the Google Earth Engine platform. The classification system assigned specific values to different land cover classes: 0 for Forest, 1 for Water, 2 for Shrubland, and 3 for built up and 4 for Agriculture. The Random Forest classifier was trained using training samples derived from Landsat images captured in the years, 2001, 2012, and 2023. Each class was represented greater than 50 training samples. The overall accuracy and kappa coefficient of the land use land cover classification was calculated using a code.

Table 6: Accuracy assessment

Year	Overall accuracy	Kappa coefficient
2001	0.9	0.89
2012	0.95	0.94
2023	0.97	0.96

Based on Table 6 the accuracy of the land use and land cover (LULC) classification for the GERD region, validated using Google Earth Engine (GEE) and Landsat satellite imagery, demonstrated consistent improvement over the study period (2001–2023). The overall accuracy rose from 0.90 (90%) in 2001 to 0.95 (95%) in 2012 and further to 0.97 (97%) in 2023, reflecting advancements in remote sensing technology and refined classification methodologies. Similarly, the Kappa coefficient, which quantifies the agreement between classified data and ground-truth references, increased from 0.89 in 2001 to 0.94 in 2012 and 0.96 in 2023. These high accuracy scores align with globally recognized standards for LULC mapping (Congalton & Green, 2019), underscoring the reliability of observed trends such as deforestation, urbanization, and reservoir expansion. The progressive enhancement in accuracy can be attributed to the integration of advanced Landsat sensors, improved machine learning algorithms and expanded ground truth validation datasets (Christofi et al., 2025). The use of GEE further ensured scalable and reproducible processing of multi-temporal satellite data, minimizing misclassification errors and enhancing spectral discrimination of complex land covers like fragmented forests and urban sprawl (Gorelick et al., 2017).

4.4. The Relationship between LULC, Climate Variably and Evapotranspiration Dynamics from the Period of 2001 to 2023

The current studies used random forest regression model to testing how AET trends explain by rainfall and LST climate variables based on R^2 in form scatter plot figure, and as well how the value of AET is parallelly increasing the water bodies land use classes.

As random forest regression result demonstrated, both rain fall and land surface temperature explanatory variables are explained the actual evapotranspiration trends from 2001-2023, the result of regression R^2 between rainfall and AET scored 0.93, this indicating rainfall strongly explain the AET trend. Similarly, the LST are another climate variable explained the AET in the present study, with value of 0.87 R^2.

In contrast, the rainfall is over explained AET rather than LST. This result indicating the trend of AET is explained by the trends of LST, and rainfall climate variables, as well as the water body similarly shown increment with AET, as the above LULC result revealed particularly in water bodies.by -based regression two scatter plots that clearly demonstrate the relationships between Actual Evapotranspiration (AET), Land Surface Temperature (LST), and rainfall in the vicinity of the Grand Ethiopian Renaissance Dam (GERD). These relationships highlight significant microclimatic changes triggered by the formation of the GERD reservoir, which has reshaped the local climate.

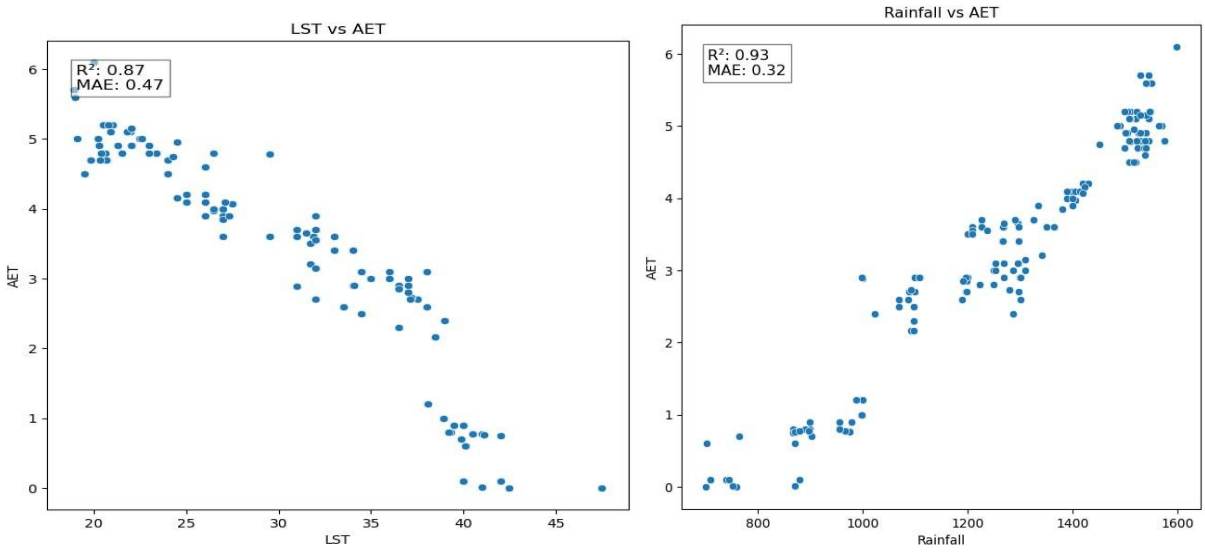

Figure 20 Random Forest regression

The spatial patterns observed in the GERD region reveal that areas with increased water coverage and vegetation exhibit elevated actual evapotranspiration (AET) rates, which actively enhance atmospheric moisture recycling. This feedback loop not only supports the observed rise in local rainfall but also underscores the bidirectional relationship between land surface processes

and regional precipitation dynamics. These findings are consistent with similar studies indicating that increased AET from reservoirs and forested areas amplifies atmospheric moisture content, subsequently promoting regional rainfall (Abdelrady et al., 2021; Mengistu et al., 2023). Additionally, AET plays a pivotal role in sustaining soil moisture and vegetation-driven transpiration, further reinforcing land-atmosphere coupling (Gebremichael et al., 2023; Deng et al., 2022).

The GERD reservoir serves as a case study of how engineered water infrastructure can modulate regional climate by fostering evaporative cooling a phenomenon that has been documented globally in large dam systems and is known to offset localized warming trends (Wu et al., 2004; Grill et al., 2015). These insights align with broader research emphasizing the dual role of land use and land cover (LULC) changes in both enhancing hydrological recycling and contributing to thermal regulation through increased surface water and vegetation (Pathak et al., 2018). Collectively, this body of evidence positions AET as a critical driver in the feedback loop between land surface modifications and regional climate behavior, reinforcing the climate-modulating potential of large-scale hydrological interventions such as the GERD.

Moreover, In the context of the GERD and its vicinity, the random forest regression analysis reveals that rainfall significantly influences Actual Evapotranspiration (AET), especially during the dam filling period. The model with rainfall as the predictor exhibits a lower MAE of 0.32, indicating more accurate predictions compared to the LST-based model. This validity is supported by studies showing that the filling of large reservoirs like the GERD leads to increased local and regional rainfall and water body expansion due to altered hydrological cycles (Gebremedhin & Kebede, 2020). The increased water availability results in higher evaporation rates, which in turn elevate AET levels consistent with prior research demonstrating that reservoir impoundment and water surface expansion enhance evapotranspiration (Yohannes et al., 2019). Simultaneously, the expansion of water bodies and increased moisture content tend to decrease Land Surface Temperature (LST) in the surrounding region due to the cooling effect of water surfaces and increased humidity (Zhang et al., 2018). These environmental modifications underscore the interconnected impacts of the GERD filling on regional hydrology and climate variables, emphasizing the importance of considering water surface dynamics and rainfall in hydrological modeling and water resource planning within this region.

.

CHAPTHER FIVE

5.CONCLUSION and RECOMMENDATION

5.1. Conclusion

This study provides crucial insights into the dynamics of actual evapotranspiration (AET) in the Benishangul Gumuz region, particularly in the vicinity of the Grand Ethiopian Renaissance Dam (GERD). The findings demonstrate that since the GERD reservoir was impounded in 2020, there has been a significant increase in AET, rising from approximately 5.4 mm/day in 2020 to 6 mm/day in 2023. These changes in AET, moisture availability, and local temperature regulation highlight the profound impact of the dam on local microclimates and regional hydrological dynamics, fostering moisture recycling and contributing to ecological resilience. The analysis also reveals that, prior to the dam's construction, AET remained relatively stable, averaging about 3 mm/day between 2001 and 2019, reflecting consistent land surface and hydrological conditions. However, with the impoundment of the reservoir, the increase in AET signals a shift in the regional hydrological cycle, driven in part by enhanced evaporation from the dam's large water body and its interaction with local temperature and precipitation patterns. Land use/land cover (LULC) analysis underscores the broader ecological transformations in the region, including deforestation, urbanization, and the expansion of water bodies and built-up areas. These LULC changes, largely attributed to the GERD's construction and operational activities, introduce both opportunities and challenges for sustainable land and water management.

The shifting land cover poses challenges for ecosystem conservation and necessitates integrated land management strategies that account for both infrastructure development and environmental sustainability. Given the significant influence of the GERD on AET, climate, and land cover, this study emphasizes the need for a holistic approach to water resource management in the Nile Basin. These results indicate that rainfall explains 93% of the variability in AET, making it a stronger predictor than LST, which explains 87% of the variance. The lower MAE in the rainfall model also indicates higher predictive accuracy. The introduction of floating solar panels on the GERD reservoir could provide an innovative solution to reduce evaporation, maintain water lev-

els, and generate renewable energy, contributing to long-term water quality monitoring and sustainable resource management. Ultimately, the findings highlight the necessity for continuous monitoring, reforestation, and responsible land use planning to enhance the resilience of the region's ecosystems and ensure the sustainable management of water resources. Collaboration among stakeholders, effective governance, and strategic planning will be essential in addressing the complexities of climate variability, infrastructure development, and regional water resource management in the Nile Basin. This study calls for a proactive, integrated approach to managing the evolving environmental conditions in the GERD region, ensuring that both the natural environment and local communities' benefit from sustainable water and land use practices.

5.2. Recommendation

The findings of the research conducted provide numerous suggestions to enhance the management of water resources.

1. The use of floating solar panels on the artificial lake of GERD: This will reduce water evapotranspiration substantially as well as aid in renewable energy generation. The Ethiopian federal government is advised to manage monitoring of water levels, vertical flow of water, and the overall quality of water in order to minimize environmental impacts. There is a need to collaborate with government agencies for optimal planning and management of this project.
2. Strategies for Integrated Land Management: Environmentalists are prompted to advance and advocate land management practices that contribute towards the sustainable coexistence of forest conservation and agricultural activities. Strategies should be formulated to minimize the adverse impacts of agricultural land expansion on forests. Environmentalists should stress emphasizing such practices to ensure ecosystem maintenance, biodiversity protection, and provision for the sustainable use of water resources.
3. Enhancing Reforestation Activities: Reforestation and restoration activities are recommended to be given high priority in areas where forests are degraded. These activities will reinstate bio-diversity, improve water holding capacity, and support overall landscape health. It is important that respective stakeholders, including government departments, environmental NGOs, and local communities, own such activities to ensure long-term success and sustainable land management.

4. Promotion of Sustainable Farming Techniques: It is recommended that the adoption of sustainable agriculture practices in the GERD region should be enhanced to save water and enhance the efficiency of water use. Techniques such as crop rotation, agroforestry, and conservation tillage can help in maintaining soil, enhancing water holding capacity, and lessening the adverse impacts of agriculture on the environment. It is necessary that farmers, agricultural extension programs, and government officials come together in promoting these practices to ensure long-term agricultural production and water resources sustainability of the GERD region.
5. Informing Agriculturalists within the GERD Region and its vicinity: Sensitize agriculturalists to the impacts of climate change on water resources and agriculture within the GERD region. The common awareness should be on release of information regarding sustainable agriculture technology such as water-saving irrigation devices and soil-saving techniques. As an agricultural expert, it is important to empower farmers with the necessary information and equipment to counter the weather changes so that they continue farming activities keeping production on and conserving water.
6. Collaborative Governance: Promote collaboration among stakeholders, including government agencies, Nongovernmental organization, and local communities, to develop and implement effective water resource management.

References

Abburu, S., & Golla, S. B. (2015). Satellite image classification methods and techniques: A review. International journal of computer applications, 119(8).

Tian, W., Liu, X., Wang, K., Bai, P., & Liu, C. (2021). Estimation of reservoir evaporation losses for China. Journal of Hydrology, 596, 126142.

Zhu, G., Sang, L., Zhang, Z., Sun, Z., Ma, H., Liu, Y., ... & Guo, H. (2021). Impact of landscape dams on river water cycle in urban and peri-urban areas in the Shiyang River Basin: Evidence obtained from hydrogen and oxygen isotopes. Journal of Hydrology, 602, 126779.

Yang, Y., Wang, Y., Cong, N., Wang, N., & Yao, W. (2024). Impacts of the Three Gorges Dam on riparian vegetation in the Yangtze River Basin under climate change. Science of The Total Environment, 912, 169415.

Zulkifli, C. Z., Garfan, S., Talal, M., Alamoodi, A. H., Alamleh, A., Ahmaro, I. Y., ... & Chiang, H. H. (2022). IoT-based water monitoring systems: a systematic review. Water, 14(22), 3621.

Tawfik, R., & Dombrowsky, I. (2017). GERD and hydropolitics in the Eastern Nile: From water-sharing to benefit-sharing?. In The Grand Ethiopian Renaissance Dam and the Nile Basin (pp. 113-137). Routledge.

Aty, M. A. (2022). Managing risks on egypt water resources security: Climate change and grand Ethiopian renaissance dam (GERD) as challenging aspects. Water Security Under Climate Change, 313-330.

Abdallah, S., Abd elmohemen, M., Hemdan, S., & Ibrahem, K. (2019). Assessment of land use/land cover changes induced by Jizan Dam, Saudi Arabia, and their effect on soil organic car-bon. Arabian Journal of Geosciences, 12, 1-11.

Abdelrady, W. A., Elshawy, E. E., Abdelrahman, H. A., Hassan Askri, S. M., Ibrahim, Z., Mansour, M., ... & Shamsi, I. H. (2024). Evaluating Physiological and Yield Indices of Egyptian Barley Cultivars Under Drought Stress Conditions. Agronomy, 14(11), 2711.

Abtew, W., & Melesse, A. (2013). Climate change and evapotranspiration. Evaporation and evapotranspiration: Measurements and estimations, 197-202.

Acquafredda, V. (2022). Regreening Ethiopia beyond climate change and environmental degradation: the political meaning of green legacy. JUNCO| Journal of UNiversities and international development Cooperation, 6(1-2).

Adamala, S., Raghuwanshi, N. S., Mishra, A., & Tiwari, M. K. (2014). Evapotranspiration modeling using second-order neural networks. Journal of Hydrologic Engineering, 19(6), 1131-1140.

Ahmad, A. (2024). Large Dams Establishment Impacts on Different Environmental Aspects: A Review. AUIQ Technical Engineering Science, 1(2), 1.

Ahmad, L., Parvaze, S., Mahdi, S., Dekhle, B., Parvaze, S., Majid, M., & Wani, F. (2017). Comparison of potential evapotranspiration models and establishment of potential evapotranspiration curves for temperate Kashmir Valley. Current Journal of Applied Science and Technology, 24(3), 1-10.

Allen, R. G., Robison, C. W., Huntington, J., Wright, J. L., & Kilic, A. (2020). Applying the FAO-56 dual Kc method for irrigation water requirements over large areas of the Western US. Transactions of the ASABE, 63(6), 2059-2081.

Almeida, D. R., et al. (2019). Agricultural expansion in the Amazon and its impacts on deforestation: A review of the literature. Environmental Science & Policy, 92, 134-144.

Amikuzino, J., & Donkoh, S. A. (2012). Climate variability and yields of major staple food crops in Northern Ghana. African Crop Science Journal, 20, 349-360

Anderegg, W. R. L., et al. (2013). Tree mortality in the western United States: patterns and drivers. Environmental Research Letters, 8(4), 045008.

Awotwi, A., Anornu, G. K., Quaye-Ballard, J. A., Annor, T., Nti, I. K., Odai, S. N., ... & Gyamfi, C. (2021). Impact of post-reclamation of soil by large-scale, small-scale and illegal mining on water balance components and sediment yield: Pra River Basin case study. Soil and Tillage Research, 211, 105026.

Awulachew, S. B., Merrey, D., Van Koopen, B., & Kamara, A. (2010, March). Roles, constraints and opportunities of small-scale irrigation and water harvesting in Ethiopian agricultural development: Assessment of existing situation. In ILRI workshop (pp. 14-16).

Azar, C. (2011). Biomass for energy: a dream come true… or a nightmare?. Wiley Interdisciplinary Reviews: Climate Change, 2(3), 309-323.

Badawy, H. A. (2009). Effect of expected climate changes on evaporation losses from Aswan High Dam Reservoir (AHDR). In Thirteenth international water technology conference, IWTC (Vol. 13, No. 2009, pp. 1-1).

Baldocchi, D. (2008). 'Breathing'of the terrestrial biosphere: lessons learned from a global network of carbon dioxide flux measurement systems. Australian Journal of Botany, 56(1), 1-26.

Bao, Z., Zhang, J., Wang, G., Chen, Q., Guan, T., Yan, X., ... & Wang, J. (2019). The impact of climate variability and land use/cover change on the water balance in the Middle Yellow River Basin, China. Journal of Hydrology, 577, 123942.

Barros, R., et al. (2019). Deforestation and changes in land use due to hydroelectric projects in Brazil.

Bastiaanssen, W. G., Menenti, M., Feddes, R. A., & Holtslag, A. A. M. (1998). A remote sensing surface energy balance algorithm for land (SEBAL). 1. Formulation. Journal of hydrology, 212, 198-212.

Basudeb Bhatta, 2011.Remote Sensing and GIS 2nd edition textbook, from (peg 361_378).

Belay, T., & Mengistu, D. A. (2019). Land use and land cover dynamics and drivers in the Muga watershed, Upper Blue Nile basin, Ethiopia. Remote Sensing Applications: Society and Environment, 15, 100249.

Berhane, A. (2018). Climate change and variability impacts on agricultural productivity and food security. Climate Weather Forecasting, 6(240), 2.

Beyene Dobo, B. D., Fassil Asefa, F. A., & Zebene Asfaw, Z. A. (2018). Effect of tree-enset-coffee based agro-forestry practices on arbuscular mycorrhizal fungi (AMF) species diversity and spore density.

Bisht, S., Singh, H., & Kumar, A. (2024). Ecosystem Services and Maintaining Their Flow in Urban Environments: Nurturing Sustainable Flow in Urban Environments. In Urban Forests, Climate Change and Environmental Pollution (pp. 447-467). Springer, Cham.

Blyth, E., & Harding, R. J. (2011). Methods to separate observed global evapotranspiration into the interception, transpiration and soil surface evaporation components. Hydrological Processes, 25(26), 4063-4068.

Boelens, R., Shah, E., & Bruins, B. (2019). Contested knowledges: Large dams and mega-hydraulic development. Water, 11(3), 416.

Brutsaert, W. (2023). Hydrology: an introduction. Cambridge university press.

Chazdon, R. L. (2008). Beyond deforestation: restoring forests and ecosystem services on degraded lands. science, 320(5882), 1458-1460.

Chen, X., Wang, L., Niu, Z., Zhang, M., Li, C. A., & Li, J. (2020). The effects of projected climate change and extreme climate on maize and rice in the Yangtze River Basin, China. Agricultural and Forest Meteorology, 282, 107867.

Chen, Z., Liu, Z., Yin, L., & Zheng, W. (2022). Statistical analysis of regional air temperature characteristics before and after dam construction. Urban Climate, 41, 101085.

Christofi, D., Metas, C., Evagorou, E., Stylianou, N., Eliades, M., Theocharidis, C., ... & Hadjimitsis, D. (2025). A Review of Open Remote Sensing Data with GIS, AI, and UAV Sup-port for Shoreline Detection and Coastal Erosion Monitoring. Appl. á Sci. á, 15, 4771.

Chu, G., Sun, Q., Zhu, Q., Shan, Y., Shang, W., Ling, Y., ... & Liu, J. (2017). The role of the Asian winter monsoon in the rapid propagation of abrupt climate changes during the last deglaciation. Quaternary Science Reviews, 177, 120-129.

Coe, D., Benítez, N., Broadhurst, T., & MOUSTAkAS, L. A. (2010). A high-resolution mass map of galaxy cluster substructure: Lens Perfect analysis of A1689. The astrophysical journal, 723(2), 1678.

Congalton, R. G., & Green, K. (2019). Assessing the accuracy of remotely sensed data: princi-ples and practices. CRC press.

Cordova, A., Dolci, J., & Gianfrate, G. (2015). The determinants of crowdfunding success: evi-dence from technology projects. Procedia-Social and Behavioral Sciences, 181, 115-124.

Creswell, J. W., Shope, R., Plano Clark, V. L., & Green, D. O. (2006). How interpretive qualita-tive research extends mixed methods research. Research in the Schools, 13(1), 1-11.

Dai, Y., Van Spronsen, J., Witkamp, G. J., Verpoorte, R., & Choi, Y. H. (2013). Natural deep eutectic solvents as new potential media for green technology. Analytica chimica acta, 766, 61-68.

Daly, E., & Porporato, A. (2005). A review of soil moisture dynamics: from rainfall infiltration to ecosystem response. Environmental engineering science, 22(1), 9-24.

Dax, T., et al. (2021). Ecological resilience and shrubland growth in areas affected by agricultur-al abandonment.

Deng, Z., Ciais, P., Tzompa-Sosa, Z. A., Saunois, M., Qiu, C., Tan, C., ... & Chevallier, F. (2022). Comparing national greenhouse gas budgets reported in UNFCCC inventories against atmospheric inversions. Earth System Science Data, 14(4), 1639-1675.

Deressa, T. T., Hassan, R. M., Ringler, C., Alemu, T., & Yesuf, M. (2009). Determinants of farmers' choice of adaptation methods to climate change in the Nile Basin of Ethiopia. Global environmental change, 19(2), 248-255.

Dingman, S. L. (2015). Physical hydrology. Waveland press.

Donohue, K., Rubio de Casas, R., Burghardt, L., Kovach, K., & Willis, C. G. (2010). Germination, post germination adaptation, and species ecological ranges. Annual review of ecology, evolution, and systematics, 41(1), 293-319.

Dube, T., & Frank, L. (2011). Impact of urban expansion and agricultural practices on land cover.

Ekka, A., Pande, S., Jiang, Y., & der Zaag, P. V. (2020). Anthropogenic modifications and river ecosystem services: a landscape perspective. Water, 12(10), 2706.

Elmqvist, T., et al. (2013). Urbanization, biodiversity, and ecosystem services: Challenges and opportunities. In Urbanization, Biodiversity and Ecosystem Services: Challenges and Opportuni-ties (pp. 1-12).

Everard, M. (2019). A socio-ecological framework supporting catchment-scale water resource stewardship. Environmental Science & Policy, 91, 50-59.

Fikadu, G., & Olika, G. (2023). Impact of land use land cover change using remote sensing with integration of socio-economic data on Rural Livelihoods in the Nashe watershed, Ethiopia. Heli-yon, 9(3).

Fischer, E. M., Rajczak, J., & Schär, C. (2012). Changes in European summer temperature variability revisited. Geophysical Research Letters, 39(19).

Franchini, M., Morossi, C., Di Marcantonio, P., Chavez, M., Gilmore, G., Randich, S., ... & Zwitter, T. (2018). Gaia–ESO Survey: INTRIGOSS A New Library of High-resolution Synthetic Spectra. The Astrophysical Journal, 862(2), 146

Funk, C., Peterson, P., Landsfeld, M., Pedreros, D., Verdin, J., Shukla, S., ... & Michaelsen, J. (2015). The climate hazards infrared precipitation with stations a new environmental record for monitoring extremes. Scientific data, 2(1), 1-21.

Gao, H., Yan, C., Liu, Q., Ding, W., Chen, B., & Li, Z. (2019). Effects of plastic mulching and plastic residue on agricultural production: A meta-analysis. Science of the Total Environment, 651, 484-492.

Gao, X., Luo, Y., Lin, Y., & Bao, X. (2022). A source of WRF simulation error for the early-summer warm- sector heavy rainfall over South China coast: Land- sea thermal contrast in the boundary layer. Journal of Geophysical Research: Atmospheres, 127(4), e2021JD035179.

Gelete, G., Gokcekus, H., & Gichamo, T. (2020). Impact of climate change on the hydrology of Blue Nile basin, Ethiopia: a review. Journal of Water and Climate Change, 11(4), 1539-1550.

Ghil, M. (2002). Natural climate variability: Can it be modeled? Climate Dynamics, 18(2), 115-131.

Gibbs, H. K., Ruesch, A. S., Achard, F., Clayton, M. K., Holmgren, P., Ramankutty, N., & Foley, J. A. (2010). Tropical forests were the primary sources of new agricultural land in the 1980s and 1990s. *Proceedings of the National Academy of Sciences*, *107*(38), 16732-16737.

Godfray, H. C. J., Beddington, J. R., Crute, I. R., Haddad, L., Lawrence, D., Muir, J. F., ... & Toulmin, C. (2010). Food security: the challenge of feeding 9 billion people. science, 327(5967), 812-818.

Gordon, L. J., Steffen, W., Jönsson, B. F., Folke, C., Falkenmark, M., & Johannessen, Å. (2005). Human modification of global water vapor flows from the land surface. Proceedings of the National Academy of Sciences, 102(21), 7612-7617.

Gorelick, N., Hancher, M., Dixon, M., Ilyushchenko, S., Thau, D., & Moore, R. (2017). Google Earth Engine: Planetary-scale geospatial analysis for everyone. Remote sensing of Environment, 202, 18-27.

Grill, G., Lehner, B., Lumsdon, A. E., MacDonald, G. K., Zarfl, C., & Liermann, C. R. (2015). An index-based framework for assessing patterns and trends in river fragmentation and flow regulation by global dams at multiple scales. Environmental Research Letters, 10(1), 015001.

Guo, Y., Jia, X., & Paull, D. (2018). Effective sequential classifier training for SVM-based multitemporal remote sensing image classification. IEEE Transactions on Image Processing, 27(6), 3036-3048.

Hamad Bin Khalifa University. (2021). Estimation of potential evapotranspiration in the Rogerm Basin, Niger using different methods. Hydrology, 9(2), 206.

Hammer, D. A., & Bastian, R. K. (2020). Wetlands ecosystems: natural water purifiers? In Constructed wetlands for wastewater treatment (pp. 5-19). CRC Press.

Harary, M. (2024). Efficient algorithms for the sensitivities of the Pearson correlation coefficient and its statistical significance to online data. arXiv preprint arXiv:2405.14686.

Hargreaves, G. H., & Samani, Z. A. (1985). Reference Crop Evapotranspiration from Temperature. Applied Engineering in Agriculture, 1(2), 96-99.

Hassan, Z., Shabbir, R., Ahmad, S. S., Malik, A. H., Aziz, N., Butt, A., & Erum, S. (2016). Dynamics of land use and land cover change (LULCC) using geospatial techniques: a case study of Islamabad Pakistan. Springer Plus, 5(1), 812.

He, J., et al. (2020). Construction of irrigation pipelines effectively improves the water-saving potential in North China: A case study of Zhangye city and beyond. Water, 12(4), 985.

Herbst, M., Rosier, P. T., McNeil, D. D., Harding, R. J., & Gowing, D. J. (2008). Seasonal variability of interception evaporation from the canopy of a mixed deciduous forest. Agricultural and forest meteorology, 148(11), 1655-1667.

Hirschi, M., Davin, E. L., Schwingshackl, C., Wartenburger, R., Meier, R., Gudmundsson, L., & Seneviratne, S. I. (2020). Soil moisture and evapotranspiration. ETH Zurich.

Hoffman, R. R., Mueller, S. T., Klein, G., & Litman, J. (2018). Metrics for explainable AI: Challenges and prospects. arXiv preprint arXiv:1812.04608.

Holl, K. D., & Aide, T. M. (2011). When and where to actively restore ecosystems. Forest ecology and management, 261(10), 1558-1563.

Holmberg, M., Junttila, V., Schulz, T., Grönroos, J., Paunu, V. V., Savolahti, M., ... & Forsius, M. (2023). Role of land cover in Finland's greenhouse gas emissions. Ambio, 52(11), 1697-1715.

Huete, A., Didan, K., Miura, T., Rodriguez, E. P., Gao, X., & Ferreira, L. G. (2002). Overview of the radiometric and biophysical performance of the MODIS vegetation indices. Remote sensing of environment, 83(1-2), 195-213.

Hurni, H., Abate, S., Bantider, A., Debele, B., Ludi, E., Portner, B., ... & Zeleke, G. (2010). Land degradation and sustainable land management in the highlands of Ethiopia.

Hussain, S., Mubeen, M., Akram, W., Ahmad, A., Habib-ur-Rahman, M., Ghaffar, A., ... & Nasim, W. (2020). Study of land cover/land use changes using RS and GIS: a case study of Multan district, Pakistan. Environmental monitoring and assessment, 192, 1-15.

Hwang, S. J., Lee, S. W., Son, J. Y., Park, G. A., & Kim, S. J. (2007). Moderating effects of the geometry of reservoirs on the relation between urban land use and water quality. Landscape and Urban Planning, 82(4), 175-183.

Irmak, A., Singh, R. K., Walter-Shea, E. A., Verma, S. B., & Suyker, A. E. (2011). Comparison and analysis of empirical equations for soil heat flux for different cropping systems and irrigation methods. Transactions of the ASABE, 54(1), 67-80.

Irmak, S., & Kukal, M. S. (2022). Evapotranspiration, Transpiration, and Evaporation Processes and Modeling in the Soil Residue Canopy System. Modeling Processes and Their Interactions in Cropping Systems: Challenges for the 21st Century, 53-114.

Jackson, R. B., Schenk, H. J., Jobbagy, E. G., Canadell, J., Colello, G. D., Dickinson, R. E., ... & Sykes, M. T. (2000). Belowground consequences of vegetation change and their treatment in models. Ecological applications, 10(2), 470-483.

Jeuland, M., Wu, X., & Whittington, D. (2020). Infrastructure development and the economics of cooperation in the Eastern Nile. In A River Flows Through It (pp. 182-202). Routledge.

Jiang, M., et al. (2018). Relationships between urban growth and land use changes in China. Sustainable Cities and Society, 39, 1-10.

Juárez, M. L. A., Ignacio, M. F. H., Silvestre, S. L. R., Romero, J. O., & Elizondo, E. C. (2022). Evaluation of the capacity of PET bottles, water aeration, and water recirculation to reduce evaporation in containers of water. Journal of King Saud University-Science, 34(4), 102046.

Jung, M., Reichstein, M., Ciais, P., Seneviratne, S. I., Sheffield, J., Goulden, M. L., ... & Zhang, K. (2010). Recent decline in the global land evapotranspiration trend due to limited moisture supply. Nature, 467(7318), 951-954.

Kambale, J. B., Nemichandrappa, M., Dandekar, A. T., & Basavaraja, D. (2022). Spatio-temporal variability and climate change impact on the crop water requirement of pigeonpea (Cajanus cajan)-A case study, north-eastern Karnataka, India. Legume Research-An International Journal, 45(6), 780-789.

Kang, T., Li, Z., & Gao, Y. (2021). Spatiotemporal variations of reference evapotranspiration and its determining climatic factors in the Taihang mountains, China. Water, 13(21), 3145.

Lal, R., Sivakumar, M. V., Faiz, S. M. A., Rahman, A. M., & Islam, K. R. (Eds.). (2010). Climate change and food security in South Asia. Springer Science & Business Media.

Lambin, E. F., Geist, H. J., & Lepers, E. (2003). Dynamics of land-use and land-cover change in tropical regions. Annual review of environment and resources, 28(1), 205-241.

Lawrence, D., D'Odorico, P., Diekmann, L., DeLonge, M., Das, R., & Eaton, J. (2007). Ecological feedbacks following deforestation create the potential for a catastrophic ecosystem shift in tropical dry forest. Proceedings of the National Academy of Sciences, 104(52), 20696-20701.

Li, G., Zhang, F., Jing, Y., Liu, Y., & Sun, G. (2017). Response of evapotranspiration to changes in land use and land cover and climate in China during 2001–2013. Science of the Total Environment, 596, 256-265.

Li, S., Wang, G., Sun, S., Hagan, D. F. T., Chen, T., Dolman, H., & Liu, Y. (2021). Long-term changes in evapotranspiration over China and attribution to climatic drivers during 1980–2010. Journal of Hydrology, 595, 126037.

Li, Z., Tang, R., Wan, Z., Bi, Y., Zhou, C., Tang, B., Yan, G., & Zhang, X. (2021). A review of current methodologies for regional evapotranspiration estimation from remotely sensed data. Sensors, 9(5), 3801-3853

Liebscher, P. (1998). Quantity with quality? Teaching quantitative and qualitative methods in an LIS master's program

Lillesand, T., Kiefer, R. W., & Chipman, J. (2015). Remote sensing and image interpretation. John Wiley & Sons.

Liu, B., Gao, X., Ma, J., Jiao, Z., Xiao, J., Hayat, M. A., & Wang, H. (2019). Modeling the present and future distribution of arbovirus vectors Aedes aegypti and Aedes albopictus under climate change scenarios in Mainland China. Science of the Total Environment, 664, 203-214.

Liu, X., et al. (2014). Challenges of managing land resources in the face of rapid development and environmental changes.

Liu, Z. (2022). Estimating land evapotranspiration from potential evapotranspiration constrained by soil water at daily scale. Science of the Total Environment, 834, 155327.

Lotsch, A., Friedl, M. A., Anderson, B. T., & Tucker, C. J. (2003). Coupled vegetation-precipitation variability observed from satellite and climate records. Geophysical Research Letters, 30(14).

Lu, N., Chen, S., Wilske, B., Sun, G., & Chen, J. (2011). Evapotranspiration and soil water relationships in a range of disturbed and undisturbed ecosystems in the semi-arid Inner Mongolia, China. Journal of Plant Ecology, 4(1-2), 49-60.

Ma, W. X., Huang, T. L., Li, X., Zhang, H. H., & Ju, T. (2015). Impact of short-term climate variation and hydrology change on thermal structure and water quality of a canyon-shaped, stratified reservoir. Environmental Science and Pollution Research, 22, 18372-18380.

Mahmud, A. A., Sultana, N., & Habib, M. E. Application of the Analytical Hierarchy Process for Comprehensive Flood Susceptibility Mapping in a Rapidly Developing Industrial Zone of Bangladesh. Available at SSRN 4978180.

Mastrorillo, M., Licker, R., Bohra-Mishra, P., Fagiolo, G., Estes, L. D., & Oppenheimer, M. (2016). The influence of climate variability on internal migration flows in South Africa. Global Environmental Change, 39, 155-169.

McDonald, A. J., et al. (2018). Water management and the role of ecosystems: Moving towards a sustainable future. Water Policy, 20(4), 781-803.

Mekonnen, M. M., & Hoekstra, A. Y. (2016). Four billion people facing severe water scarcity. Science advances, 2(2), e1500323.

Mekuria, W., Langan, S., Noble, A., & Johnston, R. (2017). Soil restoration after seven years of exclosure management in northwestern Ethiopia. Land degradation & development, 28(4), 1287-1297.

Mendicino, G., & Senatore, A. (2012). The Role of Evapotranspiration in the Framework of Water Resource Management and Planning Under Shortage Conditions. Evapotranspiration-Remote Sensing and Modeling.

Mengistu, A. G., Tesfuhuney, W. A., Woyessa, Y. E., Ejigu, A. A., & Alemu, M. D. (2025). Contrasting hydro-climatic trends and drought dynamics in Ethiopia and South Africa under climate change. Climate Dynamics, 63(2), 105.

Mishra, R. K. (2023). Fresh water availability and its global challenge. British Journal of Multidisciplinary and Advanced Studies, 4(3), 1-78.

Moreda, T. (2023). The social dynamics of access to land, livelihoods and the rural youth in an era of rapid rural change: Evidence from Ethiopia. Land Use Policy, 128, 106616.

Morid, S., & Bavani, A. R. M. (2010). Exploration of potential adaptation strategies to climate change in the Zayandeh Rud irrigation system, Iran. Irrigation and Drainage: The journal of the International Commission on Irrigation and Drainage, 59(2), 226-238.

Mostafa, H., Saleh, H., El Sheikh, M., & Kheireldin, K. (2016). Assessing the impacts of climate changes on the eastern Nile flow at Aswan. Journal of American Science, 12(1), 1-9.

Mu, Q., Zhao, M., Kimball, J. S., McDowell, N. G., & Running, S. W. (2013). A remotely sensed global terrestrial drought severity index. Bulletin of the American Meteorological Society, 94(1), 83-98.

Mu, S., Zhou, S., Chen, Y., Li, J., Ju, W., & Odeh, I. O. A. (2013). Assessing the impact of restoration-induced land conversion and management alternatives on net primary productivity in Inner Mongolian grassland, China. Global and Planetary Change, 108, 29-41.

Mumo, L., Yu, J., & Fang, K. (2018). Assessing impacts of seasonal climate variability on maize yield in Kenya. International Journal of Plant Production, 12(4), 297-307.

Nannawo, A. S., Lohani, T. K., Eshete, A. A., & Ayana, M. T. (2022). Evaluating the dynamics of hydroclimate and streamflow for data-scarce areas using MIKE11-NAM model in Bilate river basin, Ethiopia. Modeling Earth Systems and Environment, 8(4), 4563-4578.

Nassali, J., Yongji, Z., & Fangninou, F. (2020). Land cover change patterns resulting from dam construction around Lake Victoria.

Negash, S., et al. (2023). Land use land cover changes in Ethiopia: A focus on the Akaki catchment.

New, T., & Xie, Z. (2008). Impacts of large dams on riparian vegetation: applying global experience to the case of China's Three Gorges Dam. Biodiversity and Conservation, 17, 3149-3163.

Ngongondo, C., Li, L., Gong, L., Xu, C. Y., & Alemaw, B. F. (2013). Flood frequency under changing climate in the upper Kafue River basin, southern Africa: a large-scale hydrological model application. Stochastic Environmental Research and Risk Assessment, 27, 1883-1898.

Niang, A., Becker, M., Ewert, F., Tanaka, A., Dieng, I., & Saito, K. (2018). Yield variation of rainfed rice as affected by field water availability and N fertilizer use in central Benin. Nutrient Cycling in Agroecosystems, 110, 293-305.

Nouri, H., Glenn, E. P., Beecham, S., Chavoshi Boroujeni, S., Sutton, P., Alaghmand, S., ... & Nagler, P. (2016). Comparing three approaches of evapotranspiration estimation in mixed urban vegetation: Field-based, remote sensing-based and observational-based methods. Remote Sensing, 8(6), 492.

Novák, V. (2012). Evapotranspiration in the soil-plant-atmosphere system. Springer Science & Business Media.

Ouko, A. (2017). Civil conflict and its impact on deforestation and land use in the Democratic Republic of the Congo.

Ozdogan, M., Woodcock, C. E., Salvucci, G. D., & Demir, H. (2006). Changes in summer irrigated crop area and water use in Southeastern Turkey from 1993 to 2002: Implications for current and future water resources. Water resources management, 20, 467-488.

Pagano, T., & Sorooshian, S. (2002). Hydrologic cycle. University of Arizona. Tucson. AZ. USA.

Passioura, J. B., & Angus, J. F. (2010). Improving productivity of crops in water-limited environments. Advances in agronomy, 106, 37-75.

Pathak, A., Paul, S., & Ghosh, S. (2018). Land-Surface Feedback and Impacts of Land-Use Change to Indian Monsoon. Climate Change Signals and Response: A Strategic Knowledge Compendium for India, 3.

Peiman, R. (2011). Pre-classification and post-classification change-detection techniques to monitor land-cover and land-use change using multi-temporal Landsat imagery: a case study on Pisa Province in Italy. International journal of remote sensing, 32(15), 4365-4381.

Pelletier, C., Valero, S., Inglada, J., Champion, N., & Dedieu, G. (2016). Assessing the robustness of Random Forests to map land cover with high resolution satellite image time series over large areas. Remote Sensing of Environment, 187, 156-168.

Pereira, L. S., Perrier, A., Allen, R. G., & Alves, I. (1999). Evapotranspiration: concepts and future trends. Journal of irrigation and drainage engineering, 125(2), 45-51.

Porter, J. R., et al. (2014). Food security and food production systems in climate change. In Climate Change 2014: Impacts, Adaptation, and Vulnerability (pp. 1-45). Cambridge University Press.

Priyan, K. (2021). Issues and challenges of groundwater and surface water management in semi-arid regions. Groundwater resources development and planning in the semi-arid region, 1-17.

Qiu, G. Y., Zou, Z., Li, X., Li, H., Guo, Q., Yan, C., & Tan, S. (2017). Experimental studies on the effects of green space and evapotranspiration on urban heat island in a subtropical megacity in China. Habitat international, 68, 30-42.

Rahayuningsih, T., Idfi, G., & Anindyasari, A. (2019, November). The dominant factor causing potential evapotranspiration in Malang raya using geographic information systems. In IOP Conference Series: Materials Science and Engineering (Vol. 669, No. 1, p. 012048). IOP Publishing.

Ramamurthy, P., & Bou- Zeid, E. (2014). Contribution of impervious surfaces to urban evaporation. Water Resources Research, 50(4), 2889-2902.

Rosegrant, M. W. (1997). Water resources in the twenty-first century: Challenges and implications for action (Vol. 20). Intl Food Policy Res Inst.

Saatchi, S., Marlier, M., Chazdon, R. L., Clark, D. B., & Russell, A. E. (2011). Impact of spatial variability of tropical forest structure on radar estimation of aboveground biomass. Remote sensing of environment, 115(11), 2836-2849.

Said, M., Hyandye, C., Komakech, H. C., Mjemah, I. C., & Munishi, L. K. (2021). Predicting land use/cover changes and its association to agricultural production on the slopes of Mount Kilimanjaro, Tanzania. Annals of GIS, 27(2), 189-209.

Schlosser, C. A., & colleagues. (2014). The impact of climate change on hydrology and water resources. Global Environmental Change, 25, 81-93.

Schober, P., Boer, C., & Schwarte, L. A. (2018). Correlation coefficients: appropriate use and interpretation. Anesthesia & analgesia, 126(5), 1763-1768.

Sellers, P. J., Randall, D. A., Collatz, G. J., Berry, J. A., Field, C. B., Dazlich, D. A., ... & Bounoua, L. (1996). A revised land surface parameterization (SiB2) for atmospheric GCMs. Part I: Model formulation. Journal of climate, 9(4), 676-705.

Senay, G. B., Bohms, S., Singh, R. K., Gowda, P. H., Velpuri, N. M., Alemu, H., & Verdin, J. P. (2013). Operational evapotranspiration mapping using remote sensing and weather datasets: A new parameterization for the SSEB approach. JAWRA Journal of the American Water Resources Association, 49(3), 577-591.

Seneviratne, S. I., Corti, T., Davin, E. L., Hirschi, M., Jaeger, E. B., Lehner, I., ... & Teuling, A. J. (2010). Investigating soil moisture–climate interactions in a changing climate: A review. Earth-Science Reviews, 99(3-4), 125-161.

Seto, K. C., Generally, B., & Hutyra, L. R. (2012). Global forecasts of urban expansion to 2030 and direct impacts on biodiversity and carbon pools. Proceedings of the National Academy of Sciences, 109(40), 16083-16088.

Shah, A., Ali, K., & Nizami, S. M. (2021). Four decadal urban land degradation in Pakistan a case study of capital city islamabad during 1979–2019. Environmental and sustainability indicators, 10, 100108.

Sherwood, S. C., Roca, R., Weckwerth, T. M., & Andronova, N. G. (2010). Tropospheric water vapor, convection, and climate. Reviews of Geophysics, 48(2).

Shuka, K. A. M., Ke, W., Sohail Nazar, M., Abubakar, G. A., & Shahtahamssebi, A. (2022). Impact of hydrological infrastructure projects on land use/cover and socioeconomic development in arid regions Evidence from the upper Atbara and Setit Dam Complex, Kassala, Eastern Sudan. Sustainability, 14(6), 3422.

Sinclair, F., Wezel, A., Mbow, C., Chomba, S., Robiglio, V., & Harrison, R. (2019). The contribution of agroecological approaches to realizing climate-resilient agriculture. GCA: Rotterdam, The Netherlands.

Singh, N., Singh, J., Gupta, A. K., Bräuning, A., Dimri, A. P., Ramanathan, A. L., ... & Raja, P. (2021). Climate-driven acceleration in forest evapotranspiration fuelling extreme rainfall events in the Himalaya. Environmental Research Letters, 16(8), 084042.

Sinha, A., Huang, V., Livingstone, J., Wang, J., Fox, N. S., Kurganovs, N., ... & Boutros, P. C. (2019). The proteogenomic landscape of curable prostate cancer. Cancer Cell, 35(3), 414-427.

Sivakumar, B. (2011). Global climate change and its impacts on water resources planning and management: assessment and challenges. Stochastic Environmental Research and Risk Assessment, 25, 583-600.

Solomon, T., & Hyunshik, M. (2024). Trends of forest cover and prospects of Great Ethiopian Renaissance Dam (GERD) to Ethiopia and the downstream countries. Journal of Infrastructure, Policy and Development, 8(9), 6424.

Song, C., Wu, L., Xie, Y., He, J., Chen, X., Wang, T., ... & Mao, H. (2017). Air pollution in China: Status and spatiotemporal variations. Environmental pollution, 227, 334-347.

Srivastava, P. K., Han, D., Islam, T., Petropoulos, G. P., Gupta, M., & Dai, Q. (2016). Seasonal evaluation of evapotranspiration fluxes from MODIS satellite and mesoscale model downscaled global reanalysis datasets. Theoretical and Applied Climatology, 124, 461-473.

Stonestrom, D. A., Scanlon, B. R., & Zhang, L. (2009). Introduction to special section on impacts of land use change on water resources. Water resources research, 45(7).

Tan, S., Wang, H., Prentice, I. C., & Yang, K. (2021). Land-surface evapotranspiration derived from a first-principles primary production model. Environmental Research Letters, 16(10), 104047.

Tardieu, L., Roussel, S., Thompson, J. D., Labarraque, D., & Salles, J. M. (2015). Combining direct and indirect impacts to assess ecosystem service loss due to infrastructure construction. Journal of Environmental Management, 152, 145-157.

Tasgara, T. D., & Kumar, B. (2023). Assessment of land use/land cover change impact on stream-flow: a case study over upper Guder Catchment, Ethiopia. Sustainable Water Resources Man-agement, 9(1), 6.

Tesfaye, K., Kruseman, G., Cairns, J. E., Zaman-Allah, M., Wegary, D., Zaidi, P. H., ... & Erenstein, O. (2018). Potential benefits of drought and heat tolerance for adapting maize to climate change in tropical environments. Climate risk management, 19, 106-119.

Tewabe, D., & Fentahun, T. (2020). Assessing land use and land cover change detection using remote sensing in the Lake Tana Basin, Northwest Ethiopia. Cogent Environmental Science, 6(1), 1778998.

Thambawita, T. K. C. N., Munasinghe, D. S., & Yapa, L. K. K. (2023). Identification of Urban Heat Island Effect on Land Use Land Cover Changes. Journal of Geospatial Surveying, 3(2).

Thomas, R., & Hardy, C. (2011). Reframing resistance to organizational change. Scandinavian journal of management, 27(3), 322-331.

Thornton, P. K., & Herrero, M. (2010). Potential for reduced methane and carbon dioxide emissions from livestock and pasture management in the tropics. Proceedings of the National Academy of Sciences, 107(46), 19667-19672.

Trenberth, K. E. (2011). Changes in precipitation with climate change. Climate research, 47(1-2), 123-138.

Urama, K., & Ozor, N. (2011). Agricultural innovations for climate change adaptation and food security in Western and Central Africa. Agro-Science, 10(1).

Vanham, D., Hoekstra, A. Y., Wada, Y., Bouraoui, F., de Roo, A., Mekonnen, M. M., ... & Bidoglio, G. (2018). Physical water scarcity metrics for monitoring progress towards SDG target 6.4: An evaluation of indicator 6.4. 2 "Level of water stress". Science of the total environment, 613, 218-232.

Vicente-Serrano, S. M., Lopez-Moreno, J. I., Beguería, S., Lorenzo-Lacruz, J., Sanchez-Lorenzo, A., García-Ruiz, J. M., ... & Espejo, F. (2014). Evidence of increasing drought severity caused by temperature rise in southern Europe. Environmental Research Letters, 9(4), 044001.

Wang, D., Wang, F., Huang, Y., Duan, X., Liu, J., Hu, B., ... & Chen, J. (2018). Examining the effects of hydropower station construction on the surface temperature of the Jinsha River Dry-Hot Valley at different seasons. Remote Sensing, 10(4), 600.

Wang, X., Yang, G., Feng, Y., Ren, G., & Han, X. (2012). Optimizing feeding composition and carbon–nitrogen ratios for improved methane yield during anaerobic co-digestion of dairy, chicken manure and wheat straw. Bioresource technology, 120, 78-83.

Wang, Y., Li, Z., Feng, Q., Si, L., Gui, J., Cui, Q., ... & Xu, C. (2024). Global evapotranspiration from high-elevation mountains has decreased significantly at a rate of 3.923%/a over the last 22 years. Science of The Total Environment, 931, 172804.

Wang, Z., Li, Y., Zhang, J., & Wang, L. (2020). Estimation of evapotranspiration using remote sensing data: A review. Remote Sensing, 12(7), 1191

Wanniarachchi, S., & Sarukkalige, R. (2022). A review on evapotranspiration estimation in agricultural water management: Past, present, and future. Hydrology, 9(7), 123.

Welde, K., & Gebremariam, B. (2017). Effect of land use land cover dynamics on hydrological response of watershed: Case study of Tekeze Dam watershed, northern Ethiopia. International Soil and Water Conservation Research, 5(1), 1-16.

Weng, X. Z., Chen, X. L., Deng, W. Z., & Zhu, S. L. (2019). Hidden-charm pentaquarks and P c states. Physical Review D, 100(1), 016014.

World Bank (2020). Water management and its impact on downstream ecosystems: Case study of the GERD.

Wu, G., Hu, Z., Keenan, T. F., Li, S., Zhao, W., Cao, R. C., ... & Sun, X. (2020). Incorporating spatial variations in parameters for improvements of an evapotranspiration model. Journal of Geophysical Research: Bio geosciences, 125(11), e2019JG005504.

Xu, C. Y., & Singh, V. P. (2001). Evaluation and generalization of temperature- based methods for calculating evaporation. Hydrological processes, 15(2), 305-319.

Yeh, H. F. (2017). Comparison of Evapotranspiration Methods Under. Current Perspective to Predict Actual Evapotranspiration, 1.

Yeshaneh, E., Wagner, W., Exner-Kittridge, M., Legesse, D., & Blöschl, G. (2013). Identifying land use/cover dynamics in the Koga catchment, Ethiopia, from multi-scale data, and implications for environmental change. ISPRS International Journal of Geo-Information, 2(2), 302-323.

Yesuph, A. Y., & Dagnew, A. B. (2019). Land use/cover spatiotemporal dynamics, driving forces and implications at the Beshillo catchment of the Blue Nile Basin, North Eastern Highlands of Ethiopia. Environmental Systems Research, 8(1), 1-30.

Yihdego, Y., Vaheddoost, B., & Al-Weshah, R. A. (2019). Drought indices and indicators revisited. Arabian Journal of Geosciences, 12, 1-12.

Zeng, L., Schmitt, R. W., Li, L., Wang, Q., & Wang, D. (2019). Forecast of summer precipitation in the Yangtze River Valley based on South China Sea springtime sea surface salinity. Climate Dynamics, 53(9), 5495-5509.

Zeng, Y., Zhou, Z., Yan, Z., Teng, M., & Huang, C. (2019). Climate change and its attribution in three gorges reservoir area, China. Sustainability, 11(24), 7206.

Zeng, Z., Estes, L., Ziegler, A. D., Chen, A., Searchinger, T., Hua, F., ... & F. Wood, E. (2018). Highland cropland expansion and forest loss in Southeast Asia in the twenty-first century. Nature Geoscience, 11(8), 556-562.

Zeppel, M. J., Harrison, S. P., Adams, H. D., Kelley, D. I., Li, G., Tissue, D. T., ... & McDowell, N. G. (2015). Drought and resprouting plants. New Phytologist, 206(2), 583-589.

Zhang, G., Yao, T., Xie, H., Yang, K., Zhu, L., Shum, C. K., ... & Ke, C. (2020). Response of Tibetan Plateau lakes to climate change: Trends, patterns, and mechanisms. Earth-Science Reviews, 208, 103269.

Zhang, J., Terrones, M., Park, C. R., Mukherjee, R., Monthioux, M., Koratkar, N., ... & Bianco, A. (2016). Carbon science in 2016: Status, challenges and perspectives. Carbon, 98, 708-732.

Zhang, Y., et al. (2020). Impacts of the Three Gorges Dam on land cover and local ecosystems in China.

Zhang, Y., Moges, S., & Block, P. (2018). Does objective cluster analysis serve as a useful precursor to seasonal precipitation prediction at local scale? Application to western Ethiopia. Hydrology and Earth System Sciences, 22(1), 143-157.

Zhang, Y., Qi, P., & Manning, C. D. (2018). Graph convolution over pruned dependency trees improves relation extraction. arXiv preprint arXiv:1809.10185.

Zhao, M., Golaz, J. C., Held, I. M., Guo, H., Balaji, V., Benson, R., ... & Xiang, B. (2018). The GFDL global atmosphere and land model AM4. 0/LM4. 0: 2. Model description, sensitivity studies, and tuning strategies. Journal of Advances in Modeling Earth Systems, 10(3), 735-769.

Zhao, X., et al. (2020). Reforestation in China: A review of progress and prospects. Forest Ecology and Management, 464, 118059.

Zhou, H., Xu, F., Dong, J., Yang, Z., Zhao, G., Zhai, J., ... & Xiao, X. (2019). Tracking reforestation in the Loess Plateau, China after the “Grain for Green” Project through integrating PALSAR and Landsat imagery. Remote Sensing, 11(22), 2685.

Zhou, Q., Zhang, H., Fu, C., Zhou, Y., Dai, Z., Li, Y., ... & Luo, Y. (2018). The distribution and morphology of microplastics in coastal soils adjacent to the Bohai Sea and the Yellow Sea. Geoderma, 322, 201-208

Zhu, B., Zhang, Q., Yang, J. H., & Li, C. H. (2022). Response of potential evapotranspiration to warming and wetting in Northwest China. Atmosphere, 13(2), 353.

APPENDEX

This code performs land use/land cover classification in Google Earth Engine by preprocessing landsat imagery, using training data, and applying a Random Forest classifier.

```
Imports (15 entries)
var Forest: FeatureCollection (60 elements)
var water: FeatureCollection (68 elements)
var Shrubland: FeatureCollection (51 elements)
var builtup: FeatureCollection (61 elements)
var Agriculture: FeatureCollection (52 elements)
var Forest1: FeatureCollection (70 elements)
var water1: FeatureCollection (59 elements)
var Shrubland1: FeatureCollection (58 elements)
var builtup1: FeatureCollection (64 elements)
var Agriculture1: FeatureCollection (55 elements)
var Forest2: FeatureCollection (64 elements)
var water2: FeatureCollection (66 elements)
var shrubland2: FeatureCollection (56 elements)
var builtup2: FeatureCollection (76 elements)
var Agriculture2: FeatureCollection (54 elements)
// Load your boundary asset
var boundary = ee.FeatureCollection('projects/ee-enatihuny/assets/enat');

// Define the date ranges for the years
var startDate2001 = '2001-01-01';
var endDate2001 = '2001-12-31';
var startDate2012 = '2012-01-01';
var endDate2012 = '2012-12-31';
var startDate2023 = '2023-01-01';
var endDate2023 = '2023-12-31';
```

```
// Load the Landsat Collection 2 ImageCollections
var landsat7 = ee.ImageCollection('LANDSAT/LE07/C02/T1');
var landsat8 = ee.ImageCollection('LANDSAT/LC08/C02/T1');

// Function to filter, mask clouds, and create a median composite for Landsat 7
function createCompositeLandsat7(startDate, endDate) {
  var filtered = landsat7
    .filterDate(startDate, endDate)
    .filterBounds(boundary);

  function maskClouds(image) {
    var cloudMask = image.select('QA_PIXEL');
    var clouds = cloudMask.bitwiseAnd(1 << 4).eq(0); // Clouds
    var cloudShadows = cloudMask.bitwiseAnd(1 << 3).eq(0); // Cloud shadows
    return image.updateMask(clouds).updateMask(cloudShadows);
  }

  var cloudFree = filtered.map(maskClouds);

  // Create a median composite
  var composite = cloudFree.median().clip(boundary);

  // Handle scanline gaps
  var gapFilledComposite = composite.unmask(calculateGapFill(composite, cloudFree));

  return gapFilledComposite;
}


function calculateGapFill(original, cloudFree) {
  // Use the cloud-free collection to fill gaps
  var filled = cloudFree.median().clip(boundary);

  // Create a mask from the original composite
  var mask = original.mask(); // Mask to identify valid pixels

  // Replace missing values (value equals zero) with cloud-free image values
  return original.unmask(filled); // Fill gaps where original is missing with filled
}

// Function to filter, mask clouds, and create a median composite for Landsat 8
function createCompositeLandsat8(startDate, endDate) {
  var filtered = landsat8
    .filterDate(startDate, endDate)
    .filterBounds(boundary);

  var composite = filtered.median().clip(boundary);
  return composite;
}

// Create composites for the years (using Landsat 7 for 2001 now)
var landsat7Composite2001 = createCompositeLandsat7(startDate2001, endDate2001);
var landsat7Composite2012 = createCompositeLandsat7(startDate2012, endDate2012);
var landsat8Composite2023 = createCompositeLandsat8(startDate2023, endDate2023);
```

```
// Define visualization parameters
var visParams = {
  bands: ['B4', 'B3', 'B2'],  // True color visualization (RGB)
  min: 0,
  max: 3000
};

// Optional: Export the composite images to Google Drive
Export.image.toDrive({
  image: landsat7Composite2001,
  description: 'Landsat7_Composite_2001',
  scale: 30,
  region: boundary.geometry(),
  maxPixels: 1e13
});

Export.image.toDrive({
  image: landsat7Composite2012,
  description: 'Landsat7_Composite_2012',
  scale: 30,
  region: boundary.geometry(),
  maxPixels: 1e13
});
```

v

```
Export.image.toDrive({
  image: landsat8Composite2023,
  description: 'Landsat8_Composite_2023',
  scale: 30,
  region: boundary.geometry(),
  maxPixels: 1e13
});

// Define training points for each year
var trainingPoints2001 = water.merge(Forest).merge(Shrubland).merge(builtup).merge(Agriculture);
var trainingPoints2012 = Forest1.merge(water1).merge(Shrubland1).merge(builtup1).merge(Agriculture1);
var trainingPoints2023 = Forest2.merge(water2).merge(shrubland2).merge(builtup2).merge(Agriculture2);

// Sample the images for training
var training2001 = landsat7Composite2001.sampleRegions({
  collection: trainingPoints2001,
  properties: ['land'],  // Ensure class labels are in the 'land' property
  scale: 30
});
```

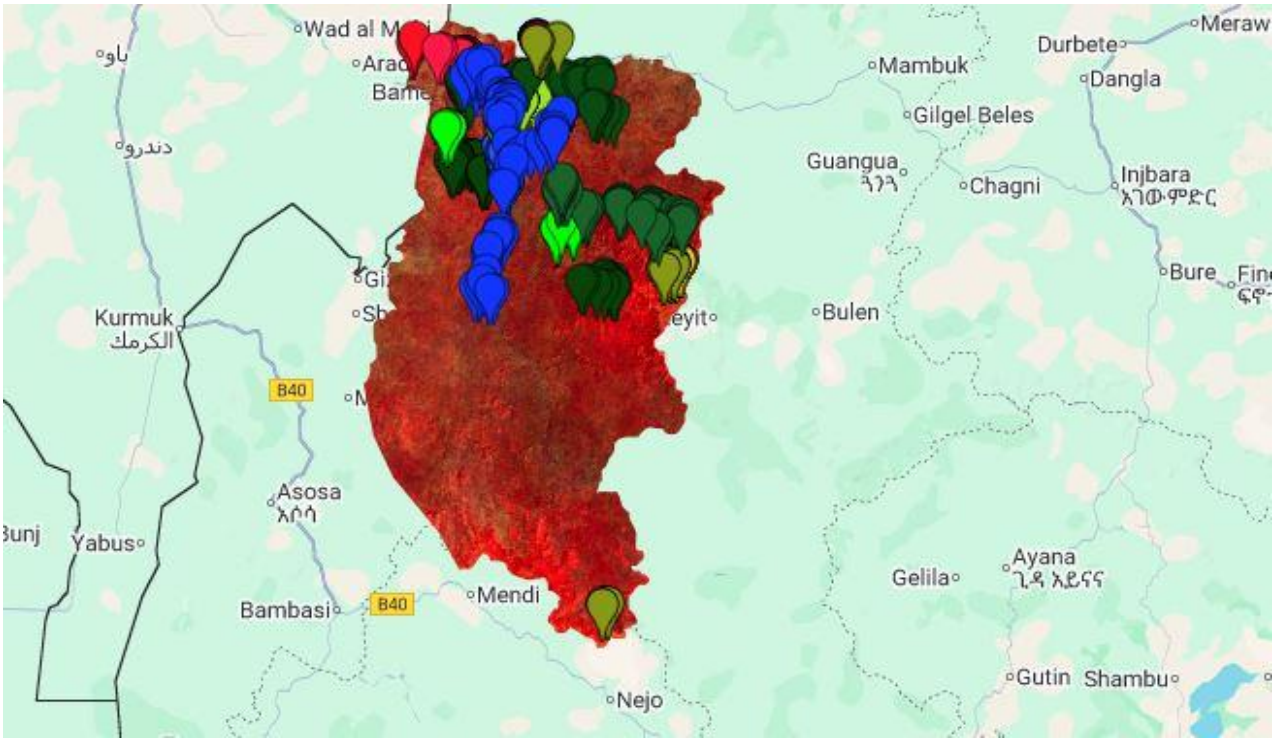


```
var training2012 = landsat7Composite2012.sampleRegions({
  collection: trainingPoints2012,
  properties: ['land'],
  scale: 30
});

var training2023 = landsat8Composite2023.sampleRegions({
  collection: trainingPoints2023,
  properties: ['land'],
  scale: 30
});

// Train the classifier using a Random Forest method for each year
var classifier2001 = ee.Classifier.smileRandomForest(50).train({
  features: training2001,
  classProperty: 'land',
  inputProperties: ['B4', 'B3', 'B2']  // Choose appropriate bands for classification
});

var classifier2012 = ee.Classifier.smileRandomForest(50).train({
  features: training2012,
  classProperty: 'land',
  inputProperties: ['B4', 'B3', 'B2']
});
```

```
var classifier2023 = ee.Classifier.smileRandomForest(50).train({
  features: training2023,
  classProperty: 'land',
  inputProperties: ['B4', 'B3', 'B2']
});

// Classify the images using the trained classifiers
var classified2001 = landsat7Composite2001.classify(classifier2001);
var classified2012 = landsat7Composite2012.classify(classifier2012);
var classified2023 = landsat8Composite2023.classify(classifier2023);

// Define visualization parameters for classified images
var classifiedVisParams2001 = {
  min: 0,
  max: 4, // Adjust based on the number of classes
  palette: [
    '#2a4700',  // forest (green)
    '#033fd6',  // water (blue)
    '#ff1d56',  // builtup (red)
    '#ffe923',  // Agriculture (yellow)
    '#2efb1b',  // shrubland (light blue)
  ]
};


var classifiedVisParams2012 = {
  min: 0,
  max: 4, // Adjust this based on the number of classes you have for 2012
  palette: [
    '#0a4b11',  // Forest1 (green)
    '#2156ff',  // Water1 (blue)
    '#ff1949',  // builtup1 (red)
    '#889916',  // Agriculture1 (yellow)
    '#00ff00',  // Shrubland1 (light blue)
  ]
};

var classifiedVisParams2023 = {
  min: 0,
  max: 4, // Adjust this based on the number of classes you have for 2023
  palette: [
    '#19642b',  // Forest2 (green)
    '#1336ff',  // Water2 (blue)
    '#ff135a',  // builtup2 (red)
    '#fffd2d',  // Agriculture2 (yellow)
    '#13ff4b',  // Shrubland2 (light blue)
  ]
};

// Visualize the classified images for each year
Map.addLayer(classified2001, classifiedVisParams2001, 'Classified 2001');
Map.addLayer(classified2012, classifiedVisParams2012, 'Classified 2012');
Map.addLayer(classified2023, classifiedVisParams2023, 'Classified 2023');
```

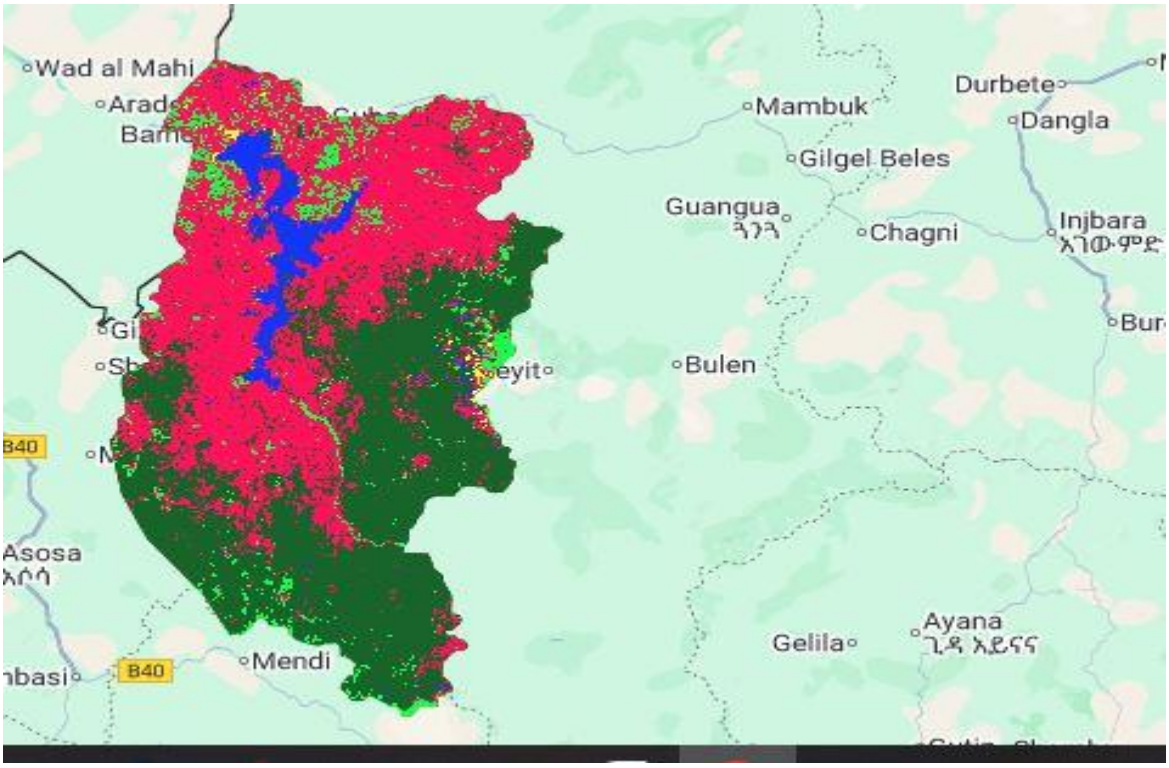


```
// Optional: Center the map on your area of interest for better visualization
Map.centerObject(boundary, 8);

// Export the classified images to Google Drive
Export.image.toDrive({
  image: classified2001,
  description: 'Classified_Image_2001',
  scale: 30,
  region: boundary.geometry(),
  maxPixels: 1e13 // Adjust if necessary
});

Export.image.toDrive({
  image: classified2012,
  description: 'Classified_Image_2012',
  scale: 30,
  region: boundary.geometry(),
  maxPixels: 1e13
});

Export.image.toDrive({
  image: classified2023,
  description: 'Classified_Image_2023',
  scale: 30,
  region: boundary.geometry(),
  maxPixels: 1e13
});
```

```
// Function to split the training points into training and validation sets
function splitTrainingValidation(trainingPoints) {
  var withRandom = trainingPoints.randomColumn('random'); // Add a random column
  var trainingSet = withRandom.filter(ee.Filter.lt('random', 0.8)); // 80% for training
  var validationSet = withRandom.filter(ee.Filter.gte('random', 0.8)); // 20% for validation
  return { trainingSet: trainingSet, validationSet: validationSet };
}

// Split training and validation sets for each year
var split2001 = splitTrainingValidation(trainingPoints2001);
var split2012 = splitTrainingValidation(trainingPoints2012);
var split2023 = splitTrainingValidation(trainingPoints2023);

// Sample the images for training
var training2001 = landsat7Composite2001.sampleRegions({
  collection: split2001.trainingSet,
  properties: ['land'], // Specify class property accordingly
  scale: 30
});

var training2012 = landsat7Composite2012.sampleRegions({
  collection: split2012.trainingSet,
  properties: ['land'],
  scale: 30
});


var classifier2023 = ee.Classifier.smileRandomForest(50).train({
  features: training2023,
  classProperty: 'land',
  inputProperties: ['B4', 'B3', 'B2']
});

// Validate the classified outputs and calculate accuracies
var validation2001 = landsat7Composite2001.sampleRegions({
  collection: split2001.validationSet,
  properties: ['land'],
  scale: 30
}).classify(classifier2001);

var validation2012 = landsat7Composite2012.sampleRegions({
  collection: split2012.validationSet,
  properties: ['land'],
  scale: 30
}).classify(classifier2012);

var validation2023 = landsat8Composite2023.sampleRegions({
  collection: split2023.validationSet,
  properties: ['land'],
  scale: 30
}).classify(classifier2023);
```

Dependent and independent variable

Below The table dependent variable is Actual evapotranspiration the independent variable is land surface temperature and rainfall.

Table 1: dependent and independent variable

AET in mm/day	Rainfall in mm/ year	LST in °C
4.1	1400	26
4.2	1300	27
3.9	1334	32
3.7	1446	31
4.1	1236	32
4.2	1330	29
3.97	1425	28.5
4	1300	25
4.1	1325	29
4.7	1425	26
4.16	1340	27
4.78	1350	25
4.8	1390	29.5
4.7	1450	27
4.8	1330	26
4.8	1450	27.5
4.7	1400	32
4.6	1390	30

4.5	1320	26.5
4.75	1452	27.3
4	1300	26.5
5	1400	26
4.07	1320	27.5
3.9	1200	27
5	1490	28.5
5	1485	26
3.85	1230	29
3.9	1220	32
3.9	1200	33
4.1	1390	31
4.7	1400	31
4.9	1100	23
5	1115	22
5.1	1120	21.99
4.8	1023	23.5
6.1	1250	20
5.2	1189	21
4.9	1036	23

5.1	1121	21.8
5.2	1200	20.5
4.79	1222	23.4
5.2	1223	20.8
5.1	1245	20.92
4.9	1004	22
4.5	989	24
5.6	1250	19
5.7	1290	18.9
5.15	1050	22
5.2	1298	21
4.9	1029	23
5.1	1290	21.8
5.2	1275	20.5
4.79	989	23.4
5.2	1300	20.8
5.1	1298	20.92
4.9	1002	22
4.5	908	24
5.6	1340	19

5.7	1345	18.9
5.15	1290	22
4.95	1187	24.5
4.8	1009	25
2.9	1000	37
2.7	998	37.5
2.73	999.5	37.2
2.6	1002	38
2.4	987	39
2.8	1024	37
3	1250	35
3.1	1254	34
2.9	1200	36.5
2.7	1197	37.1
2.85	1198	36.5
2.16	992	38.5
2.3	998	36.5
2.5	997	34.5
2.6	1070	33.5
2.7	1089	32

2.89	1000	31
2.9	998	37
2.7	999.5	37.5
2.73	1002	37.2
2.6	987	38
2.4	1024	39
2.8	1250	37
3	1254	35
3.1	1200	34
2.9	1197	36.5
2.7	1198	37.1
2.85	992	36.5
2.16	998	38.5
2.3	997	36.5
2.5	1070	34.5
2.6	1089	33.5
3.7	1027	32
3.6	1009	33
3.4	1098	34
3.1	997	34.5

3.65	1195	31.5
3.5	1200	31.7
3.55	1209	32
3	987	36
2.9	970	37
3.6	1270	31
3.4	1265	33
3.6	1267	29.5
2.9	1100	34
2.9	908	34.1
3.21	1002	31.7
3.15	1000	32
31.6	1027	31.9
3.7	1009	32
3.6	1098	33
3.4	997	34
3.1	1195	34.5
3.65	1200	31.5
3.5	1209	31.7
3.55	987	32

3	970	36
2.9	1270	37
3.6	1265	31
3.4	1267	33
3.6	1100	29.5
2.9	908	34
2.9	1002	34.1
0.9	956	39.5
0.1	880	40
0.8	900	39.3
0.01	870	41
0.8	890	39.2
0.7	902	39.9
0.6	870	40.1
1	997	38.9
1.2	1000	38.1
0.75	870	42
0.9	900	40
0.78	976	41
0.76	976	41.1

0.78	967	40.5
0.1	840	42
0.001	760	42.5
0.9	978	39.5
0.1	870	40
0.8	956	39.3
0.01	752	41
0.8	867	39.2
0.7	765	39.9
0.6	702	40.1
1	978	38.9
1.2	988	38.1
0.75	867	42
0.9	900	40
0.78	898	41
0.76	870	41.1
0.78	879	40.5
0.1	745	42
0.001	700	42.5